NATURAL AND ANTHROPOGENIC CARBONACEOUS MATERIALS FOR THE REMEDIATION OF POLYCHLORINATED BIPHENYLS FROM AQUEOUS SOLUTION

A Thesis

Presented to

the Faculty of the Department of the Civil & Environmental Engineering

University of Houston

In Partial Fulfillment

of the Requirements for the Degree

Master of Science

in Environmental Engineering

by

Bradley D. Beless

August 2013

NATURAL AND ANTHROPOGENIC CARBONACEOUS MATERIALS FOR THE REMEDIATION OF POLYCHLORINATED BIPHENYLS FROM AQUEOUS SOLUTION

Bradley D. Beless

Approved:

Chair of the Committee
Hanadi Rifai, Professor,
Civil & Environmental Engineering

Committee Members:

Debora Rodrigues,
Assistant Professor,
Civil and Environmental Engineering

Shankar Chellam, Professor,
Civil and Environmental Engineering

Suresh K. Khator, Associate Dean,
Cullen College of Engineering

Hanadi Rifai, Director,
Environmental Engineering Graduate Program

Acknowledgements

I want to first acknowledge that the completion of my master's thesis is the culmination of many people coming together to help, support and simply be there for me throughout the process. The past two years have been quite the whirlwind of an experience and unfortunately I do not have the space or memory to recognize everyone who has been there for me along the way. I can confidently say that I could not have done it alone!

Specifically, I want to give special recognition to my advisor, Professor Hanadi Rifai, for allowing me the opportunity to come to the University of Houston to learn and grow. She gave me continuous support, guidance and motivation towards realizing the goals I set out to accomplish two years ago. I have learned from her personal example to set high standards, enabling me to go beyond what I once thought possible.

I want to thank my committee members, Debora Rodrigues and Shankar Chellam, for investing in both my education and personal research. Dr. Rodrigues demonstrates a contagious enthusiasm for research coupled with the ability to keep looking towards the future, which contributed to the formulation of the original idea that grew into my thesis project. Dr. Chellam's rigorous pursuit of fundamental knowledge and precision motivated me during the second half of my project to remain diligent when the volume of work and the unknown put me at risk of compromising the quality of my work.

In addition to the professors here at UH, I want to thank Bryan Boulanger, who helped spur my love for Environmental Engineering and laboratory research during my undergraduate years at Texas A&M. Dr. Boulanger's willingness to invest in students such as myself, on a professional and personal level, inspired me to move forward towards the Environmental Engineering field.

I want to thank Fritz Claydon, Maria Modelska, Dr. Rifai, and all those who help with the GK-12 fellowship program, for the financial support and opportunity to invest in the education of the physics students at Galena Park high school. Additionally I want to recognize the teacher I was partnered with, Jeremy Ardner, for his guidance towards improving my communication and presentation abilities, as well as his continuous interest in my work and friendship over the past year.

Being in a research group has helped teach me the value of collaboration and mutual support. To all those who shared time with me in 'the lab:' Nathan Howell, Dan Burleson, Catherine Santos, Taft Tucker, Brandon Georgetown, Maria Modelska, Aparna Balasubramani, Tiffany Schmidt, Emily Sappington, Rose Sobel, Cagla Akat, Taylour Burton, Angela Johnson and Veronica By, thank you for the support and friendship along the way. Special thanks to Nathan and Catherine, who routinely offered their time and energy to provide essential guidance to my research.

Stepping outside the realm of academics, I want to give my upmost gratitude to Kate and Asher, the foundation of my support. My family is central in keeping me grounded in my priorities, of which they are top of the list. Kate is the perfect friend, wife, mom and counselor to me, who willingly sacrificed her own time and desires to help me accomplish this work. My young son, Asher, is a joy to have around, and a constant reminder that there is so much more to life than work and career. I also acknowledge all other family members: my brother, sisters, parents, grandparents and in-laws, all of whom supported me and were patient when free time was limited.

Lastly, and most significantly, I want to give thanks and all praise to Jesus Christ, who created me and guides me throughout every turn of life. I hope to ultimately point whatever success and glory back to Him, who knows and understands all the things I work so hard to try and figure out.

NATURAL AND ANTHROPOGENIC CARBONACEOUS MATERIALS FOR THE REMEDIATION OF POLYCHLORINATED BIPHENYLS FROM AQUEOUS SOLUTION

An Abstract

of a

Thesis

Presented to

the Faculty of the Department of Civil and Environmental Engineering

University of Houston

In Partial Fulfillment

of the Requirements for the Degree

Master of Science

in Environmental Engineering

by

Bradley D. Beless

August 2013

Abstract

The presence of polychlorinated biphenyls (PCBs) in the environment is a continuing challenge that presents a hazard to ecosystems and human health. The proliferation of carbon-based nanomaterials such as graphene (GE) and carbon nanotubes (CNT) has generated interest in their use as sorbent materials for the remediation of PCBs. In this study, isotherm experiments were conducted to compare the sorption of 11 PCB congeners to activated carbon (AC), black carbon (BC), GE and CNT. The Langmuir, Freundlich and Polanyi-Dubinin-Manes models were used to fit the experimental data, resulting in model parameters and distribution coefficients. AC exhibited the highest sorption of the materials tested, with average distribution coefficients 1.0, 1.5 and 2.5 orders of magnitude greater than GE, CNT and BC, respectively. Although improvements can be made to the nanomaterials, in the present study, AC proved to be the superior sorbent for PCBs in solution followed by GE and CNT.

Table of Contents

List of Figures

List of Tables

Nomenclature

Term	Explanation
AC	activated carbon
BC	black carbon
C_e	equilibrium concentration of PCBs in water (µg/L)
CNT	carbon nanotubes
CNT-OH	carbon nanotubes containing hydroxyl functional groups
CV	coefficient of variation
DI	deionized
EPA	environmental protection agency
FRE	Freundlich sorption isotherm
GC-MS	gas chromatography – mass spectrometer
GE	graphene
GO	graphene oxide
HOC	hydrophobic organic compounds
K_{ow}	octanol-water partitioning coefficient (L/L)
K_s	sorbent -water distribution coefficient (L/kg)
LAN	Langmuir sorption isotherm
MWNT	multi-walled nanotubes
PCBs	polychlorinated biphenyls
PDM	polanyi-dubinin-manes isotherm model
POPs	persistent organic pollutants
q_e	equilibrium concentration of PCBs on a sorbent material (µg/kg)
SEM	scanning electron microscope
SPME	solid-phase microextraction
SSA	specific surface area
SWNT	single-walled nanotubes

Chapter 1: Introduction and Objectives

Polychlorinated biphenyls (PCBs) have been widely studied since they were banned from production in the United States in 1979 due to their negative impacts on the environment and human health. PCBs are toxic to biotic organisms and are highly persistent in the environment, contaminating ecosystems and food chains for many years even when introduced at low concentrations [1]. A large amount of research has been conducted to investigate the physicochemical properties of PCBs to better understand their interactions within the environment. With increasing knowledge about their properties, the emphasis is now focused on how to remediate environments already contaminated with PCBs and how to more efficiently remove incidental PCBs from waste streams. PCBs are strongly hydrophobic molecules and preferentially sorb to sediments and organic matter at the bottom of natural water systems, making them especially difficult to remediate. The industries that manufactured or used PCBs were most commonly located along waterways, making industrial waterways the most common type of contaminated environment.

There have been very few methods and technologies implemented to effectively remediate waterways that are contaminated with PCBs. Currently, dredging and disposing of contaminated sediment in hazardous waste landfills is one of the most commonly used methods. Despite the simplicity of dredging, the method is extremely invasive, disruptive, costly, time consuming and may lead to a short term elevation of PCB levels in the water column. Additionally, it is also possible that residual PCBs remaining in the sediment post-dredging will continue to present high risks to humans and the environment. In an attempt to improve the quality and cost effectiveness of remediation, many researchers are looking towards new *in situ* methods with the use of amended sorbent materials as caps or incorporation into the sediment as sequestration

agents. In addition to remediating historically contaminated sites, there is also a need for improving the handling and disposing of PCBs in industrial wastewater streams. Many industries, such as chemical refineries, go to great expense to remove PCBs that continue to persist as an undesired byproduct in their waste streams. Sorbents such as activated carbon (AC) and fly ash can be used in the wastewater treatment process to remove PCBs from aqueous solution and concentrate them into a sludge stream [2].

Whether the need is sediment remediation or wastewater treatment, the use of sorbents to sequester or remove PCBs is a relatively simple and commonly used technology. AC, for example, is a conventionally used sorbent that has been tested and proven effective at removing organic pollutants such as PCBs from aqueous solution. AC is a carbon based material that is created in such a way to generate a highly porous structure that is effective at physically adsorbing a variety of pollutants. Although AC is an appealing option when choosing a sorbent, there is always a desire to seek new sorbents that are more efficient and applicable in sequestering or removing PCBs.

In addition to AC, there has been an increasing awareness of soot and char particles that demonstrate high levels of sorption towards organic pollutants such as PCBs [3-5]. These particles are byproducts of incomplete combustion and include numerous subgroups: traffic soot, wood soot, coal soot, coal, and charcoal [4], all of which can be placed under the classification of black carbon (BC). Both AC and BC have been studied as potential sorbents with applications in removing or sequestering PCBs; however, there are recently synthesized materials that exhibit similar chemical characteristics to AC and BC that have yet to be researched for their potential use as a sorbent for PCBs.

Research on nanoparticles such as graphene (GE) has rapidly accelerated over the past few years resulting in numerous findings and applications. GE is a nanoparticle that consists mostly of carbon atoms, much like its larger parent particles AC and BC.

Carbon nanotubes (CNTs) are another class of nanoparticles that demonstrate similar chemical characteristics to AC and BC but are on a nano-scale in terms of size. The effect of oxygen functional groups on the surface of CNTs is a continuing question in sorption science; therefore, CNTs with hydroxyl (-OH) functional groups are included as a sorbent in this study alongside non-functionalized CNT. GE, CNT, and CNT-OH are each similar to AC and BC in their elemental makeup yet these three materials exhibit unique properties which are not fully understood, making them candidates as potential sorbents of PCBs. Because of their unique properties (size, potential for their use as coatings, or manipulating their chemical make-up to enhance their sorptive properties), the aforementioned nanoparticles may offer exciting opportunities for managing persistent organic pollutants (POPs), such as PCBs, in the environment and in waste streams.

In this research, the sorption properties of GE, CNT and CNT-OH were investigated and compared to the more traditionally studied materials: AC and BC. More specifically, the objectives included:

- Determining which isotherm model and error function fit the experimental data best.
- Evaluating the effect that the molecular planarity of PCBs had on sorption to the five sorbents.
- Determining if the hydroxyl groups on CNT increased or inhibited the sorption of PCBs.
- Evaluating and comparing the efficiency and strength of PCB sorption to the five sorbents using the measured sorbent-water distribution coefficients and calculated isotherm parameters.

Chapter 2: Background

2.1 PCBs in the Environment

2.1.1 Production History

The production of PCBs began in 1930 and expanded rapidly due to their desirable physical properties as a heat-exchange fluid [1]. In 1930, Chester Penning wrote “Physical Characteristics and Commercial Possibilities of Chlorinated Diphenyls” in the *Journal of Industrial and Engineering Chemistry*, announcing the synthesis of PCBs and detailing their physical properties and potential applications. Penning stated in his article that, “They [PCBs] have no noticeable action upon the skin; the concentrated vapors are irritating to the nasal passages, and cause violent headaches to certain persons, but aside from this no toxic effects have been noted,” leading to the general assumption that PCBs do not cause any major adverse health risks [6]. Yet this assumption was quickly questioned because of noticeable health effects on workers, such as chloracne and liver disease [1].

A study conducted at Harvard University in 1937 demonstrated that PCBs are indeed capable of producing negative health effects in humans [7]. Occupational thresholds were created, but these warnings were largely ignored and the creation of PCBs continued. As the PCB industry grew, the list of applications grew as well, including uses such as hydraulic fluids, heat transfer fluids and high pressure lubricants, (often being used in electrical transformers and capacitors) [8]. Additional uses of PCBs continued to emerge and their market began to include more open-ended products such as inks, paints, dedusting agents, and pesticides [9]. It was not until the 1960s that serious concerns began to arise concerning the negative effect of PBCs on humans and the environment.

In 1964, Dr. S. Jensen, a Swedish scientist, was studying the contamination of DDT in the environment when he noticed an interfering peak in his gas-liquid chromatographic separator. Jensen soon realized this interfering peak in many of his environmental samples was due to the presence of PCBs. This discovery raised the concern that PCBs were becoming a widespread problem, persisting in many food chains and posing a human and ecological health threat [10]. In 1971, many United States producers of PCBs voluntarily limited the sale of PCB in open systems, but it was not until 1976 that Congress regulated the use of PCBs with the Toxic Substance Control Act (TSCA). A few years later, the Environmental Protection Agency (EPA) banned PCB production in the United States and moved towards phasing PCBs out of the existing electrical infrastructure [8]. Although the production of PCBs in the United States was halted in the 70s, the complete removal from infrastructure was not accomplished. Additionally, PCBs were being produced by many other countries besides the United States, some of which were not as quick to stop production. Although PCBs are no longer being produced, their persistent legacy is evident throughout the globe.

2.1.2 Current State of PCBs in the Environment

The environmental contamination of PCBs is a widespread problem in many parts of the U.S. and the world [11]. Although contamination with PCBs in the environment is fairly ubiquitous, trace levels of PCBs present little if any health risks, making only the areas of high contamination of interest for remediation. According to the EPA Superfund online database, 503 active sites exists in the U.S. with PCBs listed as a contaminant of concern [12]. PCBs cycle through air, water and soil/sediment, but because of their hydrophobic nature, a majority of the PCB contamination exists in soils and sediments where they can interact with benthic organisms and pore water, making their way up the food chain and becoming hazardous to ecosystems and human health.

The Hudson River is a well-known case study that exemplifies the result of how improper historic disposal causes contamination for generations to come. A recent report published by the EPA [13] describes the contamination of the Hudson River with approximately 1.3 million gallons of PCBs from two General Electric (GE) plants between the years 1947 and 1977. Much of the PCBs were adsorbed to the river sediments near the plants outfalls, but the problem was proliferated when a dam was removed in 1973, increasing the transport of PCBs downstream. Once in the sediment, chemical, biological and physical processes continuously released PCBs into the water column and biotic food chains, causing the PCBs to present health risks to the Hudson River ecology and the surrounding human population. In 1984, 200 miles of the river were placed on EPA's National Priorities List and the Hudson River quickly became one of the most studied and costly Superfund sites [14]. The EPA has currently completed Phase one of the Superfund plan by dredging approximately 283,000 cubic yards of contaminated sediment. Phase two of the project has recently begun with the goal of dredging another 2.4 million cubic yards over the next five to seven years [14].

In addition to the Hudson River, there are various other water bodies that are significantly contaminated, including but not limited to: Baltimore Harbor, San Diego Bay, Delaware River, Chesapeake Bay and New York Harbor. The growing prevalence of contaminated ecosystems provides continued motivation for researching more effective *in situ* remedies for PCB contaminated soil, sediment, and water.

2.1.3 Current Remedial Practices

The earliest method of sediment remediation was to dredge all of the highly contaminated sediments and dispose of them in hazardous waste disposal sites or treat them via *ex situ* treatment technologies. Dredging has the advantage of physically removing PCBs from a site, yet it presents many disadvantages, including high cost,

invasive nature, and the potential to mobilize PCBs that were once sequestered in sediments back into the water column. There are many different methods of dredging, some more suited for minimizing the re-suspension of contaminated sediments, but overall there is no consensus on whether dredging is an effective method of removing contaminated sediments [15-21]. An example of this uncertainty is illustrated with the Hudson River case study, where the question of whether dredging was the best technology arose and was actively debated [22]. Despite the potential ecological disadvantages of dredging, the technology provides a solution that is often more appealing than alternative and lesser known remediation methods that may or may not work as effectively.

Although dredging remains the status quo for remediating sediments contaminated with PCBs, and hydrophobic organic compounds (HOCs) in general, there are numerous alternatives that have been proposed and developed that might provide more effective and less invasive options. Examples of *in situ* sediment remediation include but are not limited to: monitored natural recovery [23, 24], enhanced microbial degradation [25-28], capping [24, 29], amendment capping [24, 29-33], iron catalyzed degradation [25, 34], and thermal desorption treatment [35-37]. It should be noted that the application of any of these methods does not have to exclude the use of others; often for optimization of site specific remediation, more than one technology can be jointly used. With that said, as research continues to develop, it is apparent by the growing number of field studies, that amendment capping is the increasingly favored choice. Moreover, the summary of the *Fourth International Battelle Conference on Remediation of Contaminated Sediments*, emphasizes the importance of amendment capping for the future of sediment remediation [24].

The technique of amendment capping, involves placing a layer of material that has a strong affinity towards PCBs on top of the contaminated sediments, impeding the

transport of PCBs into the water column and food chain. There remains many concerns and obstacles to the wide spread use of amended caps, but researchers have recently begun to address these challenges in laboratory and field studies [32].

The purpose behind amended capping is not to remove PCBs, or HOCs in general, but rather to decrease the risk of ecological and human exposure. Conventional capping uses a layer of sand or clay on top of the contaminated sediments as the amended material; however, to increase the effectiveness of sediment capping, sorbents that have stronger affinities towards PCBs are often augmented in the sand or clay layer.

Currently, activated carbon, both powder and granular, has been used as the primary sorbent material for sediment caps. AC is a conventionally used sorbent, which has been tested and proven efficient at removing organic pollutants such as PCBs from not only aqueous solution but sediment pore water as well. In addition to AC, attention has been given to other sorbents, such as naturally occurring BC [4, 38], fly ash [2], and even cellulose [39], that could potentially be an alternative to AC. To date, there has been no other sorbent material reported that is more efficient or applicable as AC for sequestering PCBs. However, in recent years the development of carbonaceous nanomaterials has renewed the interest in finding a material that surpasses AC in its ability to sequester PCBs.

2.2 Sorbents Used for PCB Sorption

2.2.1 Activated Carbon

The use of carbon materials for purification dates back to antiquity. Its first recorded uses were for the reduction of ores in bronze manufacturing and for medicinal purposes [40, 41]. Activated carbon, as we know it today, is created by taking a carbon-based material: coal, nut or coconut shell, peat, wood, coal, or anything with a primarily

carbon molecular structure, and heating it to between 600 – 800°C in the absence of oxygen [42]. This first step, called carbonization, removes all non-carbon materials and results in a more pure carbon structure. Next the material is “activated” by either a physical process, heating up the carbonized material in the presence of steam or air, or a chemical process, utilizing chemicals such as zinc chloride or phosphoric acid. The activation process further increases the porosity of the material and creates surface functional groups. These functional groups are a small molecular structure that spurs off of the main surface of a material, most often beginning with an oxygen atom being bonded with one of the surface carbon atoms. These oxygen based functional groups have been known to aid in AC’s sorption strengths to some pollutants.

On average, AC has a specific surface area (SSA) of 800 – 1500m^2/g and pore volume of 0.20 – 0.60cm^3/g [42]. The combination of high SSA and surface functional groups makes AC a very effective sorbent of most HOCs. These two properties of AC allow two different mechanisms for sorption of PCBs, and HOCs in general, to occur. First, the microporous structure of AC creates an environment where PCB molecules can diffuse into the pores and physically be entrapped in the pore space [43, 44]. To aid in this entrapment process, there is an additional chemical mechanism that occurs in which the PCB molecules are bonded by Van der Wall forces to the carbon surface of the AC [43]. The type of carbon material used as feed stock, whether it be coal or biomass for example, and the method of activation has significant effects on the pore structure and functional groups of the resulting AC product. AC created by biomass based carbon has been shown to have narrower pore structures than coal based AC [45, 46], making it more effective in entrapping HOCs yet more prone to fouling in the presence of other dissolved organics [47]. Amstaetter et al. (2012) compared both biomass and coal based AC and determined that, in the presence of sediment, the coal

based AC outperformed the biomass based AC [47]. In the present study, the same coal based AC used in Amstaetter et al. (2012) was used.

2.2.2 Black Carbon

Black carbon includes a diverse group of materials and definitions, but is most commonly defined as a product of weathered graphitic carbon rock or the result of incomplete combustion of fossil fuels and vegetation [48-52]. Due to the wide range of materials that make up the BC family, the characteristics of BC are equally as diverse. In general, BC particles consist of three-dimensional structures built of stacked aromatic carbon sheets [52, 53] with widely variable SSA ranging from 2 – 776m^2/g [4, 54-58]. The amount of BC flux into the environment has dramatically increased in the past century due to the increase in biomass burning and fossil fuel consumption set in motion by the industrial revolution [59].

It is widely accepted that the presence of BC, especially in the air, presents both environmental and human health hazards by the catalyzing of smog and linkage to respiratory and cardiovascular diseases [60-62]. Yet the presence of BC, especially in aquatic and sediment environments, has demonstrated positive environmental effects by acting as a strong binding agent for HOCs, so much so that the presence of BC has altered the way researchers model the transport of HOCs in natural environments [4, 52, 63-70]. Because of this relatively new finding, discussions concerning the implications of BC have increased over the past two decades within the realm of environmental engineering and sediment remediation [52].

In a review article written by Koelmans et al. entitled *Black Carbon: The reverse of its dark side*, the authors summarize the findings of “recent investigations [that] have now proven that BC is capable of extremely efficiently sorbing particular toxic chemicals [52].” The authors explain the mechanisms of this “extremely efficient” sorption as being

two fold; first by physical entrapment within the BC structure during formation, secondly by a reversible adsorption on the exterior surface of BC after formation. The entrapment mechanism hypothesizes that the BC particles occlude HOC molecules between their aromatic carbon layers or within internal pore volumes while being formed during combustion. The entrapment mechanism provides an extremely strong sorption between HOCs and BC and can be largely regarded as irreversible. In the present study, only virgin BC particles that have already been formed are used, thus negating the need to consider the entrapment mechanism. The second mechanism of sorption is the adsorption of HOC molecules into pore spaces and onto the exterior surface of BC particles due largely to Van der Waals interactions [52, 71].

As previously mentioned, there are many different types of BC particles: traffic soot, wood soot, coal soot, coal, and charcoal, but for the purposes of this study, one form was chosen to represent the entire BC spectrum for the purpose of comparison to the other sorbents tested. Jonker et al. (2002) tested nine different BC particle alongside AC particles of the same size distribution [4]. The results from their study showed that the charcoal had the highest sorbent-water distribution coefficients and was therefore selected as the most conservative representation of BC for this study.

2.2.3 Carbon Nanotubes

The past few decades have experienced a large increase of research and innovation on carbon based nanoparticles. Kroto et al. (1985) initiated the trend when they accidentally discovered a stable spherical structure of aromatically bonded carbon atoms commonly known as fullerenes [72]. A few years later, Sumio Iijima (2001) discovered what are now known as carbon nanotubes (CNTs) during an attempt to synthesize fullerenes [73]. CNTs are hollow cylinders of aromatically bonded carbon atoms only a few nanometers in diameter but up to several microns in length. Most

CNTs are capped with rounded ends, however, there are methods to remove the end caps and load the hollow interior of the CNT [74].

There are two main categories of CNTs: single-walled carbon nanotubes (SWNT) and multi-walled carbon nanotubes (MWNT). SWNT, as the name implies, are a single sheet of carbon atoms forming one tubular structure; MWNT are SWNTs with additional concentric shells of carbon tubes layered on the original nanotube. Figure 2.1, obtained from Choudhary and Gupta (2011) [75], illustrates the structure of single and multi-walled CNTs.

Figure 2.1: Conceptual illustration of SWNT (left) and MWNT (right).

Currently, there are three main methods of synthesizing CNTs: arc discharge, the simplest but least pure method; laser ablation, which mostly forms bundles of CNTs; and chemical vapor deposition, a more involved but precise method [76]. The average outer diameter of SWNT and MWNT range from 0.6 – 2.4nm and 2.5 – 100nm, respectively, with the interlayer thickness of MWNT being ≈0.3nm [76]. SWNTs have the highest SSA of all types of CNTs with values theoretically as high as 3000m^2/g [77], while MWNTs have SSA values that decrease inversely proportionally to the number of concentric layers, with a minimum of ≈50m^2/g [78]. As the knowledge of how CNTs are created and the technologies continue to increase, scientists will be able to better control the different

properties of CNTs: including but not limited to, inner diameter, number of carbon layers, purity, orientation, and length.

CNTs were not considered for uses as a sorbent until the early 2000s, when Long and Yang (2001) reported the superior ability of MWNTs to remove dioxins compared to AC [79]. Since then, there have been numerous studies investigating the ability of CNTs to remove various types of HOCs, with only a few focusing on PCBs specifically. Interestingly, it has been reported in the literature that the sorption affinity of HOCs to CNTs does not strongly correlate with the hydrophobicity of the HOC, as is commonly assumed with soil and sediments [80, 81]. One main mechanism of sorption proposed is the π-electron coupling that occurs between the aromatic molecules and the carbon surface of CNTl; HOCs that more willingly accept electrons have higher affinities to CNTs [80, 82]. Additionally, there has been some debate on whether the amendment of oxygen functional groups contribute little or negative effects on sorption [80, 82], or if they have an increasing effect on sorption [83]. The diameter of the CNTs also contributes to their ability to sorb with HOCs. CNTs with larger diameters have more surface area and less curvature, making it easier for the HOC molecules to interact with the CNTs [83, 84]. Additionally, researchers have begun to attach select functional groups onto CNTs to improve the sorption of HOCs. Shao et al. (2010) and Shao et al. (2011) reported the addition of cyclodextins and methyl methacrylate groups onto the walls of CNTs using the nitrogen plasma technique. Using this technology, the authors were able to successfully increase the dispersion of CNTs in the aqueous phase and the sorption of HOCs to CNTs [85, 86]. It is this unique ability to manipulate and specialize CNTs that gives them the advantage over the less malleable AC and BC.

The amount of information concerning PCB sorption onto CNTs is still limited, which is why this study has incorporated two types of CNTs for comparison. Although CNTs lack the porous structure of AC and BC, their ability to bond with HOCs through π-

electron coupling has proven adequate for sufficient PCB sorption. Additionally, because CNTs are on the order of nano and micrometers, they have a large surface area that is comparable with AC, providing numerous sorption sites for contaminates. In this study, two MWNTs, one with no functional groups and the other with hydroxyl (OH) functional groups, were chosen to further study the ability of CNTs to sorb PCBs.

2.2.4 Graphene

Activated carbon, charcoal (black carbon), and carbon nanotubes, all have, in at least some fraction, the molecular structure of stacked sheets of aromatically bonded carbon atoms. Figure 2.2, obtained from Wang et al. (2008) [87], illustrates this single sheet of honeycomb shaped carbon, which has been termed graphene (GE). Researchers have long theorized the unique properties of an isolated single layer of GE and have worked hard towards making materials with fewer and fewer layers of carbon sheets. Novoselov et al. (2004) were the first to create GE in its purest form, a single sheet of carbon one atom thick [88]. Their technique for isolating the single sheet of GE was surprisingly simple; they used common cellophane (Scotch®) tape to peel layers of GE off of a graphite flake and deposit single or few-layered GE sheets onto a substrate [89]. The impressive physical, mechanical, thermal and electrical properties measured from single or few-layered GE confirmed the theorized assumptions and generated a surge of research with the goals of developing better methods of generating GE and finding applications for the use of GE.

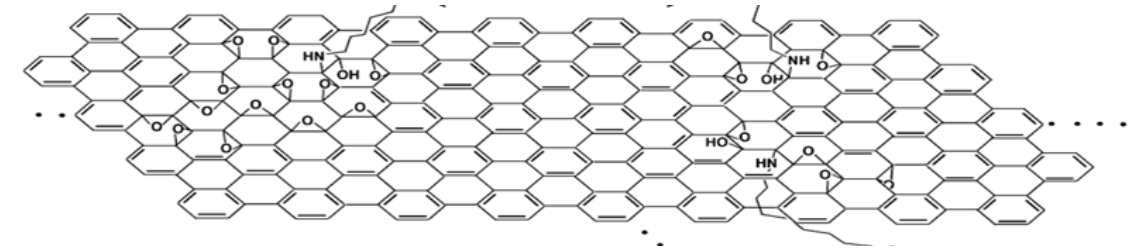

Figure 2.2: Conceptual illustration of a graphene sheet. The image realistically shows the possibilities of imperfections and oxygen functional groups.

There are four main methods of producing GE: mechanical exfoliation of graphite using adhesive tape; chemically derived graphene oxide (GO) that can be reduced to GE; thermal decomposition of silicon carbide (SiC) to remove the silicon under high temperature and vacuum; and chemical vapor deposition of hydrocarbons onto transition metal substrates [89, 90]. Currently, the difficulty of generating pure single layer GE in large amounts is still the limiting factor in expanding technological applications. Despite the difficulty with production, scientists and engineers have developed multiple uses and potential uses for GE, such as high-speed electronics, highly sensitive sensors, and use in solar cells [89].

To date, and to the best of the author's knowledge, there has been no research demonstrating the capability of GE to act as a sorbent material for HOCs. GE is the building block of the previously mentioned carbon materials, all of which have been proven to be efficient at absorbing HOCs. Although GE lacks the porous structure of AC and BC, they contain the potential for π-electron coupling similar to CNTs, while having a potentially greater surface area with more sorption sites available. Additionally, GE is highly tunable and can be the host for many different organic or inorganic functional groups, giving GE the potential for future modification to increase its sorption efficiencies [91]. GE can also be electro-deposited onto metal substrates, which could be advantageous for future filtering applications [92]. With this foundation, GE was selected as a sorbent to initiate the study of PCB sorption to GE and to compare GE against the other carbonaceous sorbents.

2.3 Physical and Chemical Properties of PCBs

In addition to understanding the properties of the sorbent materials, it is important to thoroughly understand the sorbate of interest. PCBs are formed by a single bond joining two phenyl rings with any assortment of chlorine atoms substituted for hydrogen

atoms on the 10 available carbon atoms (Figure 2.3). There are 209 different PCB congeners that can theoretically exist, each congener with a unique sequence of chlorine atoms bonded to the carbon atoms of the two phenyl rings [1].

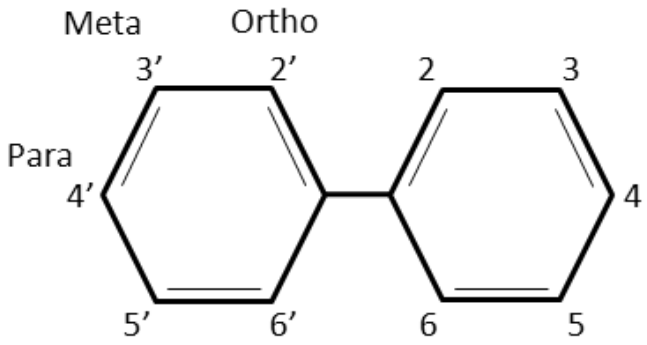

Figure 2.3: Conceptual illustration of the chemical structure of a PCB molecule.

Pure PCBs are solid at room temperature (21°C) with a melting temperature ranging from 54°C for the lowest chlorinated PCBs to 310°C for the highest chlorinated PCBs [8]. One of the most important properties of PCBs when considering fate and transport in the environment is that they are largely water-insoluble while strongly lipid-soluble. Additionally, PCBs are very resistant to degradation by oxidation, acid or bases, heat, and microbial processes [8]. The overarching trend is that the more chlorine substitutes a PCB congener has, the harder it is to degrade [34] and the more persistent it is in the environment. In contrast, different PCB congeners have varying toxic effects depending more on the positions of chlorine substitutions than the number of chlorine substitutes [93].

The physical shape and size of each PCB congener also depends on the number and positioning of the chlorine substitutes. The chlorine atom is much larger than the hydrogen atom which it replaces, with atomic mass of 35.45 and 1.01amu, respectively. Because of this size difference, the substitution of chlorine atoms plays a significant role in determining the planarity, size, and molecular weight of each PCB congener. The

planarity of a PCB congener is described by the angle between the planes formed by the two phenol rings, referred to as the dihedral angle. Congeners that are more planar will have small dihedral angles so that the two phenol rings are closely aligned and the molecule as a whole is roughly on the same plane, while non-planar molecules will have a dihedral angle around 90°. The planarity of PCB congeners primarily depends on whether there are chlorine atoms substituted in the ortho position. The dihedral angles are ≈40°, ≈60°, and ≈90° for PCB congeners with non-, mono-, and di-ortho chlorine substitutions, respectively [44, 94]. Figure 2.4 is a simplified illustration of the difference in dihedral angle for the three different ortho position possibilities; as more chlorines are substituted into the ortho positions, the angle of the two bonded phenol rings increases.

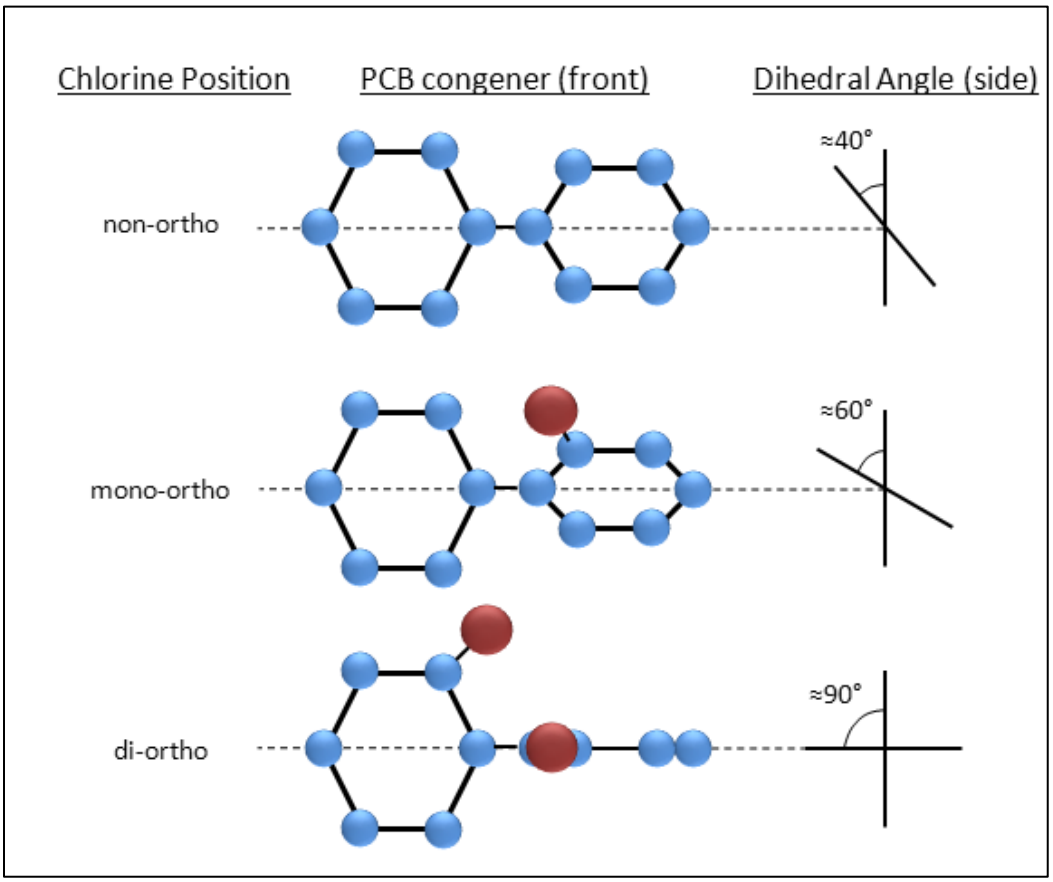

Figure 2.4: Dihedral angles for non, mono and di-ortho PCB congeners. The blue spheres represent carbon atoms, the red spheres represent chlorine atoms and the hydrogen atoms are not shown. The top of the right phenyl ring is rotating outwards.

In this study, eleven PCB congeners, numbers 1, 2, 4, 8, 15, 52, 72, 77, 138, 156 and 169, were used as the analytes of interest with two congeners, numbers 101 and 152, used as internal standards during the experimental processes (details of the specific congeners are given in Table 2.1). The eleven analyte congeners were chosen to have a wide range of hydrophobicity, described by their octanol-water partitioning coefficient (K_{ow}) and solubility (S_w), and all three ortho-position possibilities. The size of the different congener molecules, given by molecular volume (V_m), is shown to increase proportionally with molecular weight. Overall, the 11 congeners chosen cover a wide range of physical properties and adequately illustrate the variety of all 209 PCB congeners.

Table 2.1: Details and physical properties of the 13 PCB congeners used: * indicates internal standards, [a] Hawker and Connell (1988) [95], [b] Mackay et al. (1992) [96], [c] Brodsky and Ballschmiter (1988) [97] and [d] Gramatica et al. (1998) [98].

Congener	Congener Name	# of Chlorine Substitutions	Ortho-Positions	$\log(K_{ow})^a$	MW	$V_m{}^b$ (cm^3/mol)	S_w (µg/L)[c]
PCB-1	2-Chlorobiphenyl	1	mono	4.46	188.66	205.5	1431.10[d]
PCB-2	3-Chlorobiphenyl	1	non	4.69	188.66	205.5	768.55
PCB-4	2,2'-Dichlorobiphenyl	2	di	4.65	223.10	226.4	417.83
PCB-8	2,4'-Dichlorobiphenyl	2	mono	5.07	223.10	226.4	769.14
PCB-15	4,4'-Dichlorobiphenyl	2	non	5.30	223.10	226.4	94.08
PCB-52	2,2',5,5'-Tetrachlorobiphenyl	4	di	5.84	291.99	268.2	29.20
PCB-72	2,3',5,5'-Tetrachlorobiphenyl	4	mono	6.26	291.99	268.2	24.28[d]
PCB-77	3,3',4,4'-Tetrachlorobiphenyl	4	non	6.36	291.99	268.2	0.99
PCB-101*	2,2',4,5,5'-Pentachlorobiphenyl	5	di	6.38	-	-	-
PCB-138	2,2',3,4,4',5'-Hexachlorobiphenyl	6	di	6.83	360.88	310.0	1.50
PCB-152*	2,2',3,5,6,6'-Hexachlorobiphenyl	6	quad	6.22	-	-	-
PCB-156	2,3,3',4,4',5-Hexachlorobiphenyl	6	mono	7.18	360.88	310.0	1.78
PCB-169	3,3',4,4',5,5'-Hexachlorobiphenyl	6	non	7.42	360.88	310.0	0.50

2.4 Isotherm Theory

There are a variety of materials that are currently being used as sorbents, and many others which have yet to be explored. With the variety and volume of sorbent materials tested, researchers developed the isotherm approach to measure the efficiency of sorbent materials to compounds of interest. The term isotherm fundamentally means a system at constant temperature, yet in the realm of sorption science, isotherm experimentation has taken on a more specific meaning. While it is true that temperatures are held constant, isotherm experiments are specifically conducted to understand the equilibrium relationships between a sorbent and sorbate system over a wide range of equilibrium concentrations. Experimentally, isotherms are conducted in batch systems with a range of sorbent:sorbate ratios. The overarching goal of isotherm experiments is to better understand how sorbent materials interact with the sorbate of interest. More specifically, isotherm experiments are designed to enhance understanding of the characteristics of the sorbent materials, such as surface properties and sorption capacities that are crucial in comparing different sorption materials and optimizing their use [99].

2.4.1 Isotherm Models

Using mathematical models to fit the isotherm experimental results is the primary means by which sorbent characteristics and overall efficiency is determined. Researchers have developed numerous models that fit equilibrium sorption with a variety of different underlining assumptions. This section contains a brief description of the three isotherm models used in the present study.

Langmuir Isotherm Model

Irving Langmuir derived a widely used isotherm model in 1917, originally developed to describe the sorption of gasses onto activated carbon [100, 101]. The Langmuir model (LAN) has a few fundamental assumptions that are important when considering its application. First, the model assumes a homogeneous sorbent surface where only monolayer sorption can occur. Plainly put, the LAN model assumes that the sites available for sorption on a material are evenly distributed and only have the capacity of attaching to one sorbate molecule, resulting in only a single coating of sorbate molecules on the sorbent surface. In conjunction, the second assumption states that there are a finite number of sorption sites on a sorbent material that all have the same affinity to the sorbate and no interference exists between neighboring sorption sites [99, 102].

The LAN isotherm model is as follows:

$$q_e = \frac{Q_{max}^L b C_e}{1 + bC_e}, \qquad 2.1$$

where q_e is the equilibrium concentration of sorbate on the sorbent material ($\mu g_{PCB}/kg_{sorbent}$ dry), C_e is the equilibrium concentration of sorbate in the water phase ($\mu g_{PCB}/L_{water}$), Q_{max}^L is the maximum sorption capacity (µg/kg) and b is the Langmuir isotherm constant (L/µg). The LAN model is a two parameter model; the C_e value is experimentally derived and the Q_{max}^L and b values are determined by fitting the calculated q_e to the experimental q_e values. Practically, the Q_{max}^L value represents the concentration of sorbate that a sorbent material contains when saturated, and the b value empirically represents the affinity, or bond strength, between the sorbent and sorbate. Figure 2.5 depicts a theoretical curve generated from Equation 2.1. The concentration of sorbate on the sorbent increases sharply at low equilibrium

concentrations in the bulk water, eventually slowing to a plateau as the sorbent becomes saturated with the sorbate and reaches maximum sorption capacity.

The Langmuir model is widely used for a variety of sorbent materials, however, there has been debate on whether the LAN model is appropriate to use with porous sorbents such as activated carbon [44, 103, 104]. Despite the concern raised about porous materials and their lack of surface homogeneity, the LAN model provides a robust enough mathematical model to accurately fit experimental data for many different porous materials including AC and should not be neglected due to discontinuity between the assumptions and reality [5, 105].

Freundlich Isotherm Model

H.M.F. Freundlich created one of the first isotherm models in 1906 to describe non-ideal and reversible sorption [106]. The Freundlich model (FRE) is an empirically derived mathematical equation that, unlike the LAN model, allows for a heterogeneous surface and does not depend on monolayer surface coverage. The surface sorption sites can have varying levels of bond energies, with energies decreasing exponentially proportionate to distance from the sorbent surface [99].

The FRE isotherm model is as follows:

$$q_e = K_F {C_e}^n, \tag{2.2}$$

where K_F is the Freundlich constant (µg/kg)(µg/L)^n, n is the Freundlich sorption intensity parameter (unitless), and q_e and C_e are defined above. The FRE model is a two parameter model, similar to the LAN model, where the K_F and n values are fit to the experimental data by regression between the calculated q_e and the experimental q_e values. K_F is an empirically derived constant that is very similar to the distribution coefficient (K_s). Much like K_s, K_F represents the quantity of sorption between the sorbate and sorbent, with higher values representing greater sorption. The n value controls the

linearity of equation 2.2, meaning as n approaches 1 the model becomes more linear. The more linear the isotherm is the stronger the sorption is between the sorbent and sorbate. Figure 2.5 depicts a theoretical graph generated by the FRE model. The FRE model does not produce the maximum capacity plateau characteristic of the LAN model, but rather indicates a more gradual decrease of sorbate sorption rate onto the sorbent with increasing equilibrium concentrations. The lack of a plateau is a distinct part of the FRE model, allowing the potential for very high sorption levels without consideration of maximum capacity.

The FRE model, similar to LAN, has been widely used over the past century to describe the sorption of pollutants onto sorbent materials. Originally created to describe the sorption by animal charcoal, the model typically performs well with sorption experiments using porous, carbon based materials.

Polanyi-Dubinin-Manes Isotherm Model

The Polanyi-Dubinin-Manes model (PDM) is founded on the Polanyi potential theory developed in 1916 [107]. The theory was originally developed to describe the interaction of gaseous sorbates onto solid sorbent materials and was later adapted to comply with sorption of sorbates in bulk solutions. The underlying assumptions of the Polanyi theory are: sorbents have a fixed pore volume in which sorption can take place; sorption between the sorbate and sorbent occurs due to van-der Walls forces; and sorbate molecules will first concentrate at high-energy sites [108]. Allen-King et al (2002) used the Polanyi theory to derive a mathematical model for the specific purpose of fitting liquid phase sorption to carbon based sorbents [107]. The resulting model, known as the PDM model, can be considered a union of the LAN and FRE models, in which a heterogeneous surface assumption is made alongside the understanding of a maximum sorption capacity.

The PDM isotherm model is as follows:

$$q_e = Q_{max}^{P} \exp\left[-\left(\frac{RTln\left(\frac{S_w}{C_e}\right)}{Z}\right)^{d}\right], \quad 2.3$$

where Q_{max}^{P} is the maximum sorption capacity (µg/kg), R is the universal gas constant (J/mol*K), T is the temperature (K), S_w is the saturation concentration of the sorbate (µg/L), Z is the free energy parameter (J/mol), d is the energy distribution parameter (unitless) and q_e and C_e are defined above. The gas constant, temperature and saturation concentration are known for every scenario, making the PDM model a three parameter model, with Q_{max}^{p}, Z and d used for fitting the calculated q_e to the experimental q_e values. Practically, the Q_{max}^{P} value represents the maximum capacity of sorbate a sorbent material can have when saturated, the Z value represents the bond strength between the sorbate and sorbent, and the d value relates to the distribution of sorption energies. Figure 2.5 depicts a theoretical graph generated by the PDM model. Similar to the LAN, the PDM model has a maximum adsorption capacity at which the curve plateaus, indicating that there are no more available sites on the sorbent material.

The PDM model is relatively new and is not as widely used and accepted as the LAN and FRE models. However, recent studies using various kinds of BC (soots, chars, coals) have applied the PDM model and found it to fit more accurately than the general LAN and FRE models [5, 109]. For this reason the PDM, model was included in the present study.

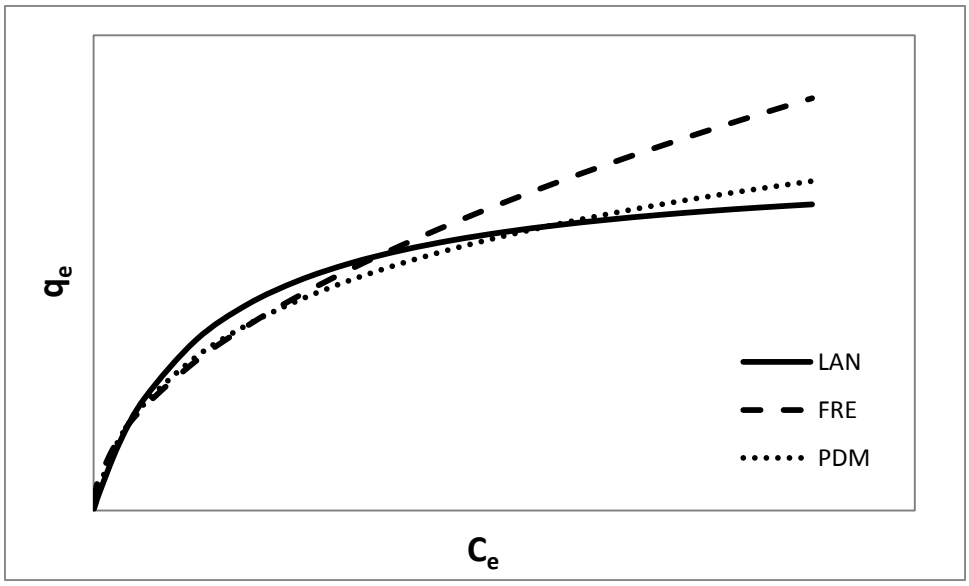

Figure 2.5: Theoretical graphs depicting the Langmuir, Freundlich, and Polanyi-Dubinin-Manes models.

2.5 Sorption of PCBs to Sorbent Materials from the Literature

The main purpose of the present study is to compare the efficiency of the nanomaterials with the more established activated and black carbon materials. As previously mentioned, there is a plethora of research on and knowledge about AC and BC, whereas there is little to no work available to understand and compare the new carbonaceous materials with the historic ones. This section presents a brief summary of the findings from the published literature concerning the adsorption of PCBs to AC, BC, CNTs and GE specifically.

There are two main criteria used to measure sorption efficiency: the distribution coefficient between the sorbent material and water (K_s), and any calculated isotherm model parameters. K_s is the ratio of sorbate concentration on the sorbent or in the water phase at equilibrium. The equation for the distribution coefficient is,

$$K_s = \frac{q_e}{C_e}, \qquad 2.4$$

where K_s is the sorbent-water distribution coefficient ($L_{water}/kg_{sorbent}$), q_e and C_e are defined above. It can be seen from equation 2.4 that increasing K_s values infer stronger sorption by the sorbent material. Although the K_s value measured can be a very useful means of determination and comparison, the value is only valid for the equilibrium concentrations at which the measurements were taken, unless the distribution is linear, in which case, the K_s is true for all concentrations.

Sorption of PCBs onto a limited amount of carbon material is seldom determined to be linear, which is why the K_s values are only compared based on the aqueous equilibrium concentrations at which the experiments were conducted. Isotherm experiments and models are used to overcome this concentration dependence when comparing sorption affinities. Because the modeled experimental data covers a wide range of aqueous equilibrium concentrations, the resulting parameters can be compared between different experimental data sets as long as the aqueous equilibrium concentrations are close to the same range. Data including K_s values and isotherm parameters were gathered from published scientific journals to lay a foundation of comparison for the five sorbent materials being tested in the present study. Table 2.2 and 2.3 give a summary of the K_s values and isotherm parameters found in the literature. All K_s values in Table 2.2 are measured for equilibrium concentration in the ng/L range. Table A.1 in Appendix A offers a more detailed list of the isotherm parameters.

Table 2.2: Summary of the distribution coefficients log(K_s) values found in the literature for sorption of PCBs to various types of sorbent materials: [a] Jonker and Koelmans (2002) [4], [b] Jantunen (2010) [5] and [c] Jonker 2006 [110].

Congener	Activated Carbon[a]	Charcoal[a]	Traffic Soot[b]	Coal[b]	Virgin Oil Mixture[c]	Weathered Oil Mixtured[c]
PCB-18	8.16	7.47	5.66	6.20	5.94	6.27
PCB-28	8.44	7.81	6.34	7.00	6.31	6.51
PCB-52	8.36	7.63	5.95	6.56	6.60	6.82
PCB-72	9.51	8.05	6.65	7.28	6.99	7.15
PCB-77	9.64	8.41	7.46	7.90	6.96	7.04
PCB-101	9.18	7.90	6.49	7.11	7.36	7.53
PCB-118	9.45	8.12	7.05	7.61	7.66	7.69
PCB-126	9.87	8.39	7.53	7.85	7.52	7.61
PCB-138	9.55	7.96	6.92	7.43	7.91	8.11
PCB-156	9.71	8.11	7.32	7.71	8.13	8.21
PCB-169	9.75	8.20	7.58	7.74	8.18	8.27

Table 2.3: Summary of the isotherm parameters found in the literature for sorption of PCBs to various types of sorbent materials. The cells highlighted in green have units of (µg/kg)(µg/L)^n and the cells highlighted in blue have units of (ng/kg)(ng/L)^n.

Lead Author	Year	Sorbent Material(s)	Particle Sizes	PCB analytes	LAN Q_{max}*10^6 (ug/kg)	LAN b (L/ug)	FRE K_F *10^6 (x/kg)(x/L)^n	FRE n_F (-)	PDM Q_{max} *10^6 (ug/kg)	PDM Z (kJ/mol)	d (-)
Cornelissen	2004	BC	-	3, 4	-	-	0.035 - 0.26	0.62 - 0.92	-	-	-
McDonough	2008	AC	40 - 75um	4, 12, 18, 52, 53, 54, 72, 77, 126	-	-	4.6 - 890	0.57 - 1.08	-	-	-
Koelmans	2009	BC with HA	<150um	18, 28, 52, 72, 77, 101, 118, 126, 138, 156, 169	0.45 - 0.92	4 - 200	-	-	0.52 - 3.9	5.6 - 24.3	1.3 - 5.3
Jantunen	2010	Soot, coal	<50um	18, 28, 52, 72, 77, 101, 118, 126, 138, 156, 169	0.05 - 0.29	9.6 - 1300	0.16 - 19	0.5 - 0.92	0.12 - 360	0.5 - 26	0.9 - 7
Shao	2010	MWNT-g-CD	nano	15, 20	235 - 261	-	-	-	-	-	-
Shao	2011	MWNT-g-pMMA	nano	15	~240	~6	-	-	-	-	-
Amstaetter	2012	AC	<50um	101	-	-	5000 - 8100	1.11 - 1.22	-	-	-

The log(K_s) values gathered in Table 2.2 clearly show the superiority of AC over the other types of carbon and oil, with log(K_s) values on average 1.85 log-units higher. Of the three types of BC (charcoal, traffic soot and coal), charcoal proved to have the highest log(K_s) value and therefore the strongest sorption to PCBs. The charcoal log(K_s) values were on average 1.2 log-units higher than traffic soot and coal for PCB congeners with 3 and 4 chlorine substitutions, but only 0.7 log-units higher for PCB congeners with 5 and 6 chlorine substitutions. As the number of chlorine substitutions increase so does the congener hydrophobicity, indicating that the type of BC has less of an impact on sorption for more hydrophobic congeners.

Table 2.3 also demonstrates the superiority of AC to various types of BC. Caution must be taken when comparing the log(K_F) values between the two studies conducted with AC and those with BC because, as the colors indicate, the experiments with AC resulted in a lower equilibrium concentration, which naturally leads to higher sorption parameters. With this in mind, it is observed that the log(K_F) values for AC are orders of magnitude higher than those for BC. The only LAN model parameters available were for CNTs and BC materials. The Q_{max} value for MWNTs with methyl methacrylate (pMMA) and β-cyclodextrin (CD) are many orders of magnitude greater than the Q_{max} values for experiments using BC.

Unfortunately, there are many gaps in the data available in the literature. For example, few recent studies conducted with AC used the LAN model at environmentally relevant equilibrium concentrations. Additionally, only the studies using BC materials use the PDM model, making comparisons to other types of sorbent materials difficult. Not only is the data available concerning sorbent interaction with PCBs sparse, but the data that is available was conducted using different methods and different units to calculate the isotherm parameters, introducing difficulties when making comparisons. This study seeks to fill the data gap in such a way that the sorbent materials in question can be

accurately compared against each other. Additionally, this study goes beyond what has been published in the literature to date by introducing GE as a possible sorbent material and taking a closer look at CNT materials. The main goal is to provide a wealth of distribution coefficients and isotherm parameters for the five sorbents being tested, as well as determining which sorbent material is the most efficient in removing PCBs from aqueous solution.

Chapter 3: Materials and Methods

3.1 Materials

3.1.1 Chemicals and Lab Materials

The thirteen PCB congeners (listed in Table 2.1) were acquired from AccuStandard, New Haven, CT, with a declared purity of >99%. The PCBs came as a solution in either hexane or acetone, sealed in amber glass ampoules. The 11 analyte congeners were prepared as a cocktail by AccuStandard, while the two internal standard congeners were prepared individually. The organic solvents used in this research included: acetone (ACS standards, ≥99.9% purity; VWR, West Chester, PA), acetonitrile (HPLC grade, ≥99.8% purity; EMD, Philadelphia, PA), hexanes (HPLC grade, ≥99.9% purity; Fisher Scientific, Fair Lawns, NJ), methanol (ACS standards, ≥99.8 purity; VWR) and toluene (ACS standards, ≥99.97% purity; Fisher Scientific). Other chemicals included: sodium azide (≥99% purity; Alfa Aesar, Ward Hill, MA), anhydrous calcium chloride (≥90% purity; EM science, Gibbstown, NJ) for use in water, and anhydrous calcium chloride (≥98.6% purity; J.T. Baker, Phillipsburg, NJ) for use when drying organic solvents.

Solid-phase microextraction (SPME) fibers were manufactured at Poly Micro Industries with a glass fiber core, diameter of 1000µm, and a 35µm outer coating of Polydimethylsiloxane (PDMS), such that the overall outer diameter of the SPME fibers were 1070µm. Boston round amber glass bottles (narrow mouth) of volume 60 and 240ml were obtained from VWR international. Threaded septa caps with silicone/Polytetrafluoroethylene (PTFE) were used in combination with the glass bottles. Additionally, 2ml Agilent amber glass auto-sample vials were used with red septa caps and 250µl footed inserts.

3.1.2 Sorbents

Activated Carbon and Black Carbon

AquaSorb® BP2 activated carbon (AC) was selected based on its demonstrated sorptive capabilities discussed in Amstaetter et al. (2012) [47]. A sample of the AquaSorb® BP2 was obtained from Jacobi Carbons Inc., Columbus, OH. The AC is a bituminous coal based powder with declared moisture content of ≤8% and ash content ≤18%. Charcoal Green® Pure Biochar Mixed was obtained from buyactivatedcharcoal.com for use as the black carbon (BC) in this study. Charcoal Green® Pure Biochar Mixed contains a mixture of hardwoods (oak, maple, alder, white alder, black hawthorne, birch, cherry, black walnut and lilac) and was prepared using the pyrolysis method with no chemical additives or additional treatment. Ten pounds of the Charcoal Green® Pure Biochar Mixed were obtained, with the contents ranging from fine powder to large chucks. The hardwood charcoal was chosen to closely resemble the charcoal used in Jonker and Koelmans (2002) [4], which was reported to have the highest distribution coefficient for PCBs compared to the five other black carbon materials they tested. Because of the similarities in BC materials between the Jonker and Koelmans and the present study, the specific surface area (SSA) reported in the Jonker and Koelmans study was used. Table 3.1 lists the SSA values used for the AC, BC, CNT, CNT-OH and GE as well as the source material and method of production. As shown in Table 3.1, SSA values range from 150 - 1150m^2/g, with AC having the highest and BC having the lowest.

To properly compare the AC and BC sorbents, similar particle size distributions were obtained from the selected materials by weighing sieve fractions. To create an approximate particle distribution, the AC and BC sorbents were sorted using a #100, 140, and 230 sieve, resulting in the diameter bins of 150-100µm:100-60µm:<60µm. The

weight fractions of AC and BC for each of the size bins were 0.59:0.29:0.12 and 0.62:0.28:0.10, respectively. Once AC and BC were screened for size, they were washed in aqueous solution containing 0.01M of calcium chloride and 25mg/L of sodium azide to remove any soluble ash or other impurities. The washing consisted of placing the AC and BC sorbents into high strength glass centrifuge tubes in aqueous solution and mixing end over end for 24 hours. The tubes containing AC and BC were then centrifuged in a Labnet centrifuge (HERMLE Labortechnik) for 20mins at 3000g and 120mins at 3600g, respectively, after which the supernatant was then discarded. The centrifuge tubes were again filled with fresh aqueous solution and the process repeated a total of three times, by which time the supernatant was visually clear. The AC and BC sorbents were then placed into separate clean metal plates and dried in an oven at 80°C until constant mass was achieved; the sorbents were subsequently dried at 105°C for one hour. Once dry, the AC and BC sorbents were gently ground with a pestle and mortar to undo any clumping that occurred during the drying phase and were passed through a #100 sieve. This method of washing was similar to that used by Jonker and Koelmans (2002) [4].

Particle size distribution analysis was conducted on the AC and BC sorbents using a Mastersizer 2000 (Malvern Instruments, Worcestershire, England). Prior to measurement, a batch of each sorbent was prepared at a concentration of 1g/L in aqueous solution with 0.01M of calcium chloride and 0.25mg/L of sodium azide. The batches were horizontally shaken at 100rpm for 24 hours to simulate the conditions in the isotherm batch reactors. After 24 hours of shaking, the aqueous solution containing the sorbent materials was fed into the small volume dispersion unit and the particle size distributions were measured. Each sorbent material was run three times and the resulting distributions were averaged.

Further analysis was conducted on the AC and BC sorbents using a 6010LA scanning electron microscope (SEM) (JOEL, Peabody, MA). Dry powder samples of each material were spread on top of an adhesive carbon conductive tape to provide a secure layer of the sorbent material. Images of the AC and BC were taken along with energy dispersive spectroscopy (EDS) elemental analysis. The EDS analysis was completed under high vacuum with a voltage of 15kV and approximately 1000 counts per second (cps).

Graphene and Carbon Nanotubes

The graphene (GE), carbon nanotubes (CNT) and carbon nanotubes with hydroxyl functional groups (CNT-OH) were obtained from Cheap Tubes Inc., Brattleboro, VT. HDPlas Graphene NanoPlatelets, research grade (grade 4), were used as provided by the supplier. The GE was synthesized by the supplier using a split plasma process with argon as the plasma process gas and natural graphite as the source material. The resulting GE contained less than 3 layers of graphene sheets with an average thickness of <3nms. The lateral dimensions of each platelet are in the range of 1-2µm, with the reported specific surface area (SSA) of >750m^2/g (Table 3.1) and purity of >99% by weight.

Short multi-walled carbon nanotubes were used as provided by the supplier for both the CNT and CNT-OH sorbents. The CNT and CNT-OH were synthesized using a catalytic chemical vapor deposition (CCVD) method, purified, and shortened using an extrusion process. The resulting CNT and CNT-OH sorbents had an outer diameter <8nm and lengths in the range of 0.5 – 2.0 µm. The reported SSA was >500m^2/g (Table 3.1), with the ash content <1.5% and nanotube purity >95% by weight. The CNT-OH was functionalized with hydroxyl groups to 5 – 7% by weight.

Further analysis was conducted on the GE, CNT and CNT-OH sorbents using a 6010LA scanning electron microscope (SEM) (JOEL, Peabody, MA). The sorbent materials were prepared, imaged and analyzed in the same manner as the AC and BC described above. Additionally, particle size distribution of the GE, CNT and CNT-OH sorbents were measured as described above.

Table 3.1: Summary of the specifications for the five sorbent materials used.

Sorbent	Source Material	Poduction Method	Approximate SSA (m^2/g)
AC	Coal	Steam Activation	1150[a]
BC	Hardwood	pyrolysis	150[b]
CNT	n/a	CCVD	500[c]
CNT-OH	n/a	CCVD	500[c]
GE	graphite	Split Plasma	700[c]

3.2 Sorption Isotherm Development

3.2.1 Experimental Design

Batch Reactor Setup

Isotherm experiments were conducted in 240ml Boston amber glass bottles with the exception of the AC isotherms, which were conducted in 60ml Boston amber glass bottles. The 60ml batch size was selected for the AC isotherms to ensure that adequate detection of PCBs on the 2cm SPME fibers would be achieved. The bottles, which were used as batch reactors, were capped with a threaded cap and silicone/PTFE septa to minimize the loss of analyte due to volatilization. The glass bottles, and all other glassware used during experimentation, were cleaned before and after use with the method recommended in EPA Method 8082A for cleaning PCB contaminated glassware [111].

The sorbent materials were added to the clean batch reactors followed by the aqueous solution to encourage initial mixing of the sorbent in the aqueous solution. The BC, CNT, CNT-OH and GE sorbents were measured on a Mettler Toledo Classic electric scale (AB304-S) to ±0.1mg accuracy and transferred to the batch reactors using aluminum foil. AC could not be measured on the scale due to the small mass used in each batch; instead, a stock solution was made with AC concentration of 0.1mg/ml and the batch reactors loaded by pipetting 0.5ml from the stock solution into the batch reactors. Although the AC was suspended in the stock solution, therefore equal dispersion was not assumed, preliminary tests showed that with thorough mixing of the stock solution during pipetting, consistent masses of AC could be transferred.

With the sorbent material loaded, each reactor was filled with either 220 or 50ml of Millipore water, leaving 20 or 10ml of headspace, respectively. Table 3.2 depicts the specific amounts of sorbent materials and aqueous solution used for the isotherm experiments. The mass of sorbent added to the batch systems were determined by the strength of the sorbent, the stronger the sorbent the lower the mass added to the batch system so that there would be detectable levels of PCBs remaining in the SPME fiber phase. The Millipore water used was from a MODULAB Water System when operating at ≥18MΩ-cm, with calcium chloride added to 0.01M so that the water had a realistic ionic strength, and sodium azide added to 25mg/L as a biocide. After the sorbent and water, a specific length of SPME fiber was added to each batch reactor for the purpose of measuring the equilibrium analyte concentrations. The SPME fibers were cut to a length of either 1 or 2cm and cleaned using sequential washing of hexane, acetonitrile and aqueous solution as reported in Lu et al. (2011) [112]. The success of the fiber cleaning method was confirmed by measurement using gas chromatography–mass spectrometry (GC-MS) as described in the following section.

Table 3.2: Summary of the experimental design for the isotherm experiments.

Sorbent	Aqueous Volume (ml)	Length of Fiber (cm)	Sorben Conc. (mg/L)	PCB Mix Conc. (µg/L)
AC	50	2	1	0.5 - 50
BC	220	1	200	0.5 - 50
CNT	220	2	50	0.5 - 50
CNT-OH	220	2	100	0.5 - 50
GE	220	2	25	0.5 - 50

Once the batch reactors were loaded with the three phases: aqueous, sorbent and SPME fiber, the cocktail of 11 PCB congeners, in acetone, was injected using a gas-tight micro syringe to create six different initial PCB concentrations for the isotherm experiments (0.5, 1, 3, 10, 25 and 50µg/L). The stock PCB congener cocktail was spiked in volumes ranging from 25 - 100µl for the 50ml AC batch reactors and 30 - 220µl for all other sorbent materials. These injection volumes resulted in acetone:water ratios at least five times lower than the 1% (v/v) limit suggested by Schwarzenbach et al. (2003) to avoid cosolvency interference [71]. Immediately after the PCB cocktail was added, the batch reactors were capped tightly and gently swirled to encourage the PCB congeners that were at concentrations above their aqueous saturation limits to contact the sorbent materials and SPME fiber.

The specific designs of each of the different sorbent isotherms were constructed to optimize the amount of PCBs partitioning onto the SPME fibers while minimizing the PCB concentrations used. SPME materials in general are designed to act similar to a probe, which measures the amount of a substance *in situ* but does not significantly alter the environment in which it is measuring. Within a batch reactor, there is a fixed mass of PCBs which can partition between the three phases. To preserve the environment under investigation, sorbent-water partitioning, the SPME phase was not to remove a significant proportion of the total PCBs within the system. It was under this constraint that the mass of sorbent and length of SPME fiber were chosen for each isotherm set,

ideally resulting in detectable quantities of PCBs partitioned to the SPME fiber but not more that 5% of the total mass of PCBs in the system.

In addition to the batch reactors spiked with PCBs, two controls without PCBs were prepared: one with the sorbent material and the SPME fiber in the aqueous solution and the other with just the SPME fiber in the aqueous solution. All samples, including the controls, were prepared in triplicate. Once an isotherm set, consisting of 24 batch reactors, was assembled, the set was securely placed in an Innova 44r (New Brunswick Scientific Co.) incubator shaker with a temperature of 20°C (±0.5) and horizontal gyration of 100rpm. To allow adequate time for equilibrium to be established, the samples were shaken for 28 days. Although the equilibrium times between the sorbents and aqueous phases are commonly reported around hours and days, the equilibrium time between the SPME fiber and the aqueous phases is on the order of weeks. Allowing 28 days (4 weeks) for equilibrium in this research was based on previous studies [39, 112]. Additionally, preliminary experiments of similar design were run for 21, 28 and 35 days, with no significant difference in PCBs measured on the SPME fibers between the three run lengths, indicating that 28 days was a conservative run length that ensured that equilibrium was reached.

SPME Fiber Extraction and PCB analysis

After 28 days of shaking, the samples were taken off of the shaker and the SPME fibers were retrieved by pouring the aqueous solution through a mesh screen. Each SPME fiber was wiped with a damp Kimwipe until visually clean of any sorbent material. The SPME fibers were then placed into a 250µl footed insert contained in a 2ml auto-sample vial. The 1 and 2cm SPME fibers were submerged in 150µl or 250µl of hexane, respectively, prepared with the internal standard, PCB-101, at the concentration of 100µg/L. To ensure maximum extraction of PCBs from the SPME fibers by the

hexane, the SPME fibers were left in the footed insert, which did not result in any interference with the automated injector needle. Once the fibers were submerged in the auto-sample vials, they were tightly capped and place in the freezer (-18°C) for storage.

A gas chromatography – mass spectrometer (GC-MS) (Agilent Technologies, 6890N GC with 5973 MSD) was used to measure the concentration of PCBs extracted off of the SPME fibers. The GC-MS was calibrated using a five point linear calibration curve with inverse concentration weighting, resulting in r^2 values >0.993. Ultra high purity helium gas was used as the carrier within an Agilent HP-5 capillary column (length=60m, inner diameter=0.250mm, film coating=0.25µm). To analyze the samples, they were first removed from storage (storage time <7days), allowed to reach room temperature, and lightly agitated to encourage equal PCB dispersion. An automated sequence was programed to run each isotherm set, with a continuing calibration verification (CCV) sample run at least every 10 samples. Additionally, two sample duplicates, one at the beginning and one at the end of the sample set, were conducted. After the septa were punctured by the injector needle, the caps were replaced in order to minimize solvent loss, and the entire isotherm set was placed back in the freezer for storage.

Using the calibration curve described above, a quantitation method was established to systematically determine the concentration of the 11 analyte PCB congeners from the generated ion spectrograph. A substantial difference in the amount of internal standard in the calibration samples compared to the analyte samples was found, which caused a bias in the generated analyte concentrations. To correct for the bias, the internal standard responses for the five calibration samples were manually adjusted so that they had the same median value as the distribution of internal standard responses in each isotherm set. By making this adjustment, any unnecessary concentration adjustments due to internal standard responses were minimized. Table A.2 in Appendix A contains the values of the internal standard responses for the

calibration set and each isotherm set, along with the manual adjustments made for the quantitation method.

3.2.2 Theory

Solid Phase Microextraction Design Criteria

There are a variety of designs for batch isotherm experiments, the simplest being the use of only aqueous and sorbent phases and measuring the analyte concentrations in both of the two phases. This simple design was not sufficient for the present study for two main reasons. First, when using the two phase design, it is necessary to completely separate the aqueous and sorbent phases for analyte measurement. This proved difficult because of the nano-sized sorbents being used. Second, there was a limitation to the detection of the analyte such that higher concentrations of the analyte or larger volumes were required for adequate detection. The addition of a third phase complicates the experimental design, but it allows for analyte detection at lower, more realistic, equilibrium concentrations and removes the necessity to separate the aqueous and sorbent phases. The main difficulty of using SPME fibers was the risk of altering the PCB partitioning between the aqueous and sorbent phases compared to what it would be without the SPME fiber present. In other words, if the SPME fibers were to remove a significant mass of PCBs from the aqueous-sorbent subsystem, then the SPME would stop acting like a probe and becomes a true third phase. As mentioned previously, significant is defined in the present study as uptake of ≥5% of the total analyte mass by the SPME fibers.

When designing the experimental procedure for the present study, the results from a preliminary study were used to estimate the affinity of the SPME fibers and each sorbent material to PCBs. This information was used to adjust the mass of sorbent or

length of SPME fiber in order to maintain, as closely as possible, the partitioning of PCBs onto the SPME fibers to less than 5% of the total analyte mass. Table 3.2 summarizes the resulting experimental design criteria used to achieve this PCB fraction.

Calculating PCB Concentrations in the Sorbent and Aqueous Phase

In the experimental method described above, only the PCBs that partition to the SPME fiber were measured; therefore, it is important to consider the means by which the PCB quantities in the aqueous and sorbent phase were generated. To begin the process, a linear correlation equation developed by Lu et al. (2007) was used to calculate the SPME fiber – water partitioning coefficients ($K_{f\text{-}w}$) the octanol-water partitioning coefficient (K_{ow}) as the independent variable. Lu et al. used their own data as well as data from Mayer et al. (2000) [112, 113] to form the correlation. The correlation was generated through control experiments that measured the equilibrium concentrations of HOCs in the water and SPME phase. The equation derived by Lu et al. is as follows,

$$\log\left(K_{f-w}\right) = 1.06(\pm 0.058)\log(K_{ow}) - 1.16(\pm 0.35), \qquad 3.1$$

where K_{ow} is the octanol-water partitioning coefficient, and $K_{f\text{-}w}$ is the SPME fiber-water partitioning coefficient (L_{water}/L_{PDMS}) [112]. An r^2 value of 0.94 was achieved for the correlation between the K_{ow} and the $K_{f\text{-}w}$ with the ≈25 data points. The data points used spanned a log(K_{ow}) range from 4.5 – 7.5, which is the same log(K_{ow}) range of the 13 PCB congeners used in the present study. The K_{ow} values used to develop equation 3.1 were from Hawker and Connell (1988) [95], and are listed for the 13 PCB congeners in the present study in Table 2.1.

Using the known K_{ow} value, equation 3.1 was used to generate $K_{f\text{-}w}$. Qualitatively, the $K_{f\text{-}w}$ value represents the ratio between the concentration of PCBs on

the SPME fiber and the concentration of PCBs in the aqueous phase. Mathematically, this ratio can be represented as,

$$K_{f-w} = \frac{C_f}{C_e}, \quad 3.2$$

where C_f is the concentration of PCBs on the SPME fiber ($\mu g_{PCB}/L_{PDMS}$), and C_e is the equilibrium concentration of PCBs in the aqueous phase ($\mu g_{PCB}/L_{water}$). Once the K_{f-w} values were calculated from equation 3.1 and the C_f values were measured, the remaining unknown, C_e, could be determined using equation 3.2. Finally, with the concentration of PCBs known for the SPME fiber and aqueous phases, conservation of mass was assumed for the system such that the concentration of PCBs in the sorbent phase (q_e) was calculated. The conservation of mass for the batch systems were as follows:

$$M_{tot} = q_e(m_s) + C_f(V_f) + C_e(V_w), \quad 3.3$$

where M_{tot} is the total mass of each PCB congener in the system (µm), m_s is the mass of sorbent (kg), V_f is the volume of PDMS (L), and V_w is the volume of aqueous solution (L). C_e is the only unknown in equation 3.3 and can therefore be solved for each of the 11 analyte congeners. Table 3.3 outlines the parameter values used in equation 3.3.

Table 3.3: Summary of the parameter values used to solve equation 3.3 for each batch reactor and each PCB congener.

Sorbent	V_w (L)	V_f (L)	M_s (kg)	M_{tot} (µg)
AC	0.05	2.28E-06	5.00E-08	0.025 - 2.5
BC	0.22	1.14E-06	4.40E-05	0.11 - 11
CNT	0.22	2.28E-06	1.10E-05	0.11 - 11
CNT-OH	0.22	2.28E-06	2.20E-05	0.11 - 11
GE	0.22	2.28E-06	5.50E-06	0.11 - 11

Once the concentration values for all three phases were known (C_f, q_e, C_e), the resulting data was used to analyze the efficiency of each sorbent material to each of the 11 PCB congeners. One resulting measurement was the distribution coefficients (K_s) for

each sorbent material (equation 2.4). Additionally, isotherm plots were graphed by plotting C_e on the x-axis and q_e on the y-axis. Models for isotherm graphs were fit to the experimental data in order to gain better insights into the mechanisms and efficiency of the interaction between the sorbent and analyte. The isotherm modeling process is described below.

Isotherm Modeling

The Langmuir (LAN), Freundlich (FRE) and Polanyi-Dubinin-Manes (PDM) isotherm models were fit to the experimental data using both Microsoft Excel (2010) and IBM SPSS Statistics (v.21). In Excel, the Solver add-in was used to minimize the error function by changing the model parameters. In SPSS, the non-linear regression sequence was used to compute the model parameters along with standard error and confidence intervals. All of the model regressions were performed using the non-linearized equations of the isotherm models given in equations 2.1 – 2.3. In almost all cases, the parameters generate by excel matched those generated by SPSS; the disagreeing values only had slight differences between the generated parameters.

The two error functions used to minimize the model error were the sum of squared errors (SSE) and hybrid fractional error function (HYBRID). The SSE and HYBRID functions used were,

$$SSE = \sum_{i=1}^{n} (q_{e,model} - q_{e,meas})_i^2 \qquad 3.4$$

$$HYBRID = \frac{100}{c-p} \sum_{i=1}^{n} \frac{(q_{e,model} - q_{e,meas})^2}{q_{e,meas}}_i, \qquad 3.5$$

where $q_{e,model}$ are the values calculated by the isotherm model (µg/kg), $q_{e,meas}$ are the experimental values (µg/kg), c is the number of points being compared and p is the degrees of freedom. Regressions between the three models and the experimental data

were performed using both error functions and the resulting isotherm parameters were compared for precision.

3.3 Mass Balance Confirmation Measurements

Experiments were conducted to isolate the three phases (water, sorbent, SPME) and measure the concentrations of PCBs in each to confirm the conservation of mass assumption. The BC triplicate (C=50µg/L) was chosen for mass balance measurements because the BC material was easly to separated using a filter and had the highest sorbent mass, ideal for PCB detectability. To measure the PCBs in each phase, the contents of each batch reactor were vacuum filtered through a glass fiber filter (1µm pore size) such that the BC and SPME fiber were retained on the filter and the aqueous phase was collected in a clean glass container. The SPME fiber was wiped with a damp Kimwipe, removing only a small amount of the BC from the total mass, and submerged in hexane as described previously. The aqueous phase was sealed in glass containers and stored in a refrigerator (2°C). The BC retained on the filters were dried in an oven at 80°C until constant mass was achieved and then at 105°C for 1hr, after which the mass was measured on an electronic scale. A preliminary study was conducted to subtract the mass of the filters from the BC/filter system, by averaging the mass of five filters. In the preliminary study, the same volume of water was passed through the five filters and dried using the same regimen, resulting in five masses of which the average was taken for use in the mass balance experiment. Using the average mass of a dried filter, the mass of the BC retained on the paper was calculated using the equation,

$$m_s = m_{tot} - m_{filter}, \quad 3.6$$

where m_s is the mass of the sorbent (kg), m_{tot} is the mass of the filter and sorbent together (kg), and m_{filter} is the average mass of the preliminary filters (kg). Once the mass of BC was calculated for each of the triplicates, the samples were stored in the

refrigerator (2°C). In addition to the BC triplicates, a control of clean aqueous solution was filtered and processed in the same manner.

A liquid-to-liquid extraction method was used to extract the PCBs from the aqueous phase. Before extraction, PCB-152 was added to each sample (mass = 0.1µg) for use as an extraction standard. The sample aqueous phase, approximately 250ml, was poured into a 500ml separatory funnel along with 100ml of hexane. The sample was shaken and the two phases separated and collected. This process was repeated once more with 100ml of fresh hexane resulting in 200ml of total hexane used for PCB extraction. The hexane was dried using anhydrous calcium chloride powder, after which the calcium chloride powder was removed using a vacuum filter. The dry hexane was transferred into a clean spherical glass flask and completely evaporated using a Büchi Rotavapor (R-205), such that the PCBs were retained on the glass. One milliliter of fresh hexane was swirled around the spherical flask and then transferred into a 2ml auto-sample vial, after which the hexane was completely evaporated using nitrogen gas. This process was repeated a total of 3 times. Finally, 0.5ml of hexane, containing PCB-101 as an internal standard (C=100µg/L), was added to the auto-sample vials. The vials were then capped, vigorously shaken, and measured using the GC-MS procedure detailed previously.

A soxhlet extraction method was used to extract the PCBs from the BC sorbent phase. The dried filters containing the BC material were placed in custom soxhlet extractors and extracted with approximately 70ml of toluene. The extraction was allowed to cycle for 16hrs as described for charcoal in the research done by Jonker and Koelmans (2002a and 2002b) [4, 65]. Once the extraction was complete, the toluene was evaporated and PCBs transferred from the soxhlet glassware to the auto-sample vials and analyzed using the same method as that described for the liquid-to-liquid extraction.

Chapter 4: Results and Discussion

4.1 Sorbent Characterization

4.1.1 Scanning Electron Microscope (SEM) Analysis

Images of the five sorbent materials were taken with the SEM, with magnifications ranging from x450 to x4500. Figure 4.1 shows the resulting images of the sorbent materials. The AC particle in Figures 4.1a and b illustrates the heterogeneous and porous nature of the surface of AC. The extensive network of ridges and valleys produce the micro and mesopores that gives AC its large surface area and allows PCBs to sorb through surface interaction and physical containment. The BC particle in Figures 4.1c and d illustrates a much more homogeneous surface structure compared to AC, with an overall smooth surface and systematic 'wafer' like pores.

The CNT-OH in Figure 4.1e was aggregated together, yet the individual fibers that made up the aggregates were clearly seen. In contrast, the fibers of the non-functionalized CNT in Figure 4.1f, while also aggregated, were less clearly distinguished amongst the aggregate at the same magnification as CNT-OH. The GE material in Figure 4.1g was also aggregated, with each individual platelet forming what looks like scales on the larger aggregate. Figure 4.1g confirmed the approximate lateral dimensions of each GE platelet to be 2-3μm, as reported by the supplier. It should be noted that these images were taken before mixing in aqueous solution; therefore, the aggregate characteristics observed for the CNT, CNT-OH and GE materials were subject to change when submerged and mixed in water.

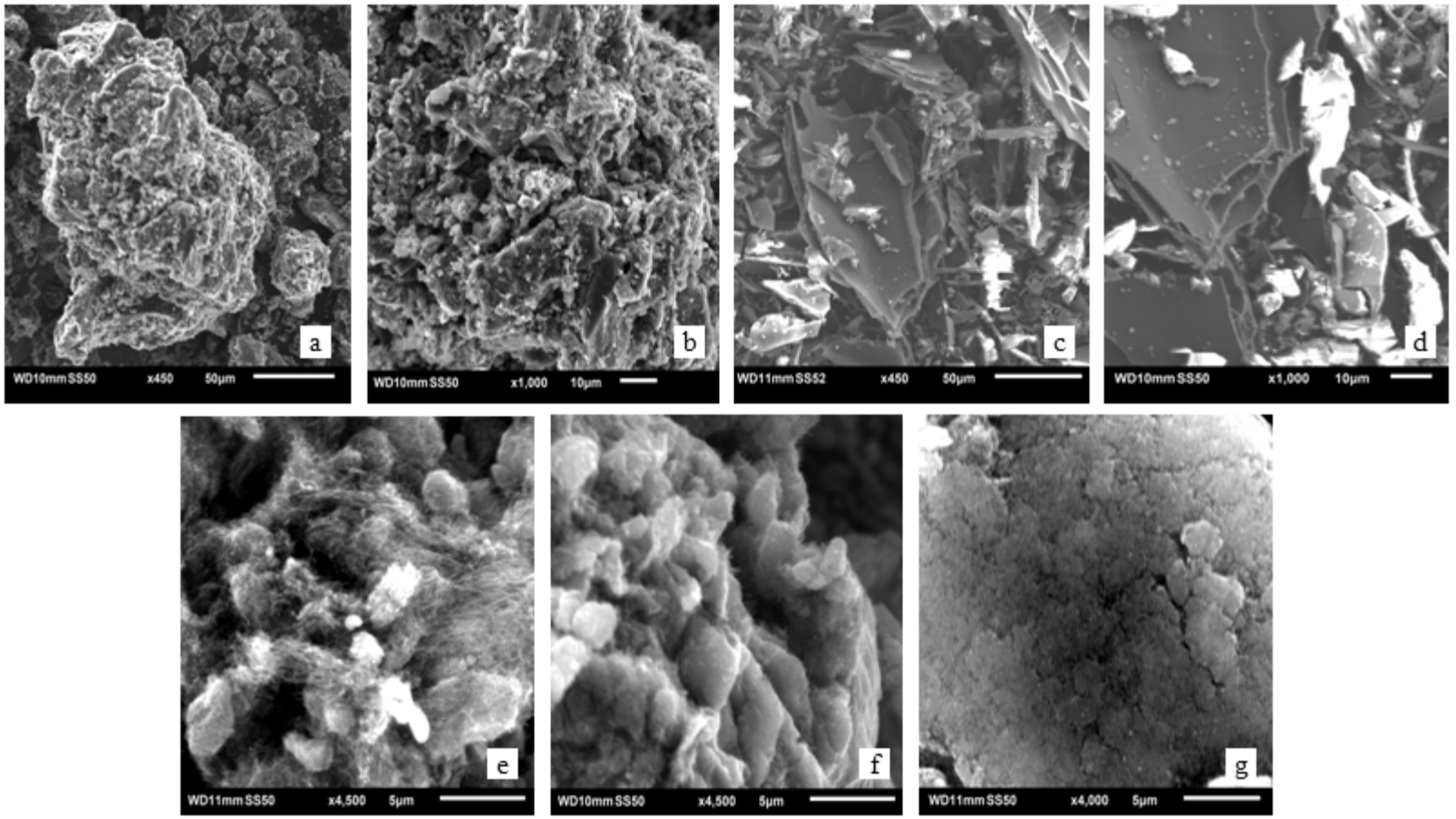

Figure 4.1: Scanning electron microscope images of a) full image of an activated carbon particle, b) zoomed in image of the same activated carbon particle, c) full image of a black carbon particle, d) zoomed in image of the same black carbon particle, e) carbon nanotubes functionalized with hydroxyl groups, f) non-functionalized carbon nanotubes and g) graphene.

In addition to images, energy dispersive spectroscopy (EDS) elemental analysis was conducted to determine the atomic makeup of the five sorbent materials. Table 4.1 summarizes the atomic mass fractions of the five sorbent materials. As expected, carbon consisted of the majority of the atomic structure in all five of the materials. BC had the lowest carbon content with 79.1% and the highest level of oxygen with 18.7%. The small amount of oxygen present in AC was most likely due to functional groups that are commonly reported in small amounts on the surface of AC. The trace amounts of metals and minerals such as aluminum and silicon are also commonly found in AC.

Only carbon atoms were detected on the CNT, compared to 7.6% mass of oxygen in the CNT-OH. The elemental comparison between the CNT and CNT-OH confirms that the CNT material used contained no oxygen functional groups, while the CNT-OH contained a significant amount of functional groups, meeting the quantity advertised by the supplier of 5 – 7% functionalization by weight. The GE material was predominately carbon, with only a trace amount of oxygen present. This small amount of oxygen, much like AC, was likely due to small amounts of oxygen functional groups that inevitably form on the edges of the GE sheets and can only be removed with additional treatment. The results of the EDS indicates that the five sorbent materials received from the suppliers met the desired requirements for the purpose of this study.

Table 4.1: Atomic mass fractions determined from the EDS elemental analysis.

AC	atom	C	:	O	:	Al	:	Si
	mass %	93.4		4.0		1.2		1.4
BC	atom	C	:	O	:	Ca		
	mass %	79.1		18.7		2.2		
CNT	atom	C						
	mass %	100						
CNT-OH	atom	C	:	O				
	mass %	92.4		7.6				
GE	atom	C	:	O				
	mass %	98.6		1.4				

4.1.2 Particle Size Distribution

Approximate size distributions of AC and BC were initially created through weighing sieve fractions. On the other hand, the CNTs and GE came from the supplier with specifications on the dimensions of the individual particles, but with no information concerning the aggregates that naturally form in the atmosphere and in aqueous solution. The individual CNT, CNT-OH, and GE particles were in the nanoscale size range, yet they readily flocculated due to their hydrophobic nature and formed aggregates of unknown sizes. Koelmans et al. (2009) concluded that the sorption strength of charcoal is to some extent dependent on particle size [109]; therefore, creating similar size distributions was important when comparing the five sorbent materials.

The data in Figure 4.2 shows that all five sorbent materials formed very similar size distributions when mixed in aqueous solution with 0.01M ionic strength. The AC and BC distribution curves were nearly identical, the only difference being a slightly higher quantity of larger particles in the BC sample compared to the AC sample. The CNT, CNT-OH and GE samples were not in the nanoscale size range, but instead formed aggregates with size distribution ranges that were very similar to the AC and BC sorbents. Aggregated GE formed the largest size distribution of the five materials due to its strong hydrophobic nature and stackable sheets.

Interestingly, the AC, BC and GE samples formed distinct 1-mode peaks with approximately the same distribution ranges (see Table 4.2 for percentile information). In contrast, both CNT samples exhibited distributions covering a wider range of particle sizes, with a plateau, or even a second mode, spanning over the diameters 20 – 110µm. This behavior could indicate that aggregates formed by the GE flakes stacking upon each other resulted in a more natural ‘particle like’ aggregate, while the fibrous CNT

materials formed more amorphous aggregates. The difference in aggregate characteristics formed by the GE and CNT materials could play an important role in their efficiency as a sorbent; however, the role of aggregate characteristics was not investigated closely in this study.

Table 4.2: Summary of the 10th, 50th and 90th percentile particle diameters for the five sorbent materials.

Sorbent Material	Particle Diameter Percentile (µm)		
	10th	50th	90th
AC	15	50	108
BC	17	54	141
CNT	10	39	166
CNT-OH	15	56	202
GE	26	92	217

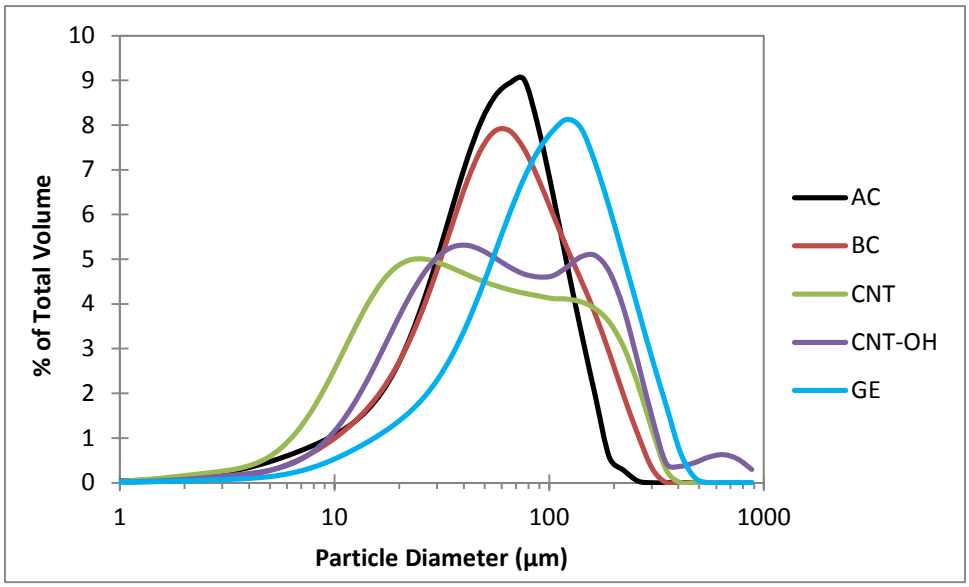

Figure 4.2: Particle size distribution curves for the five sorbent materials.

To optimize the surface area available for interaction with the analyte, the hydrophobic nanomaterials need to be chemically disperse when used in aqueous solution; however, by allowing CNT, CNT-OH and GE to aggregate, this study attempts to represent the natural environment in which the remediation of PCBs is needed. Overall, there is no statistical difference ($p > 0.05$) between the five particle-size

distributions, assuring that no bias is introduced due to differences between sorbent particle size distributions.

4.2 Sorbent-Water Distribution Coefficients

Sorbent-water distribution coefficients (K_s) are important numeric values that describe sorption affinity between a sorbent and analyte at a specific equilibrium concentration. Table 2.2 in Section 2.5 summarized published K_s values for AC, oils and various types of BC (soot, coal and charcoal), all reported at equilibrium concentrations in the ng/L range. Only the batches with aqueous equilibrium concentrations in the 0.5 – 50ng/L range were used to compare the K_s values measured in this study with those published in the literature. In other words, the K_s values for each sorbent-congener combination were measured only for the samples that resulted in aqueous equilibrium concentrations in the above range. Equation 2.4 was used to calculate K_s, resulting in a value that represents the ratio of PCBs in the sorbent phase compared to the aqueous phase. Averages of at least three K_s values for each congener-sorbent combination were calculated and are detailed in Table 4.3. Figure 4.3 graphically illustrates the resulting K_s values.

Table 4.3: Log transformed K_s values [log(K_s)] measured for each sorbent material with each of the 11 PCB congeners at ng/L equilibrium concentration levels. The ± values indicate the standard deviation from the average, * indicates that the K_s value measured used results for aqueous equilibrium concentrations slightly higher than the 50ng/L maximum and # indicates K_s values measured for aqueous equilibrium concentration slightly lower than the 0.5ng/L minimum specified.

Congener	K_s ($L_{water}/kg_{sorbent}$)				
	AC	BC	CNT	CNT-OH	GE
PCB-1	7.39 ± 0.13	4.75 ± 0.03	5.52 ± 0.11	4.90 ± 0.05	5.92 ± 0.05
PCB-2	7.94 ± 0.14	5.40 ± 0.17	5.97 ± 0.22	5.61 ± 0.22	6.26 ± 0.24
PCB-4	7.33 ± 0.13	4.30 ± 0.05*	4.85 ± 0.07*	4.09 ± 0.06*	5.48 ± 0.05
PCB-8	7.80 ± 0.20	5.29 ± 0.06	6.33 ± 0.07	5.68 ± 0.10	6.68 ± 0.09
PCB-15	8.47 ± 0.25	6.01 ± 0.10	7.24 ± 0.12	6.85 ± 0.10	7.42 ± 0.07
PCB-52	7.80 ± 0.09	5.28 ± 0.08	6.55 ± 0.13	5.88 ± 0.14	7.13 ± 0.14
PCB-72	8.40 ± 0.18	5.88 ± 0.10	7.38 ± 0.22	6.69 ± 0.22	7.68 ± 0.21
PCB-77	9.05 ± 0.37	6.46 ± 0.13	8.30 ± 0.10	7.84 ± 0.19	8.25 ± 0.18
PCB-138	8.69 ± 0.23	6.40 ± 0.08	7.70 ± 0.15	7.09 ± 0.13	8.07 ± 0.17
PCB-156	9.14 ± 0.31	6.99 ± 0.06	8.49 ± 0.11	7.83 ± 0.15	8.52 ± 0.40
PCB-169	9.82 ± 0.23	7.54 ± 0.10	9.61 ± 0.11#	9.17 ± 0.29#	8.80 ± 0.47

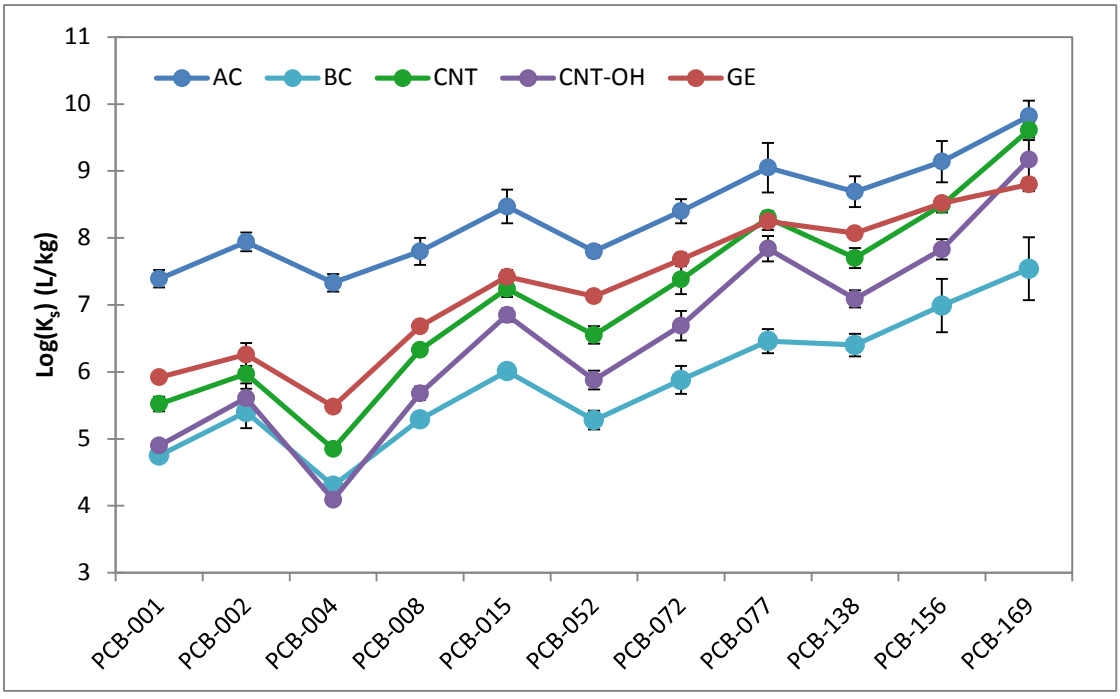

Figure 4.3: Line graph of log(K_s) values for each of the 11 PCB congeners and five sorbent materials. Each dot represents the average measured log(K_s) value for that congener-sorbent combination.

4.2.1 Comparison between Sorbent Materials

Figure 4.3 clearly illustrates that AC has larger K_s values compared to the other four materials. That superiority is most dramatic for the smallest PCB congeners and declines with increasing congener chlorination. Based solely on observation, it appears that GE has the second highest K_s values, with CNT, CNT-OH and BC having sequentially smaller K_s values. Numerically, the average of the differences in log(K_s) values between the sorbents for each 11 congeners shows that AC is 2.5, 1.8, 1.3, and 1.1 log units greater than BC, CNT-OH, CNT and GE, respectively. The difference between AC and the three nanomaterials decreases as the congeners increase but remains the same for BC. The differences between AC and the other four sorbents for PCB-1 are 2.6, 2.5, 1.9 and 1.5 log units for BC, CNT-OH, CNT and GE, respectively. Comparatively, the differences between AC and the four sorbents for PCB-169 are 2.3, 0.7, 0.2 and 1.0 log units for BC, CNT-OH, CNT and GE, respectively. At the higher chlorinated PCB congeners, the CNT materials begin to have higher log(K_s) values than GE and approach those of AC.

Statistically, the AC log(K_s) values were greater than ($p < 0.05$) the four sorbents for all 11 congeners with the exception of CNT for PCB-169, for which there was no statistically significant difference. GE was statistically greater than ($p < 0.05$) CNT, CNT-OH and BC for all congeners except PCB-77, 156 and 169, for which either no statistical difference between GE and CNT was found or CNT was significantly greater than GE. CNT is statistically greater than ($p < 0.05$) CNT-OH and BC for all PCB congeners. CNT-OH is statistically greater than ($p < 0.05$) BC for all congeners except PCB-1, for which there was no statistical difference, and PCB-4, for which BC was statistically greater than CNT-OH. Table 4.4 summarizes the statistical rankings based on log(K_s) values for

the five sorbents. Overall, AC has strongest sorption to the 11 PCBs followed sequentially by GE, CNT, CNT-OH and BC.

Table 4.4: Statistical rankings of the five sorbent materials determined by K_s values. K_s distributions statistically greater (95% confidence) are indicated by > and no statistical difference in K_s distributions by =.

Congener	Sorbent K_s Rank								
	1		2		3		4		5
PCB-1	AC	>	GE	>	CNT	>	CNT-OH	=	BC
PCB-2	AC	>	GE	>	CNT	>	CNT-OH	>	BC
PCB-4	AC	>	GE	>	CNT	>	BC	>	CNT-OH
PCB-8	AC	>	GE	>	CNT	>	CNT-OH	>	BC
PCB-15	AC	>	GE	>	CNT	>	CNT-OH	>	BC
PCB-52	AC	>	GE	>	CNT	>	CNT-OH	>	BC
PCB-72	AC	>	GE	>	CNT	>	CNT-OH	>	BC
PCB-77	AC	>	GE	=	CNT	>	CNT-OH	>	BC
PCB-138	AC	>	GE	>	CNT	>	CNT-OH	>	BC
PCB-156	AC	>	GE	=	CNT	>	CNT-OH	>	BC
PCB-169	AC	=	CNT	>	GE	>	CNT-OH	>	BC

4.2.2 Planarity Effect

In addition to using the log(K_s) values for sorbent comparison, Table 4.3 and Figure 4.3 present distinct characteristics concerning PCB planarity that are important to understand. The main factor for increasing sorption of a PCB congener is the hydrophobicity of the congener, often associated with the K_{ow} value. The log(K_{ow}) values of the 11 PCB congeners, given in Table 2.1, increase linearly with each congener and do not show any clear or systematic differences for changing ortho arrangements. If the strength of sorption is only based on the hydrophobicity of each congener, the resulting experimental log(K_s) values would follow a similarly smooth linear curve to that of the log(K_{ow}) values. However, as observed in Figure 4.3, the log(K_s) numbers generated in these experiments were generally sloped linearly upward, but followed a stair step pattern instead of a smooth curve. This deviation from the smooth linear curve was

caused by the planarity effect. For example, each of the five sorbents have decreasing log(K_s) values for PCBs 4, 52 and 138 compared to the less hydrophobic congeners immediately before them. This reduction in log(K_s) occurs because PCBs 4, 52 and 138 all have 2 chlorines in their ortho positions compared to the congeners that are immediately before them in the list, which are all non-ortho congeners. Assuming that hydrophobicity and planarity are the only two factors causing sorption, to determine the extent of the planarity effect the data must be normalized by hydrophobicity.

The slope of the log(K_s) values plotted for each sorbent over all 11 congeners were similar to that of the log(K_{ow}), with a -6% difference between the average of the five sorbent slopes to that of log(K_{ow}). This result indicates that when considering all 11 congeners together, consisting of a mix of planar and non-planar PCBs, the five sorbent materials closely resemble sorption due to hydrophobicity.

To look at the planarity effect more closely, the slopes of the log(K_s) values for the three congeners in the homolog groups 2, 4 and 6 were compared with the slope of the log(K_{ow}) values for those same congeners. The ortho-positioning of each of the three homolog groups were arranged in the following order: the first congener with the lowest log(K_{ow}) was di-ortho, the second congener was mono-ortho, and the third congener with the highest log(K_{ow}) was non-ortho. Theoretically, if increasing planarity had no effect on sorption, the slope of the measured log(K_s) would be the same as the log(K_{ow}), just as in the case where all 11 congeners were considered. But if increasing planarity causes increasing sorption, then the slope of the measured data would be greater than that of log(K_s).

The results of this analysis showed that the average slopes of the five sorbent materials are 64, 62 and 51% greater than the slopes of the log(K_{ow}) values for homolog groups 2, 4 and 6, respectively. The specific numbers are arbitrary, and simply demonstrate that planar congeners experience greater sorption than can be described

by hydrophobicity alone. However, because the homolog group with 6 chlorines had less of a positive difference than groups with 2 and 4 chlorines, it appears that the planarity effect reduceed with increasing hydrophobicity. As the congeners increase in chlorination and become more and more hydrophobic, the strength of the hydrophobic forces dampers any affect caused by molecular shape. Koelmans et al. (2009) additionally hypothesized that the increase in molecular size of more chlorinated congeners could be the cause of the dampened planarity effect [109].

4.2.3 Evaluation of Sorption Site Availability

By looking at Figure 4.3 carefully, it was apparent that the log(K_s) values for AC and BC as well as CNT and CNT-OH closely mirrored each other. To view this trend in more detail, Figure 4.4 was duplicated from Figure 4.3 with the exclusion of GE. CNT and CNT-OH were the exact same material, the only difference being that CNT-OH contained approximately 7.5% (wt.) hydroxyl (-OH) surface functional groups. Prior to this study, there has been disagreements concerning the effect of oxygen functional groups on the surface of sorbent materials. Gotovac et al. (2007) reported that acid functionalization of SWNT improved the adsorption of phenanthrene in toluene solution [83]. Other studies investigating the sorption of organic chemicals onto CNT found that the sorbates prefer to sorb to the surface of the CNT rather than functional groups [82], or that the presence of oxygen functional groups had little to no effect on overall sorption [80]. Many researchers have concluded that π-π bonding between the aromatic phenyl rings of PCB molecules and the CNT surface is the primary mechanisms for sorption, yet there exists little evidence that PCB molecules form any chemical bonds with oxygen functional groups.

In the present study, Figure 4.4 shows that the log(K_s) values for CNT-OH were slightly less than CNT for all 11 congeners, evidence that the presence of oxygen

functional groups impedes the sorption of PCBs in aqueous solution. Numerically, the log(K_s) values for CNT-OH correlate almost perfectly with those of CNT (R^2=0.993), but are reduced by an average of 0.57 (±0.14) for all 11 congeners. The correlation proves that the two CNT materials act very similar to each other, making the presence of hydroxyl groups the only cause for reduction in log(K_s). Because the PCBs were able to sorb with the carbon surface of CNT, the oxygen functional groups that were attached to the surface of CNTs were simply blocking potential sorption sites and reducing the sorption capacity. It is important to note that a neutral pH was used for the present study, such that some of the hydroxyl groups were potentially deprotonated, resulting in a negatively charged oxygen group remaining. If the pH was substantially reduced, the hydroxyl groups would protonate, which could lead to a different result when interacting with PCBs. Although hydroxyl groups impeded sorption at neutral pH, not all functional groups reduce sorption. Research conducted by Shao et al. added functional groups known to sorb well with PCBs to the surface of CNTs, with the net effect of increasing the number of sites and strength of PCB sorption to the CNT material [85, 86].

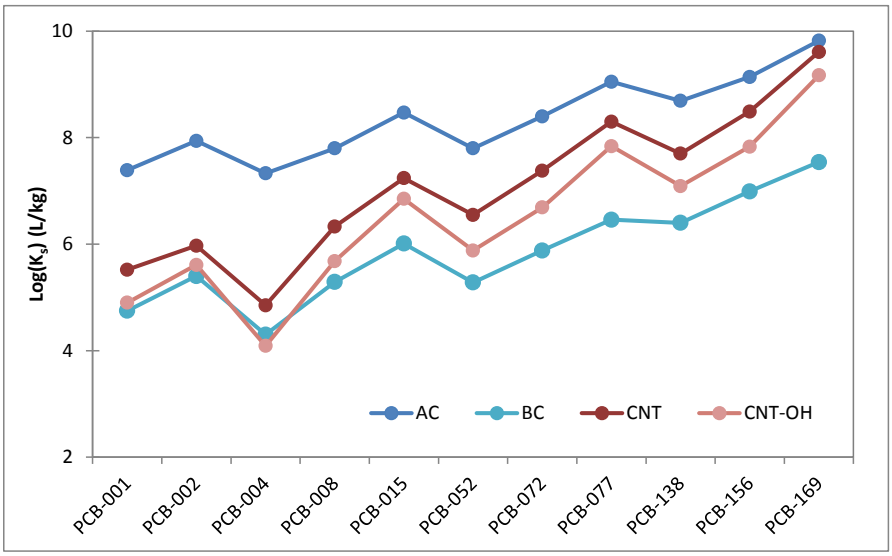

Figure 4.4: Line graph of log(K_s) values for each of the 11 PCB congeners and AC, BC, CNT and CNT-OH. The red colors illustrate the difference in sorption between CNT and CNT-OH due to functionalization, and the blue colors illustration the difference in BC and AC due to surface structure.

AC and BC were more different by nature than the two CNT materials: AC was made from a coal stock whereas the BC was made from hardwood. Despite this difference, both had a carbon rich source and were prepared by heating to high temperatures in the absence of oxygen. In addition to the difference in source material, the main difference between AC and BC was that AC was steam activated, causing a more porous structure and therefore a higher surface area. Interestingly, the graphed $\log(K_s)$ values of AC and BC for the 11 congeners closely mirror each other. The $\log(K_s)$ values for BC correlate well with AC (R^2=0.973), but are on average 2.50 (±0.23) less. The sorption mechanisms are more complex for AC and BC due to their heterogeneous surfaces, yet the correlation indicates that the reduction of sorption in BC is due to its smaller surface area and therefore less available sites for PCB sorption. While surface area plays a strong role in determining sorption capacities, other factors, such as oxygen functional groups as discussed previously, also affect how PCBs sorb to a material.

4.2.4 Comparison to Values in the Literature

The present study was modeled after similar studies conducted by various researchers for the sorption of PCBs to carbonaceous materials, making it a valuable endeavor to compare the current results with those published in the literature. The importance of comparison was twofold: first as a gauge of replicability, if similar research was conducted then similar results should occur, and second to determine the sorption capabilities of the new nanomaterials relative to the traditional materials that have already been established. Tables 2.2 and 2.3 in Section 2.5 summarized the $\log(K_s)$ values measured for the sorption of activated carbon, charcoal, coal, traffic soot and a mixture of hydrocarbon oils. Figure 4.5 compares carbonaceous materials from the literature to those used in the present study.

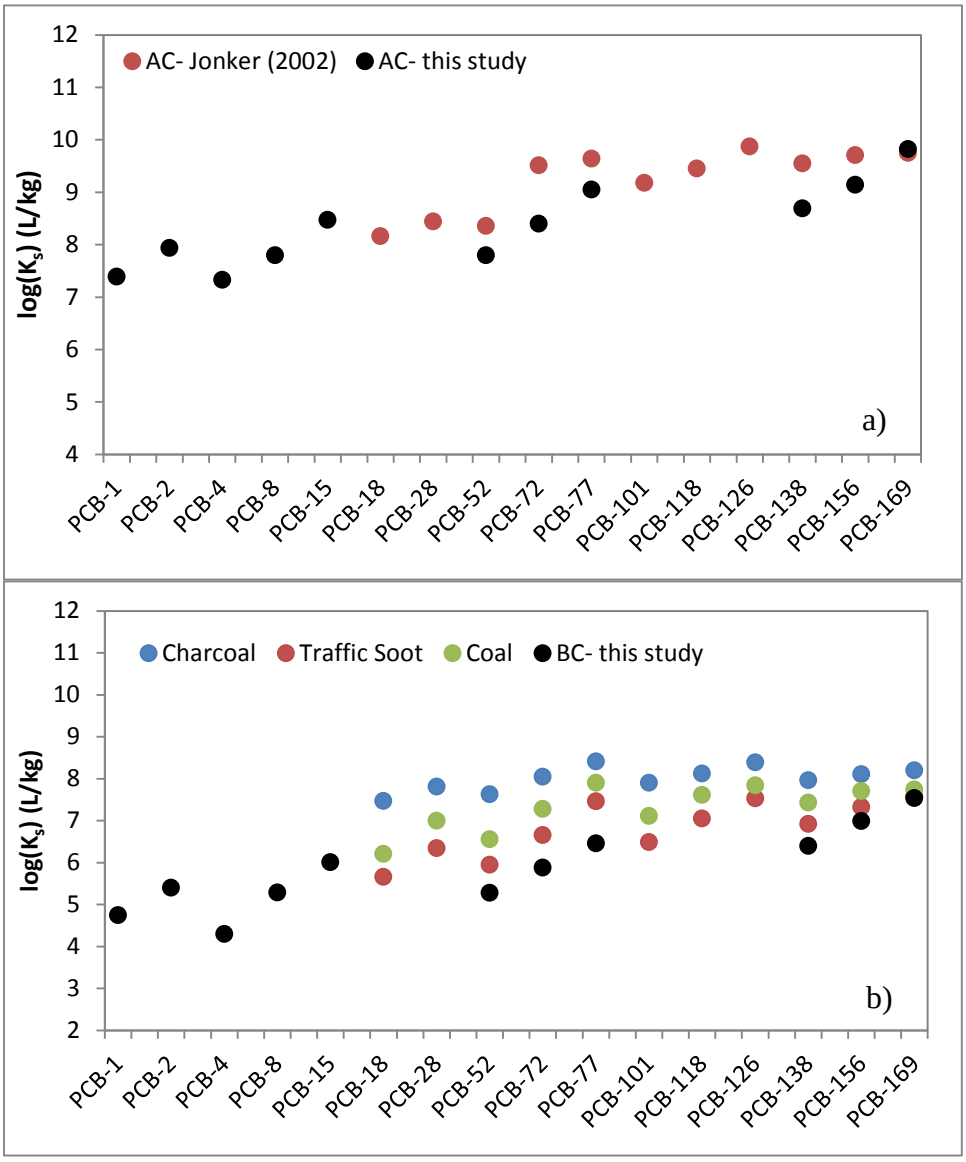

Figure 4.5: Comparison of log(K_s) values from the literature for a) activated carbon and b) three types of black carbon materials. The activated carbon and charcoal values were reported in Jonker and Koelmans [4]. The traffic soot and coal values were reported in Jantunen et al. [5].

Six congeners were collectively used by all studies: PCB-52, 72, 77, 138, 156 and 169. The log(K_s) values for the AC in the present study were slightly lower than those reported in Jonker and Koelmans (2002) [4]. The average difference in log(K_s) between the six congeners used in both studies was 0.60 (±0.39). The trend in log(K_s) values between PCB-52, 72 and 77 were similar between the two studies, however,

there was a noticeable difference between PCB-138, 156 and 169. For the three largest congeners, the log(K_s) values of the present study increased at a greater value from one congener to the next than those in the literature. Figure 4.5b depicts a significant difference between the BC materials found in the literature and the material used in the present study. The BC for this study was intended to be similar to the charcoal (blue dots) in Jonker and Koelmans (2002) [4], yet there was an average of 1.64 (±0.65) difference between the log(K_s) values of the six similar congeners.

There are a few reasons why this difference might have occurred. First, the charcoal prepared by Jonker and Koelmans was from tree bark, while the BC in the present study was prepared from the wood portion of the tree. This slight difference in source material could yield a significant structural difference and therefore cause differences in the number of available sites for PCB interaction. Additionally, the BC material in the present study was collected by sieving the powder from the large chucks instead of grounding the chunks into the appropriate particle sizes. Subsequent to conducting this research, the author learned that the powder material that comes off the larger chunks are mostly broken pieces of the larger chunks and are not consistent with the porous nature true of the larger pieces. This error in methodology could contribute to the reduced log(K_s) values in the present study. Lastly, the particle size of the materials in the present study (<150µm) are larger than the activated carbon and charcoal materials in the Jonker and Koelmans study (<50µm). As previously mentioned, smaller particles of the same material can lead to naturally higher sorption [109]. With these considerations, it is important to take into account the above comparison between sorption strengths of the five sorbent materials. The present study concluded that BC was the weakest sorbent, yet this conclusion may only be applicable for the specific BC used for these experiments.

To gain a more complete understanding of the capability of CNT and GE to act as sorbent materials for PCBs, it was important to compare their experimental data not only with the data gathered in the present study, but with any similar data available. Figure 4.6 compares the log(K_s) values for CNT and GE to activated carbon and various forms of black carbon for the six shared PCB congeners. For PCB-52, 72 and 77, the CNT and GE log(K_s) values were contained within the same spectrum of the three types of BC: charcoal, traffic soot and coal. For the more chlorinated and hydrophobic PCBs: 138, 156 and 169, the CNT and GE log(K_s) values were greater than the spectrum of log(K_s) values for the three BC materials. While the GE and CNT materials performed as superior sorbents to BC in the present study, based on comparison to additional published results, it cannot be concluded that GE and CNT are superior sorbents to all types of naturally occurring BC materials for the full spectrum of PCB congeners.

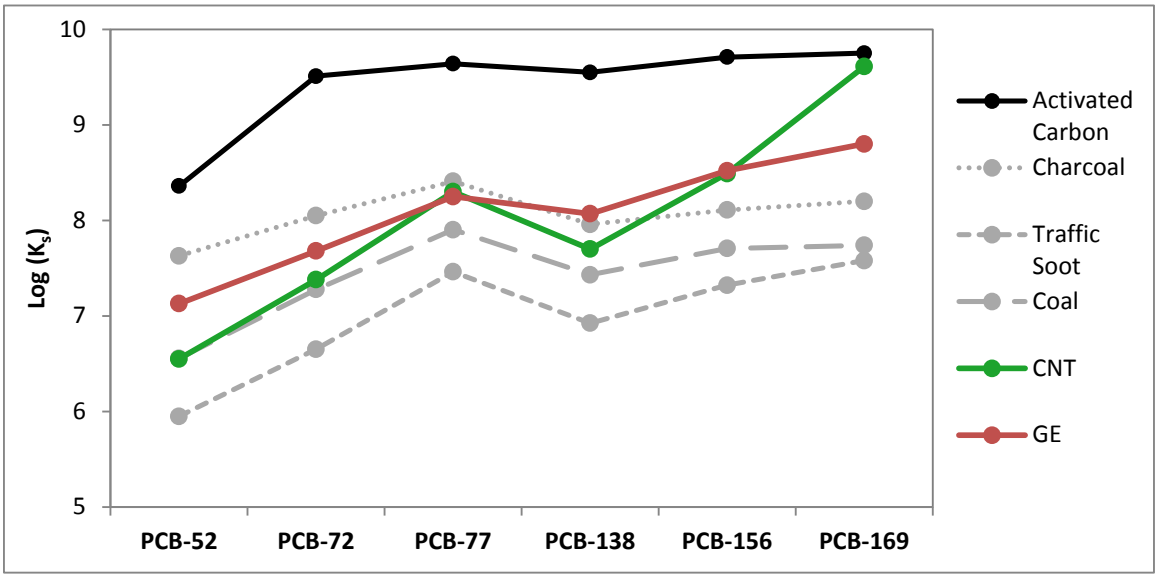

Figure 4.6: Comparison of log(K_s) values for GE and CNT (from this study) to activated carbon and three types of black carbon from the literature. The activated carbon and charcoal values are reported in Jonker and Koelmans [4]. The traffic soot and coal values are reported in Jantunen et al. [5].

4.3 Sorption Isotherms

4.3.1 Experimental QA/QC

Evaluation of Triplicates, Duplicates, and Controls

During the experimentation and data gathering, numerous measures were taken to assure the quality of the gathered data. Two types of experimental controls were used during each isotherm set, a triplicate batch consisting of SPME fibers in the aqueous solution and an additional triplicate batch consisting of SPME fibers and sorbent in aqueous solution. These controls were used to determine if any contamination was unintentionally introduced into the system through: 1) PCBs retained on improperly cleaned glassware, 2) PCBs retained on improperly cleaned SPME fibers, 3) PCBs introduced by the sorbent materials themselves, or 4) any other PCB contamination that could have occurred during the entirety of creating, handling and processing the batch systems. The results of the controls for the five sorbent sets all returned with no analyte detection except for those in the GE isotherm set, in which a small amount of the analyte PCBs were detected in the control triplicates. When analyzing the samples with the GC-MS, the six control samples were always the last to be run; therefore, one possible explanation is that the injector wash solvent had evaporated to a point at which the injector needle was not being properly washed between samples. This is a possible explanation of why trace amounts of analyte, introduced by injector contamination, were measured in the controls. Despite this one instance, the results from the control samples proved that the systems were maintained clean and no detectable contamination was introduced.

Sample duplicates were run when analyzing analyte concentrations with the GC-MS. Two duplicates were run for every isotherm set analyzed, one high concentration

and one low concentration sample, by running the sample twice in a row and comparing the resulting concentrations. The average percent difference between each the parent sample and duplicate was 5%, indicating that the GC-MS was performing consistently and precisely.

Following standard practice, samples were prepared in triplicates so that any laboratory inconsistency and/or human error were accounted for. The coefficient of variation (CV) (standard deviation/mean) of each triplicate set was calculated in order to gauge the precision achieved within the triplicates. A large CV value indicates that the standard deviation is proportionately larger than the average, meaning that there is high variation between the triplicates. A reference value often used is CV=0.5, meaning that the standard deviation is half of the mean value, at which the influence of variation can start to be significant. CV values were calculated for the 55 sorbent-congener combinations and combined together for overall analysis. The median value of all CV values was 0.18, with 93% of all triplicates having CV values less than 0.5. These results show that the measured triplicates, as a whole, had low variation. The AC isotherm set had the highest average CV value of 0.32 compared to all of the other sorbents, which was reasonable because the AC samples were performed in smaller batch sizes and more prone to triplicate variation due to laboratory inconsistency. Overall, the analysis of sample triplicates indicated that the measured variation was reasonable.

Appropriate Use of SPME Fibers

Section 3.2.2 discussed the importance of designing the experimental set up such that the solid phase microextraction (SPME) fibers only sorbed a small fraction of the total PCBs in the system. Upon completion of the experiments, the percent of total PCBs on the fiber was calculated and checked to make sure that the SPME fiber did not remove too much PCBs from the system. The percent mass of PCBs on the SPME fiber

was confirmed to be under the ideal 5% mark for all of the sorbents except for the AC samples with initial concentrations of 10, 25 and 50µg/L. For PCB-1, 4, 8, 52, 72 and 138, the fraction of PCB mass on the SPME fiber ranged from 2 – 60%. The congeners with percent PCB mass of >20% on the SPME fiber were considered too altered and the results were discarded. This criterion resulted in the removal of 30 results between the six congeners listed above for the AC isotherm set.

Mass Balance

A primary assumption made for calculating the PCB equilibrium concentration of the sorbent (q_e) and water (C_e) phases was that the batch system maintained adequate mass balance. The PCBs in the water, sorbent and SPME fiber phases were extracted for three batch samples containing a total of 44mg BC, 220ml water and 11µg of each PCB congener. The mass of each PCB congener was measured, and the fraction of PCBs in each of the three phases was calculated by dividing the mass of an individual phase by the total PCBs in the system (11µg). The bar graph in Figure 4.7 depicts the average fraction in the water, sorbent and fiber phases for the three samples measured.

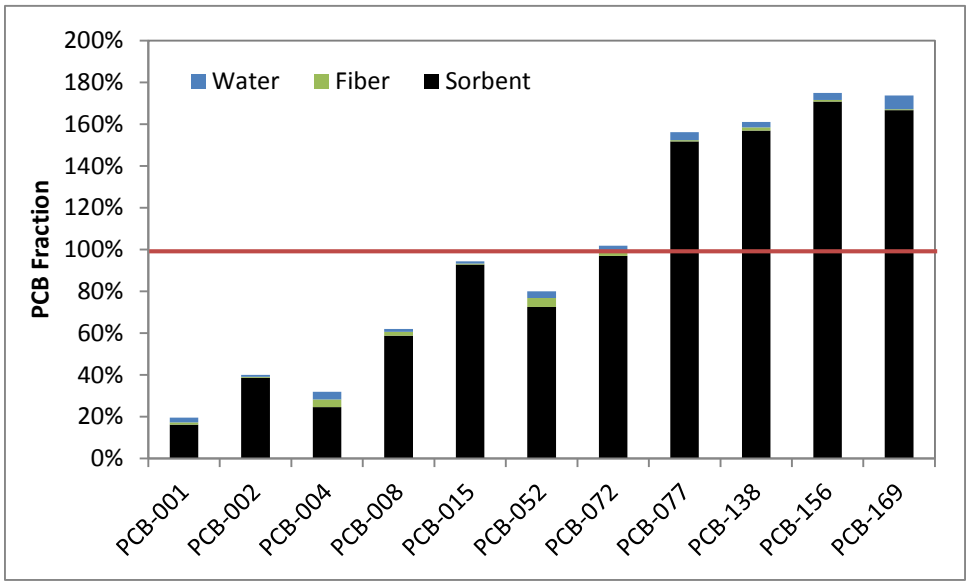

Figure 4.7: Average PCB mass fractions for the three samples measured in the water, sorbent and fiber phases. The red line indicates the ideal 100% mark.

Theoretically, the sum of the PCB mass fraction in the three phases should be 100%. However, it was observed that there were significantly less total PCBs for the lower congeners, and significantly more than 100% total PCBs for the higher congeners. The fraction of PCBs on the sorbent phase followed expectations, with small fractions in the less hydrophobic congeners and increasing fractions as the congeners became more chlorinated. The fraction of PCBs in the fibers also, to some extent, followed expectations, with higher mass fractions in the lower congeners where more PCBs are in the water phase and therefore available for sorption on the fibers. In contrast, the PCBs in the water did not exhibit expected behavior and contained small mass fractions across all the congeners. Theoretically, there should be more PCBs in the water phase for the lower congeners, filling the gap between the sorbent and fibers phases and the 100% mark. It should be noted that the water samples were stored for a long time (≈4 weeks) in glassware with ample head space before they were extracted. During this storage time, PCBs could have volatilized and been lost from the water.

Despite these uncertainties, the average of the total PCBs found for each of the 11 congeners was precisely 100%. Overall, while there is reason for questions to be raised concerning the details of the mass balance results, the averaged mass balance for all 11 congeners in the three samples confirms adequate conservation of mass. In addition to the mass balance experiments performed, the experimental procedure followed and equipment used in the present study closely followed those of many other published methods, all of which have confirmed adequate mass balance within their batch systems [47, 67, 114].

4.3.2 Model Fit Comparison

Three isotherm models: Langmuir (LAN), Freundlich (FRE) and Polanyi-Dubinin-Manes (PDM), were fit to the experimental data as described in Section 3.2.2 in Chapter

3. The three models were selected because of their different underlying assumptions and potential to describe sorption mechanisms. In addition to the three models, two types of error functions: sum of squared errors (SSE) and hybrid fractional error function (HYBRID), were used during the regressions to fit the models to the experimental data. The following section provides a discussion on how accurately each of the models fit the experimental data and the precision achieved by the two error functions.

Comparison of LAN, FRE and PDM

The 11 PCB congeners used created a spectrum of plotted curve shapes, ranging from data that quickly plateaued at low q_e concentrations to data that continued to increase linearly for the equilibrium concentrations achieved. With such a diverse data set, one model might fit some sorbent-congener combinations best while another model might fit best for other sorbent-congener combinations. The modeled values of q_e were correlated to the experimental data and the R^2 values were used to determine the best fit model for each sorbent-congener combination. In addition to the R^2 values, the total errors generated by the error functions were compared between the three models. As presumed, the best fit model found by highest R^2 values compared closely to the best fit model found by lowest total error generated, therefore the results from R^2 was primarily used for model fit comparison. The R^2 value was generated for each of the sorbent-congener combinations (n=55) using the three models. The highest R^2 value was considered to be the best fit model; however, the R^2 values of the three models were often very close to one another due to very similar fits. To avoid excluding a model that fit very closely to the best model but was a few numeric units lower than the best fit model, all models within a ±1% difference of the best fit model were considered to collectively be the best fit models. Therefore, it would be reasonable to conclude that all three models fit the data equally well, or that any combination of two of the models fit the

data equally well. The bar graph in Figure 4.8 shows which model(s) best fit the experimental data for the 55 sorbent-congener combinations when using either of the error functions (see Table A.3 for detailed R^2 results).

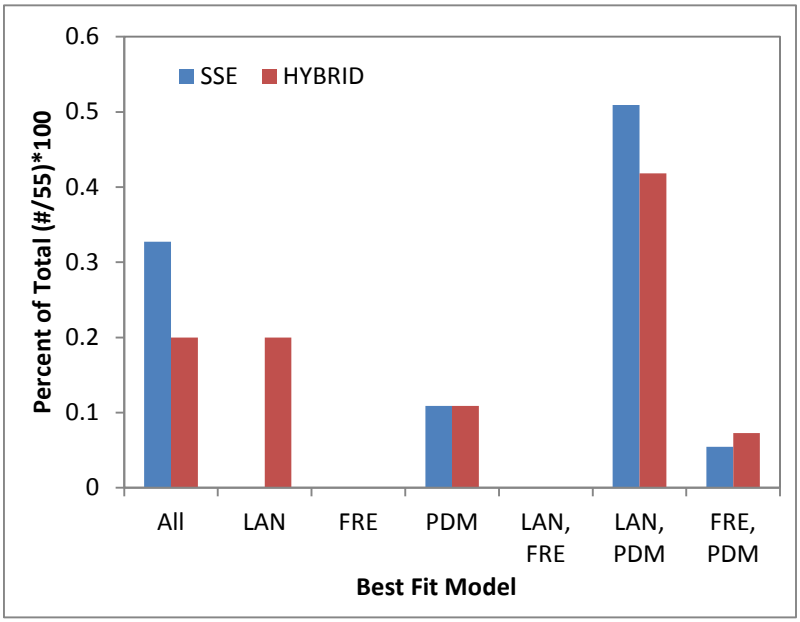

Figure 4.8: Best model fit results for the 55 sorbent-congener combinations for each of the two error functions.

A substantial number of the 55 sorbent-congener combinations had R^2 values within 1% difference of each other, whereas there were only a few instances where a single model fit best. The FRE model fit the experimental data the least accurately, with no sorbent-congener combination where FRE achieved the best fit without either PDM or both PDM and LAN also achieving best fit. When using the SSE error function, PDM was included as the best fitting model for all 55 combinations. However, for the HYBRID error function, there were 11 combinations in which LAN was the sole best fit model, with all of the 44 remaining combinations including PDM in some fashion. Interestingly, the PDM model shared best fit with both LAN (LAN-PDM) and FRE (FRE-PDM), indicating that it was capable of modeling both plateau like behavior as well as gradual increases with no plateau. Based on these results, the PDM was considered the most precise and robust model for sorption between the five materials and the 11 PCB congeners.

The conclusion presented here is similar to that of Jontunen et al. (2010), who investigated seven different types of isotherm models for the sorption of PCBs with carbonaceous sorbents and found that PDM was the most preferred model. Not only was PDM robust enough to fit a wide spectrum of experimental data, but the resulting parameters of maximum sorption capacity and bond energy were more useful and practical compared to the parameters of LAN and FRE. Overall, of the three models used in the present study, the newly developed PDM model was the most desirable for use with PCB sorption to carbonaceous materials.

Comparison of SSE and HYBRID

The primary difference between the SSE and HYBRID error functions are how they distribute the minimization of error. The SSE function simply reduces the error between the modeled q_e and the experimental q_e values, leading to bias towards the higher concentrations where the error is typically greatest; in contrast, the HYBRID function places priority on reducing the error for lower concentrations [99]. Figure 4.9 provides isotherm graphs illustrating the sorption of PCB-8 to BC to visually illustrate the different model fits resulting from the two error functions. The graphs visually confirm the mathematical bias introduced by the error functions. The three models fit the experimental data best for the higher concentrations when SSE was used, seen most dramatically for FRE in the normal scale. In contrast, the models fit more accurately for the lower concentrations when the HYBRID error function was used, seen most dramatically for the PDM model in the logarithmic scale. The SSE error function created better fits for the normal scale graphs (Figure 4.9a and c); however, the errors in the lower concentrations can be clearly seen when the scales were log normalized. The HYBRID error function notably out-performed SSE over the full range of equilibrium concentrations, as seen in the log normalized graphs (Figure 4.9b and d).

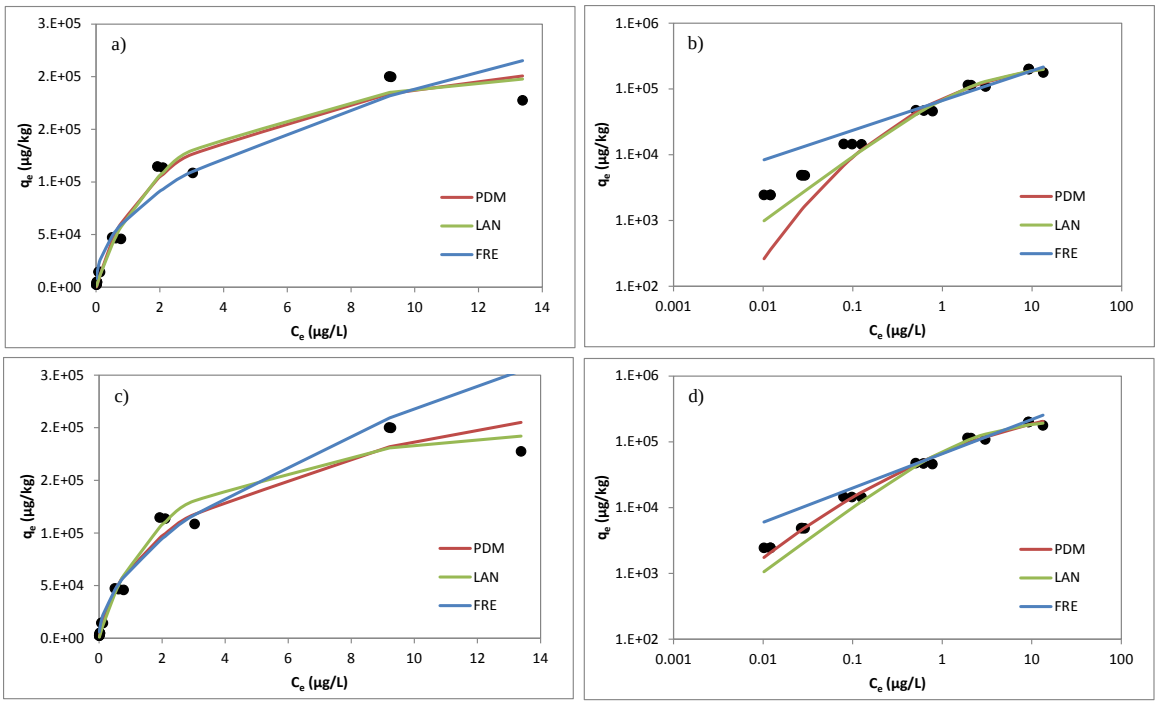

Figure 4.9: Isotherm graphs for the sorption of PCB-8 to BC, where a) shows the models fit with SSE in normal scale, b) is SSE in logarithmic scale, c) shows the model's fit with HYBRID in normal scale and d) is HYBRID in logarithmic scale.

Isotherm models should ideally evenly fit the experimental data, with the model line transecting all of data points as closely as possible. However, it was preferable to emphasize better model fits at lower concentrations, where equilibrium concentrations were low and there was little risk of sorbent saturation. By emphasizing better model fits for lower concentrations, the generated model parameters were biased towards actual environmental contamination levels, and therefore more relevant for use in environmental applications. With this understanding, it is clear that the HYBRID error function is preferred over the SSE. Interestingly, the R^2 values were slightly lower for models fit with HYBRID, average differences being -1, -3 and -1% for LAN, FRE and PDM respectively, yet the slight deficiency in model fit for higher concentrations is preferential to a more precise model fit at lower concentrations.

In addition to the preferential bias towards low concentrations, the HYBRID error function provides a more precise approach, evidenced by the reduction of standard

errors compared to SSE. The standard errors produced for the model parameters on average were 30 or 17% of the parameter value for models using SSE or HYBRID, respectively. The reduction of standard error needed to describe a modeled parameter was indicative of the precision induced by the HYBRID error function. Based on the findings from comparing the three models and two error functions, the PDM model computed using the HYBRID error function produced the most precise and accurate results for the five sorbents and 11 congeners used in this study.

4.3.3 Model Graphs

Before going into detail about the generated model parameters, it was important to understand the big picture results presented by the isotherm experiments. The experimental data was organized and plotted in Figure 4.10 and 4.11, to aid in the conceptualization of isotherm results. Figure 4.10 shows the sorption of all 11 PCB congeners onto each of the five sorbents, whereas Figure 4.11 shows the sorption of all five sorbents onto each of the 11 congeners, both in log-log scale. The PDM model (using the HYBRID error function) was chosen to fit the experimental data in Figures 4.10 and 4.11 because of its superior fit covering the full range of aqueous concentration as discussed above.

The organization of the isotherm data in Figure 4.10 allowed for comparison between the 11 congeners for each of the five sorbent materials. These graphs present many pieces of information; one important piece being the range of PCB concentrations in the aqueous phase. Ideally, the greater range of aqueous equilibrium concentration (C_e) achieved in the isotherm experiments, the more applicable the isotherm results are for general use. The isotherm samples were spiked with initial concentrations of PCBs varying by two orders of magnitude (C=0.5 – 50µg/L), resulting in C_e values for each individual congener that covered approximately 2 – 4 orders of magnitude. Additionally,

the C_e values for all of the 11 congeners spanned from pg/L to ug/L, with the bulk of concentrations being in the ng/L range. These resulting equilibrium concentrations were comparable to what has been commonly reported in the literature and found in contaminated environments.

By comparing the isotherm curves of the 11 congeners, the more chlorinated congeners were observed to generally have lower values of C_e. Similar to the results presented for the log(K_s) values, the hydrophobicity along with the planarity of the congener played an important role in sorption with the sorbent material. An example of the planarity effect can be seen by comparing the isotherm curve of PCB-1 with PCB-4. The log(K_{ow}) values 4.46 and 4.65 for PCB-1 and PCB-4, respectively, indicate that PCB-4 is more hydrophobic, yet for all five sorbents the more planar PCB-1 was removed in greater quantities than PCB-4. Overall, the graphs in Figure 4.10 illustrate that PCBs were removed from water proportionate to increasing log(K_{ow}) values coupled with increasing planarity.

Another important observation was that lower congeners had more non-linear curves than those of the mostly linear log-log curves of higher chlorinated congeners. The plateaus formed for the lower congeners meant that sorption capacity on the sorbent material was reached and that no further sorption of those congeners could occur. This transition from non-linear curves for the lower congeners to linear curves for the higher congeners was likely due to competition for sorption sites, indicating that the sorbent materials neared saturation for the batch samples with high PCB mass (initial PCB concentration of 25 and 50µg/L). If saturation was approached, then the more chlorinated and hydrophobic congeners would preferably sorb, leaving fewer available sorption sites for the less chlorinated and hydrophobic congeners. As a whole, site competition between the 11 congeners caused less sorption between the sorbent and congeners than if each congener was in a separate system by itself and there was no

cross-congener competition for sorption sites. Jantunen et al. (2010) performed a study that investigated this theory by running two sets of samples, one with a mixture of congeners and another with just one of the congeners from that mix. It was found that sorption competition between congeners began when the sorbate surface coverage reached >35% of available surface area on coal [5]. The recognition that sorption competition likely occurred in the present study was important, especially when considering the isotherm parameters generated for the less chlorinated congeners.

Interestingly, the plateaued curves indicative of sorption competition was apparent for the sorption of all 11 congeners onto GE, leading to the conclusion that GE was saturated to the extent that even the more chlorinated congeners had to compete for sorption sites. The competition effect is fairly equal amongst all five sorbents for the lower chlorinated congeners, but unique to GE for the more chlorinated congeners. This competition amongst the higher congeners in the GE isotherm would cause the dampening of sorption for GE more so than any other sorbent material, which could explain why CNT and CNT-OH surpass GE in the sorption of PCBs for the three most chlorinated congeners. Sorbent saturation and the competition between congeners that it creates does not invalidate the isotherm parameters for the GE isotherms or the lower chlorinated congeners in general, one reason being that saturation can certainly occur in actual application, but it is important to acknowledge the dampening effect saturation had on the efficiency of sorption when comparing different sorbents and congeners.

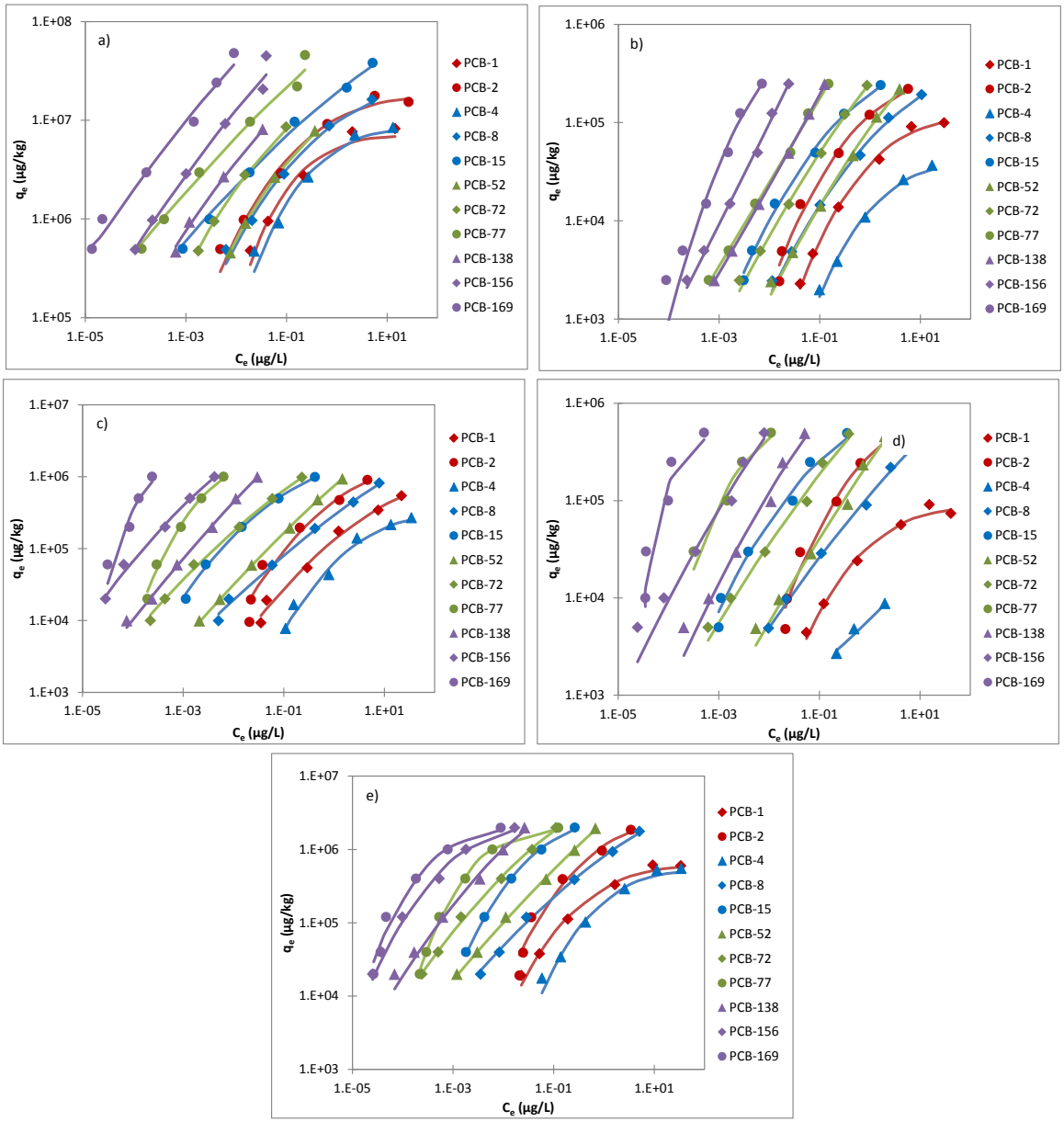

Figure 4.10: Isotherm curves for the 11 congeners onto each of the five congeners. The lines plotted to the experimental data were generated from the PDM model using the HYBRID error function. a) is AC b) is BC c) is CNT d) is CNT-OH and e) is GE.

The graphs shown in Figure 4.11 illustrate the sorption that occurred for each of the 11 congeners onto the five sorbent materials. The relative values of q_e represent the quantity of sorption for each sorbent material to the particular PCB congener. The results were similar to those generated from the distribution coefficients (K_s) discussed in Section 4.2; however, the isotherm plots were a useful visual tool to confirm the findings discussed with the K_s. One helpful piece of information confirmed here was that the isotherms for each sorbent material were performed over the same general C_e range, justifying the direct comparison of the resulting isotherm parameters. Overall, the graphs in Figure 4.11 reinforce the conclusion that AC exhibited the greatest sorption to the 11 PCB congeners, with subsequent sorption occurring for GE, CNT, CNT-OH and BC, respectively.

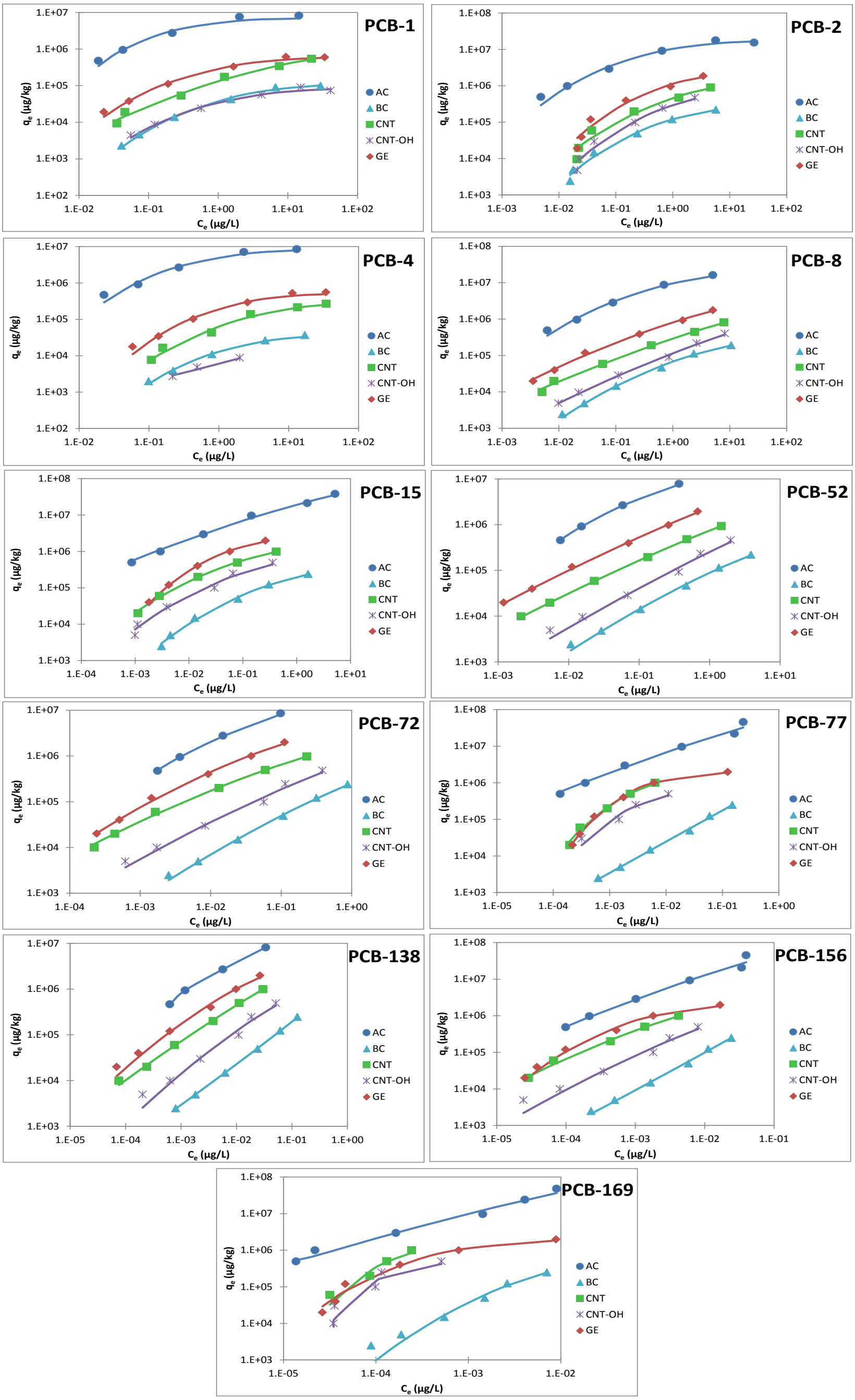

Figure 4.11: Isotherm curves for the five sorbent materials and each of the 11 PCB congeners. The lines plotted to the experimental data were generated from the PDM model using the HYBRID error function.

4.3.4 Model Parameters

The LAN, FRE and PDM model parameters, given in equations 3.4 - 3.5, were important for gaining a more specific understanding of how the PCB congeners interact with the five sorbent materials. Tables 4.5 - 4.7 list the parameters generated using either the SSE or HYBRID error function for every sorbent-congener combination tested. The remainder of the section is focused on the analysis of these parameters.

The LAN parameter, Q_{max}^{L}, reported in Table 4.5, shows that AC had the largest sorption capacity compared to the four other sorbent materials, with GE, CNT, CNT-OH and BC following in subsequent order. Interestingly, the Q_{max}^{L} value from the LAN model and the Q_{max}^{P} value generated from the PDM model show consistently similar results, with standard errors often overlapping. The only instance of substantially different Q_{max} values were those generated by PDM using the HYBRID error function. The overall consistency of the Q_{max} values generated demonstrates the similarity and functionality of the LAN and PDM models.

According to the resulting b values generated by the LAN model, AC has greater affinity for sorption with PCBs than BC. Both materials are primarily constructed with stacked carbon sheets, the main difference being that AC is highly porous while BC has a smoother surface with less pore volume. With this understanding, the sorption of PCBs due to containment in the pore spaces of AC was stronger than that of the primarily surface sorbing BC. However, in contradiction with the sorption capacity, the b values showed that GE, CNT and CNT-OH have higher affinities than AC for certain PCB congeners. Despite AC having a larger capacity for PCBs due to its greater surface area and available sorption sites, the sorption between the three nanomaterials was stronger than that of AC for the planar PCB congeners. The b values for the nanomaterials are the same or only slight greater than the AC b values for the lesser chlorinated and non-

planar congeners but became substantially greater for the more chlorinated congeners (PCBs with six chlorines or more). Researchers studying the sorption of HOCs with CNT materials have attributed the strong sorption bond between HOCs and the carbon surface to π-π electron coupling forces [80, 82], whereas the sorption mechanism for PCBs to AC is largely contributed to containment in pore spaces. The b values indicate that the smooth carbon surface of the nanomaterials provides a stronger bond with the PCB congeners, especially for the planar congeners that can lay flat on the surface, than that of the heterogeneous and porous AC.

The Z values, representing bond energy between the PCB congeners and the sorbent materials, reveal a similar phenomenon as the b values. Despite the greater capacity of AC, the nanomaterials created a stronger bond to planar PCB congeners than AC. The bond energy between the planar congeners, PCB-15, 77 and 169, all indicated stronger bonds to GE, CNT and CNT-OH than AC and BE. Additionally, the Z values for the nanomaterials have a much greater reaction to the planarity of the congener, showing a consistent and substantial increase in bond energy for the planar congeners compared to the non-planar congeners. The AC and BC materials showed very little increase or decrease due to the planarity of a congener, indicating that the planarity effect is less important for sorbent materials of which pore confinement is the primary mechanism. Interestingly, for both AC and BC, there was a downward trend in the Z values until the congeners with six chlorine substitutes, indicating that there could be an optimal point where steric hindrance was overcome by the hydrophobic effect. Between the three nanomaterials, GE consistently demonstrated greater bond energies with PCB compared to the CNT materials except for the most chlorinated congeners.

The d value in the PDM model is generally reported in the literature to be between 1 and 5 [115], with values closer to 1 indicating Freundlich type sorption [116]. The resulting d values in this research ranged from 1.4 – 5.5, 1 – 3.5, 1.2 – 6.3, 1.1 – 9.6

and 1.2 – 4.2 for AC, BC, CNT, CNT-OH and GE, respectively (only values for the HYBRID error function shown). The d values for the five sorbent materials tested were consistently higher than 1, which indicates that the sorption site energies were not distributed exponentially away from the sorbent surface, but rather acted more like the Langmuir assumption of single site energy distribution. This result coincides with the comparison in the model fitting analysis, proving that the five sorbent materials fit more consistently with LAN as compared to the FRE model.

The K_F values generated from the FRE model compare closely to the K_s values discuss thoroughly in Section 4.2. The n values reinforce the curve linearity conclusions made when observing the graphs in Figure 4.10. The n values for each of the sorbent materials trends upwards with increasing chlorination toward the value of 1, with BC having the strongest increasing trend and GE having the weakest. The positive correlation between linearity and hydrophobicity again indicates that sorption increases because of the increasing hydrophobic forces, even to the point of dampening the effects of planarity or steric hindrance.

Table 4.5: Isotherm parameter results for the Langmuir model. The (±) indicates standard deviation and ~ indicates that no standard deviation was derived for that value.

SSE

Congener	$Q_{max}{}^{L}*10^{6}$ (ug/kg)					b (L/ug)				
	AC	BC	CNT	CNT-OH	GE	AC	BC	CNT	CNT-OH	GE
PCB-1	8.6 ± 1	0.11 ± 0.005	0.62 ± 0.047	0.086 ± 0.008	0.64 ± 0.052	2.7 ± 1.5	0.51 ± 0.097	0.22 ± 0.055	0.66 ± 0.29	0.8 ± 0.32
PCB-2	17 ± 0.91	0.26 ± 0.009	1.2 ± 0.086	0.66 ± 0.072	2.4 ± 0.17	2.4 ± 0.68	0.95 ± 0.1	0.58 ± 0.11	0.95 ± 0.24	0.86 ± 0.16
PCB-4	8.7 ± 0.89	0.04 ± 0.004	0.28 ± 0.026	0.012 ± 0.002	0.59 ± 0.065	1.9 ± 0.76	0.46 ± 0.18	0.3 ± 0.11	1.4 ± 0.57	0.44 ± 0.2
PCB-8	17 ± 1.4	0.23 ± 0.012	1.1 ± 0.09	0.58 ± 0.074	2.4 ± 0.19	1.8 ± 0.73	0.42 ± 0.062	0.33 ± 0.067	0.25 ± 0.074	0.53 ± 0.11
PCB-15	42 ± 4.2	0.3 ± 0.014	1.2 ± 0.046	0.63 ± 0.08	2.6 ± 0.16	1.1 ± 0.4	2.5 ± 0.35	9.6 ± 1.1	9.8 ± 3.2	13 ± 2.1
PCB-52	12 ± 1.4	0.4 ± 0.042	1.6 ± 0.088	0.91 ± 0.21	3.6 ± 0.45	5.5 ± 1.6	0.31 ± 0.062	0.94 ± 0.1	0.47 ± 0.18	1.7 ± 0.39
PCB-72	12 ± 1.7	0.46 ± 0.056	1.4 ± 0.063	0.77 ± 0.12	3.1 ± 0.3	22 ± 7.2	1.2 ± 0.25	10 ± 1.1	4 ± 1.3	15 ± 3.1
PCB-77	51 ± 12	0.8 ± 0.18	2 ± 0.33	0.73 ± 0.12	2.1 ± 0.08	11 ± 7.9	3 ± 0.9	160 ± 45	190 ± 64	150 ± 18
PCB-138	13 ± 1.7	2 ± 1.6	2.3 ± 0.19	0.97 ± 0.24	3.2 ± 0.49	48 ± 13	1.1 ± 1	26 ± 3.5	18 ± 7.4	54 ± 16
PCB-156	62 ± 28	7.2 ± 5	1.8 ± 0.16	1 ± 0.26	2.3 ± 0.13	31 ± 29	1.5 ± 3.8	300 ± 52	110 ± 46	500 ± 83
PCB-169	59 ± 13	0.77 ± 0.21	3.6 ± 3.2	0.72 ± 0.18	2.2 ± 0.13	250 ± 130	66 ± 24	1300 ± 1400	3700 ± 1800	1300 ± 240

HYBRID

Congener	$Q_{max}{}^{L}*10^{6}$ (ug/kg)					b (L/ug)				
	AC	BC	CNT	CNT-OH	GE	AC	BC	CNT	CNT-OH	GE
PCB-1	7 ± 1.9	0.11 ± 0.009	0.55 ± 0.06	0.079 ± 0.01	0.57 ± 0.08	3.5 ± 1.2	0.53 ± 0.08	0.35 ± 0.12	0.83 ± 0.22	1.2 ± 0.28
PCB-2	16 ± 0.73	0.25 ± 0.01	1.1 ± 0.1	0.73 ± 0.37	2.4 ± 0.25	2.8 ± 0.66	0.99 ± 0.08	0.8 ± 0.2	0.7 ± 0.27	0.9 ± 0.21
PCB-4	8 ± 0.88	0.036 ± 0.006	0.27 ± 0.04	0.012 ± 0.002	0.52 ± 0.1	2 ± 0.36	0.54 ± 0.16	0.29 ± 0.07	1.4 ± 0.63	0.55 ± 0.19
PCB-8	15 ± 2.4	0.22 ± 0.03	0.91 ± 0.15	0.55 ± 0.13	2 ± 0.41	2.5 ± 1	0.47 ± 0.13	0.56 ± 0.36	0.26 ± 0.18	0.86 ± 0.27
PCB-15	32 ± 2.5	0.29 ± 0.02	1.1 ± 0.09	0.64 ± 0.17	2.6 ± 0.4	3 ± 0.89	2.8 ± 0.49	13 ± 2.7	8.1 ± 3.5	12 ± 1.5
PCB-52	12 ± 0.71	0.39 ± 0.04	1.4 ± 0.12	1.1 ± 0.91	3.2 ± 0.19	5.3 ± 0.79	0.32 ± 0.06	1.2 ± 0.23	0.33 ± 0.2	2 ± 0.27
PCB-72	~ 12	0.45 ± 0.07	~ 1.2	0.83 ± 0.52	~ 2.8	20 ± 2.9	1.2 ± 0.25	14 ± 1.6	3.1 ± 1.4	18 ± 1
PCB-77	~ 38	0.83 ± 0.39	~ 2.6	~ 0.82	~ 2.2	20 ± 7.4	2.8 ± 1.2	96 ± 7.5	130 ± 14	110 ± 9.7
PCB-138	~ 12	~ 1.7	~ 2.1	~ 1.3	~ 3.4	55 ± 6.9	1.3 ± 0.05	29 ± 1	10 ± 1.6	46 ± 3.6
PCB-156	~ 44	~ 3.9	~ 1.7	~ 1.3	~ 2.3	50 ± 11	2.7 ± 0.12	310 ± 17	62 ± 7.7	450 ± 30
PCB-169	~ 62	~ 2.5	~ 16	1.1 ± 0.03	~ 2.3	180 ± 55	15 ± 0.94	210 ± 21	1100 ± 290	930 ± 140

Table 4.6: Isotherm parameter results for the Freundlich model. The (±) indicates standard deviation and ~ indicates that no standard deviation was derived for that value.

SSE

Congener	K_F *10^6 (ug/kg)(ug/L)^n					n (-)				
	AC	BC	CNT	CNT-OH	GE	AC	BC	CNT	CNT-OH	GE
PCB-1	4.5 ± 0.75	0.036 ± 0.005	0.14 ± 0.012	0.033 ± 0.006	0.25 ± 0.041	0.25 ± 0.07	0.33 ± 0.05	0.45 ± 0.03	0.28 ± 0.06	0.28 ± 0.06
PCB-2	8.6 ± 1	0.1 ± 0.006	0.41 ± 0.019	0.28 ± 0.018	0.98 ± 0.051	0.23 ± 0.04	0.45 ± 0.04	0.52 ± 0.03	0.54 ± 0.06	0.51 ± 0.04
PCB-4	4.3 ± 0.6	0.012 ± 0.002	0.074 ± 0.014	0.006 ± 0.0004	0.19 ± 0.04	0.3 ± 0.07	0.4 ± 0.07	0.38 ± 0.06	0.47 ± 0.09	0.32 ± 0.07
PCB-8	8.8 ± 0.73	0.067 ± 0.005	0.29 ± 0.016	0.13 ± 0.015	0.79 ± 0.043	0.37 ± 0.05	0.45 ± 0.04	0.49 ± 0.03	0.53 ± 0.06	0.49 ± 0.04
PCB-15	19 ± 0.98	0.19 ± 0.008	1.5 ± 0.06	0.72 ± 0.095	3.7 ± 0.4	0.41 ± 0.03	0.47 ± 0.04	0.46 ± 0.02	0.43 ± 0.07	0.49 ± 0.05
PCB-52	14 ± 1.4	0.089 ± 0.005	0.74 ± 0.011	0.27 ± 0.017	2.4 ± 0.11	0.59 ± 0.07	0.66 ± 0.05	0.63 ± 0.02	0.68 ± 0.08	0.64 ± 0.05
PCB-72	31 ± 6.2	0.26 ± 0.009	2.2 ± 0.074	0.79 ± 0.088	6.8 ± 0.86	0.57 ± 0.07	0.69 ± 0.05	0.54 ± 0.02	0.57 ± 0.07	0.58 ± 0.05
PCB-77	77 ± 17	1.2 ± 0.12	31 ± 13	4.6 ± 2.1	3.8 ± 0.6	0.5 ± 0.12	0.82 ± 0.05	0.69 ± 0.08	0.51 ± 0.09	0.32 ± 0.05
PCB-138	67 ± 13	1.7 ± 0.23	13 ± 1.3	3.5 ± 1	16 ± 4.7	0.62 ± 0.05	0.92 ± 0.06	0.73 ± 0.03	0.68 ± 0.09	0.6 ± 0.07
PCB-156	270 ± 160	10 ± 2	32 ± 8.2	12 ± 6	8.4 ± 2.1	0.64 ± 0.17	1 ± 0.05	0.64 ± 0.04	0.69 ± 0.09	0.36 ± 0.05
PCB-169	440 ± 250	16 ± 5.6	1200 ± 1800	19 ± 18	9.8 ± 2.8	0.51 ± 0.11	0.84 ± 0.07	0.87 ± 0.18	0.5 ± 0.12	0.34 ± 0.05

HYBRID

Congener	K_F *10^6 (ug/kg)(ug/L)^n					n (-)				
	AC	BC	CNT	CNT-OH	GE	AC	BC	CNT	CNT-OH	GE
PCB-1	3.1 ± 0.86	0.024 ± 0.002	0.11 ± 0.009	0.024 ± 0.003	0.64 ± 0.02	0.3 ± 0.09	0.47 ± 0.05	0.54 ± 0.03	0.37 ± 0.05	0.27 ± 0.05
PCB-2	6.2 ± 0.66	0.083 ± 0.02	0.35 ± 0.03	0.24 ± 0.031	0.83 ± 0.08	0.33 ± 0.03	0.6 ± 0.07	0.65 ± 0.04	0.74 ± 0.07	0.68 ± 0.04
PCB-4	3.3 ± 0.54	0.009 ± 0.001	0.048 ± 0.007	0.006 ± 0.0003	0.12 ± 0.01	0.38 ± 0.07	0.47 ± 0.06	0.5 ± 0.04	0.5 ± 0.07	0.42 ± 0.07
PCB-8	7.8 ± 1.2	0.066 ± 0.005	0.27 ± 0.009	0.11 ± 0.008	0.73 ± 0.04	0.46 ± 0.05	0.52 ± 0.05	0.54 ± 0.02	0.61 ± 0.04	0.55 ± 0.02
PCB-15	18 ± 0.89	0.19 ± 0.02	1.7 ± 0.15	0.83 ± 0.3	4.7 ± 1.3	0.45 ± 0.02	0.6 ± 0.04	0.55 ± 0.03	0.57 ± 0.07	0.63 ± 0.05
PCB-52	15 ± 1.8	0.082 ± 0.004	0.74 ± 0.02	0.25 ± 0.02	2.5 ± 0.2	0.66 ± 0.04	0.74 ± 0.04	0.67 ± 0.01	0.78 ± 0.12	0.69 ± 0.03
PCB-72	~ 37	0.27 ± 0.02	2.4 ± 0.12	0.86 ± 0.28	8.5 ± 1.2	0.65 ± 0.01	0.76 ± 0.03	0.59 ± 0.02	0.68 ± 0.1	0.67 ± 0.02
PCB-77	70 ± 11	1.3 ± 0.08	~ 71	8.8 ± 0.75	5.4 ± 1	0.51 ± 0.04	0.85 ± 0.02	0.85 ± 0.01	0.66 ± 0.02	0.49 ± 0.03
PCB-138	77 ± 9.3	1.6 ± 0.13	15 ± 0.79	5.2 ± 2.4	25 ± 0.6	0.66 ± 0.05	0.93 ± 0.02	0.77 ± 0.009	0.83 ± 0.08	0.71 ± 0.008
PCB-156	~ 230	12 ± 0.87	~ 47	~ 23	16 ± 0.97	0.64 ± 0.02	1 ± 0.02	0.7 ± 0.009	0.82 ± 0.01	0.51 ± 0.03
PCB-169	~ 440	~ 38	~ 9600	~ 200	24 ± 0.36	0.54 ± 0.03	1 ± 0.02	1.1 ± 0.01	0.84 ± 0.02	0.53 ± 0.02

Table 4.7: Isotherm parameter results for the Polanyi-Dubinin-Manes model. The (±) indicates standard deviation and ~ indicates that no standard deviation was derived for that value.

SSE

Congener	Q_{max}^{PDM} *10^6 (ug/kg)					Z (kJ/mol)					d (-)				
	AC	BC	CNT	CNT-OH	GE	AC	BC	CNT	CNT-OH	GE	AC	BC	CNT	CNT-OH	GE
PCB-1	8.4 ± 1.3	0.11 ± 0.008	1.1 ± 0.4	0.087 ± 0.012	0.65 ± 0.079	22 ± 1.3	18 ± 0.54	12 ± 2.4	18 ± 1.2	19 ± 1.2	6.4 ± 3.5	4.6 ± 0.91	1.9 ± 0.53	4.5 ± 1.8	4.4 ± 1.5
PCB-2	17 ± 1.2	0.3 ± 0.032	2.3 ± 0.79	0.76 ± 0.23	2.8 ± 0.53	20 ± 0.76	17 ± 0.68	13 ± 2.1	17 ± 1.6	17 ± 1.1	5.1 ± 1.4	3.4 ± 0.51	2.1 ± 0.48	3.7 ± 1.2	3.4 ± 0.72
PCB-4	8.6 ± 1.2	0.041 ± 0.008	0.28 ± 0.041	0.74 ± 1.1	0.58 ± 0.082	18 ± 1.1	14 ± 1.3	13 ± 1	6.1 ± 55	14 ± 1.2	4.9 ± 2.1	3.4 ± 1.3	3.3 ± 1.2	1.1 ± 5.3	3.9 ± 1.6
PCB-8	20 ± 4.3	0.26 ± 0.041	1.2 ± 0.31	0.73 ± 0.35	4.7 ± 2.3	18 ± 1.5	15 ± 0.92	14 ± 1.5	13 ± 2.5	12 ± 3	3.5 ± 1.1	3.2 ± 0.7	2.8 ± 0.77	2.7 ± 1.2	2 ± 0.63
PCB-15	43 ± 9	0.34 ± 0.05	2 ± 0.3	0.69 ± 0.21	2.6 ± 0.38	13 ± 1.6	14 ± 0.88	15 ± 1	18 ± 1.7	19 ± 0.74	2.3 ± 0.78	3 ± 0.6	2.5 ± 0.32	3.9 ± 1.7	4.6 ± 0.97
PCB-52	13 ± 5.8	0.35 ± 0.074	2.8 ± 0.71	0.65 ± 0.18	5 ± 2.5	13 ± 2.3	7.1 ± 0.91	6.9 ± 1.1	9 ± 0.99	9.3 ± 2.3	2.9 ± 1.3	1.9 ± 0.44	1.5 ± 0.24	3 ± 1.2	2 ± 0.71
PCB-72	16 ± 8.8	0.56 ± 0.22	3.7 ± 1.1	0.74 ± 0.25	4.3 ± 1.8	16 ± 3.1	8.7 ± 1.8	9.5 ± 1.5	13 ± 1.5	14 ± 2.2	3.2 ± 1.6	2 ± 0.61	1.6 ± 0.24	3.4 ± 1.5	2.8 ± 0.94
PCB-77	39 ± 11	0.66 ± 0.29	1.5 ± 0.31	0.56 ± 0.081	2 ± 0.077	8.4 ± 1.8	4.7 ± 1.4	15 ± 0.78	15 ± 0.46	14 ± 0.26	2.5 ± 1.8	1.4 ± 0.4	4.8 ± 1.3	7 ± 2.4	4.1 ± 0.46
PCB-138	12 ± 3.4	2.1 ± 2.8	4.6 ± 2.1	0.63 ± 0.14	2.4 ± 0.39	13 ± 1.5	2.9 ± 2.8	7.3 ± 1.8	11 ± 0.67	13 ± 0.54	3.2 ± 1.2	1.1 ± 0.51	1.6 ± 0.36	4.6 ± 1.8	5.1 ± 1.5
PCB-156	34 ± 9.7	1.4 ± 1.2	2.8 ± 1.4	0.6 ± 0.11	2.1 ± 0.15	13 ± 1.1	8.2 ± 2.7	15 ± 2.5	16 ± 0.45	18 ± 0.36	7 ± 7	2.1 ± 0.82	2.8 ± 0.96	8.3 ± 2.9	6 ± 1.2
PCB-169	37 ± 6	0.3 ± 0.022	1.1 ± 0.11	0.56 ± 0.095	2.2 ± 0.17	15 ± 0.73	13 ± 0.18	20 ± 0.13	21 ± 0.42	17 ± 0.53	11 ± 9.4	7.1 ± 1.1	28 ± 7.9	13 ± 5.1	4.5 ± 0.85

HYBRID

Congener	Q_{max}^{PDM} *10^6 (ug/kg)					Z (kJ/mol)					d (-)				
	AC	BC	CNT	CNT-OH	GE	AC	BC	CNT	CNT-OH	GE	AC	BC	CNT	CNT-OH	GE
PCB-1	7 ± 1.9	0.12 ± 0.027	0.98 ± 0.21	0.086 ± 0.022	0.61 ± 0.21	22 ± 1.5	17 ± 1	13 ± 1.1	18 ± 1.4	19 ± 1.7	5.5 ± 1.9	3.5 ± 0.42	2.1 ± 0.22	3.7 ± 0.72	3.9 ± 0.7
PCB-2	17 ± 1	0.31 ± 0.038	1.6 ± 0.26	0.88 ± 0.93	2.7 ± 0.3	20 ± 0.64	16 ± 0.73	15 ± 1.1	16 ± 2.1	17 ± 0.55	3.5 ± 0.4	3.2 ± 0.28	2.8 ± 0.39	3.2 ± 0.78	3.5 ± 0.23
PCB-4	8.3 ± 2.6	0.038 ± 0.021	0.29 ± 0.14	0.1 ± 0.012	0.51 ± 0.2	18 ± 1.4	14 ± 2.1	13 ± 1.6	5.6 ± 1.8	15 ± 1.5	4 ± 1	3.3 ± 0.9	2.8 ± 0.88	1.1 ± 1.3	3.6 ± 0.72
PCB-8	23 ± 11	0.36 ± 0.13	3.3 ± 1.2	2 ± 0.61	5.9 ± 1.1	17 ± 1.5	13 ± 1.5	8.7 ± 1.1	7.7 ± 1.8	11 ± 0.87	2.8 ± 0.39	2.2 ± 0.28	1.4 ± 0.12	1.4 ± 0.26	1.7 ± 0.11
PCB-15	~ 71	0.41 ± 0.11	1.9 ± 0.31	1 ± 0.32	3.1 ± 0.9	9.2 ± 0.37	13 ± 1.1	15 ± 0.92	15 ± 1.6	18 ± 0.7	1.4 ± 0.06	2.4 ± 0.26	2.5 ± 0.23	2.5 ± 0.65	3.7 ± 0.26
PCB-52	18 ± 2.6	0.52 ± 0.25	3.9 ± 0.81	2.1 ± 0.83	12 ± 0.5	11 ± 1.1	5.5 ± 1.1	5.5 ± 0.66	4.4 ± 1.2	5.5 ± 0.26	2.3 ± 0.45	1.4 ± 0.19	1.2 ± 0.08	1.2 ± 0.25	1.2 ± 0.05
PCB-72	~ 26	1.1 ± 0.45	4 ± 0.61	2.5 ± 0.51	8.4 ± 1	13 ± 0.51	6 ± 1.1	9.2 ± 0.8	6.9 ± 1.6	11 ± 0.51	2.2 ± 0.19	1.4 ± 0.17	1.6 ± 0.1	1.4 ± 0.34	1.8 ± 0.09
PCB-77	32 ± 4.3	1.2 ± 0.52	2.1 ± 1.7	0.8 ± 0.77	2.1 ± 0.23	10 ± 1	2.9 ± 0.95	13 ± 1.4	13 ± 1.7	14 ± 0.46	2 ± 0.46	1 ± 0.16	3.3 ± 0.57	3.4 ± 2.7	3.7 ± 0.3
PCB-138	~ 28	2.6 ± 0.86	7.3 ± 1.4	2.3 ± 0.75	6.8 ± 4.9	8.1 ± 0.25	2.5 ± 0.55	5.7 ± 0.42	5.8 ± 1.2	8.4 ± 1.1	1.6 ± 0.07	0.97 ± 0.09	1.3 ± 0.06	1.5 ± 0.32	1.7 ± 0.22
PCB-156	~ 130	4.9 ± 0.3	7.7 ± 1.1	6.7 ± 0.67	2.5 ± 0.18	7.1 ± 0.52	4.6 ± 0.21	9.8 ± 0.67	6.7 ± 1.1	17 ± 0.49	1.4 ± 0.12	1.4 ± 0.04	1.7 ± 0.13	1.5 ± 0.3	3.4 ± 0.46
PCB-169	~ 180	0.89 ± 0.68	2.3 ± 0.11	0.6 ± 0.74	2.2 ± 0.069	7.3 ± 0.44	9.4 ± 1.4	19 ± 0.36	20 ± 0.99	17 ± 0.47	1.4 ± 0.09	2.4 ± 0.78	6.3 ± 0.97	9.6 ± 7	4.2 ± 0.46

Chapter 5: Conclusions and Summary

This thesis examined the sorption between 11 PCB congeners and five types of carbonaceous materials in aqueous solution at environmentally relevant concentrations. Activated carbon is a well-established sorbent material and is commonly used for removing HOCs from water, with current studies underway to investigate the ability of AC to sequester HOCs in sediments. Black carbon is a class of naturally occurring carbonaceous particles that have recently been recognized for their strong sorption with HOC. Graphene and carbon nanotubes have become increasingly available over the past decade, giving cause for their investigation as sorbent materials with HOCs, and PCBs in specific. The chemical characteristics and structure of GE and CNT are similar to that of AC and BC, making them ideal candidates for being a strong sorbent material to PCBs.

Isotherm experiments were conducted in batch reactors using a three phase approach with water, sorbent and SPME fibers. The concentration of PCBs on the SPME fiber was used to calculate the equilibrium concentrations in the water and on the sorbent materials. The data from the isotherm experiments were used to measure partitioning coefficients as well as fitted with the Langmuir, Freundlich and Polanyi-Dubinin-Manes models to generate isotherm parameters. Additionally, images of the sorbent surfaces along with particle size distribution analysis were conducted in order to better understand how the sorbent materials behave in solution.

The SEM images and particle size distribution analysis demonstrated that even though the individual GE, CNT and CNT-OH particles were on the nanoscale, they quickly formed aggregates that reduce their surface area available for sorption. The particle size distributions of either the aggregates or particles in solution for the five sorbent materials were similar, ranging from 5 – 150µm. AC had an extremely

heterogeneous surface, whereas the surface of BC was more smooth and homogeneous. The surfaces of individual GE and CNT particles were homogeneous sheets of carbon, yet the aggregates they form were amorphous in shape and contained pore spaces.

Of the three isotherm models used, the PDM model fit the data most consistently with FRE fitting the least. The HYBRID error function outperformed the SSE error function in accurately portraying the full range of concentrations used when fitting the isotherm parameters with the experimental data. While the optimum isotherm model and error function changes for each sorbent-congener combination, the use of PDM with the HYBRID error function was best suited for modeling the variation in sorbent materials and congeners.

The planarity of a PCB congener had clear effects on its sorption with the sorbent materials; the more planar the congener, the higher and stronger the sorption was. The planarity of a congener had stronger effects for GE, CNT and CNT-OH because the bonds between PCBs and the smooth carbon surface of the nanomaterials relies more on molecular structure than physical containment in the pores of AC and BC. The planarity effect led to higher and stronger sorption between sorbent materials, yet the effect of molecular planarity was dampened with increasing hydrophobicity.

The K_s, Q_{max}^{L}, Q_{max}^{p} and K_F values generated for the five sorbent materials all indicate that AC had the highest sorption capacity to the 11 PCB congeners, with GE, CNT, CNT-OH and BC coming in subsequent order. However, the b and Z values indicated that GE, CNT and CNT-OH had a stronger bond with the planar congener than AC and BC. Additionally, the ranges of d values generated agreed with the model fitting analysis, in that the five sorbent isotherms more closely resembled the assumptions of the Langmuir model.

Overall, the results of this study do not support the use of GE or CNT as sorbents in their natural state over AC. The positive aspects of GE and CNT are that they can be altered and further designed to improve upon their ability to act as sorbent materials with PCBs. Further research is needed to investigate how to increase the available sorption sites of GE and CNT while in solution, such that they are comparable or more than those for AC. Other promising techniques for improving sorption of GE and CNT is the addition of specialized functional groups, or the alteration of their diameter and surface, all of which have potential in increasing the sorption capacity and strength of these nanoparticles to PCBs.

References

1. Dobson, S.; van Esch, G. J. *Polychlorinated biphenyls and terphenyls: Environmental Health Criteria 140*; World Health Organization: Geneva, Switzerland, 1993.

2. Nollet, H.; Roels, M.; Lutgen, P.; Van der Meeren, P.; Verstraete, W., Removal of PCBs from wastewater using fly ash. *Chemosphere* **2003,** *53*, (6), 655-665.

3. Jonker, M. T. O.; Koelmans, A. A., Polyoxymethylene Solid Phase Extraction as a Partitioning Method for Hydrophobic Organic Chemicals in Sediment and Soot. *Environmental Science & Technology* **2001,** *35*, (18), 3742-3748.

4. Jonker, M. T. O.; Koelmans, A. A., Sorption of polycyclic aromatic hydrocarbons and polychlorinated biphenyls to soot and soot-like materials in the aqueous environment: Mechanistic considerations. *Environmental Science and Technology* **2002a,** *36*, (17), 3725-3734.

5. Jantunen, A. P. K.; Koelmans, A. A.; Jonker, M. T. O., Modeling polychlorinated biphenyl sorption isotherms for soot and coal. *Environmental Pollution* **2010,** *158*, (8), 2672-2678.

6. Penning, C. H., Physical Characteristics and Commercial Possibilities of Chlorinated Diphenyl. *Industrial & Engineering Chemistry* **1930,** *22*, (11), 1180-1182.

7. Drinker, C. K.; Warren, M. F.; Bennett, G. A., The Problem of Possible Systemic Effects From Certain Chlorinated Hydrocarbons. *Industrial Hygiene and Toxicology* **1937,** *19*, 283-311.

8. George, C. J.; Bennett, G. F.; Simoneaux, D.; George, W. J., Polychlorinated biphenyls a toxicological review. *Journal of Hazardous Materials* **1988,** *18*, (2), 113-144.

9. *Polychlorinated biphenyls: a report*; 9780309028851; National Academy of Sciences: Washington D.C, 1979; p 182.

10. Jensen, S., Report of a New Chemical Hazard. *New Scientist* **1966,** *32*, 612.

11. Schierow, L., PCBs: Background and Update. In Division, E. N. R. P., Ed. 1992.

12. EPA Search Superfund Site Information. http://cumulis.epa.gov/supercpad/cursites/srchsites.cfm (12/4/2012).

13. Klawinski, G.; LaPoma, J. *First Five Year Report for Hudson River PCBs Superfund Site*; U.S Environmental Protection Agency: New York, 2012.

14. EPA. Husdon River Cleanup. http://www.epa.gov/hudson/cleanup.html#quest1 (12/4/2012).

15. Bremle, G.; Larsson, P., PCB Concentration in Fish in a River System after Remediation of Contaminated Sediment. *Environmental Science & Technology* **1998,** *32*, (22), 3491-3495.

16. Su, S. H.; Pearlman, L. C.; Rothrock, J. A.; Iannuzzi, T. J.; Finley, B. L., Potential Long-Term Ecological Impacts Caused by Disturbance of Contaminated Sediments:A Case Study. *Environmental Management* **2002,** *29*, (2), 234-249.

17. Weston, D., Jarman, WM, Cabana, G, Bacon, CE,Jacobson, LA. , An evaluation of the success of dredging as remediation at a DDT-contaminated site in San Francisco Bay, California, USA. *Environmenatl Toxicology and Chemistry* **2002,** *21*, 2216-2224.

18. Bergen, B. J.; Nelson, W. G.; Mackay, J.; Dickerson, D.; Jayaraman, S., Environmental Monitoring Of Remedial Dredging At The New Bedford Harbor, Ma, Superfund Site. *Environmental Monitoring and Assessment* **2005,** *111*, (1-3), 257-75.

19. Madenjian, C. P.; Jude, D. J.; Rediske, R. R.; O'Keefe, J. P.; Noguchi, G. E., Gender difference in walleye PCB concentrations persists following remedial dredging. *Journal of Great Lakes Research* **2009,** *35*, (3), 347-352.

20. Engwall, M.; Naf, C.; Broman, D.; Brunstrom, B., Biological and Chemical Determination of Contaminant Levels in Settling Particulate Matter and Sediments: A Swedish River System before, during, and after Dredging of PCB-Contaminated Lake Sediments. *Ambio* **1998,** *27*, (5), 403-410.

21. Voie, O. A.; Johnsen, A.; Kristin Rossland, H., Why biota still accumulate high levels of PCB after removal of PCB contaminated sediments in a Norwegian fjord. *Chemosphere* **2002,** *46*, (9-10), 1367-1372.

22. Angelo, W. J., PCB Dredging Is Unclear Option. In Engineering News-Record: 2001; Vol. 246.

23. Vita, C., Johanson, P., Leisle, D., Marine Sediment Monitoring and Natural Recovery at the Bremonton Navel Complex. In *Battelle sediment conference proceedings*, Columbus 2011.

24. Forstner, U.; Apitz, S., Sediment remediation: U.S. focus on capping and monitored natural recovery. *Journal of Soils and Sediments* **2007,** *7*, (6), 351-358.

25. Mikszewski, A. *Emerging Technologies for the In Situ Remediation of PCB-Contaminated Soils and Sediments: Bioremediation and Nanoscale Zero-Valent Iron*; National Network for Environmental Management Studies Fellow: 2004.

26. *Final Report: Enhanced Microbial Dechlorination of PCBs and Dioxins in Contaminated Dredge Spoils*; USEPA Research Project: Rutgers University: 1999.

27. Baladi, S. M.; Lewis, C. M.; Ganguly, A.; Morrow, A. G.; Shoffner, L. R.; Blundy, R. F.; Nakagawa, P. F.; Mundy, S. T.; Anderson, L.; Adams, K., The use of enhanced bioremediation at the Savannah River Site to remediate pesticides and PCBs. *Remediation Journal* **2003,** *14*, (1), 5-20.

28. Ee, L. A.; Zhao, H.; Obbard, J. P., Recent advances in the bioremediation of persistent organic pollutants via biomolecular engineering. *Enzyme and Microbial Technology* **2005,** *37*, (5), 487-496.

29. Cornelissen, G.; Amstaetter, K.; Hauge, A.; Schaanning, M.; Beylich, B. r.; Gunnarsson, J. S.; Breedveld, G. D.; Oen, A. M. P.; Eek, E., Large-Scale Field Study on Thin-Layer Capping of Marine PCDD/F-Contaminated Sediments in Grenlandfjords, Norway: Physicochemical Effects. *Environmental Science & Technology* **2012,** *46*, (21), 12030-12037.

30. Cho, Y.-M.; Ghosh, U.; Kennedy, A. J.; Grossman, A.; Ray, G.; Tomaszewski, J. E.; Smithenry, D. W.; Bridges, T. S.; Luthy, R. G., Field Application of Activated Carbon Amendment for In-Situ Stabilization of Polychlorinated Biphenyls in Marine Sediment. *Environmental Science & Technology* **2009,** *43*, (10), 3815-3823.

31. Millward, R. N.; Bridges, T. S.; Ghosh, U.; Zimmerman, J. R.; Luthy, R. G., Addition of Activated Carbon to Sediments to Reduce PCB Bioaccumulation by a Polychaete (Neanthes arenaceodentata) and an Amphipod (Leptocheirus plumulosus). *Environmental Science & Technology* **2005,** *39*, (8), 2880-2887.

32. Ghosh, U.; Luthy, R. G.; Cornelissen, G.; Werner, D.; Menzie, C. A., In-situ Sorbent Amendments: A New Direction in Contaminated Sediment Management. *Environmental Science & Technology* **2011,** *45*, (4), 1163-1168.

33. Cornelissen, G.; Krusa, M. E.; Breedveld, G. D.; Eek, E.; Oen, A. M. P.; Arp, H. P. H.; Raymond, C.; Samuelsson, G.; Hedman, J. E.; Stokland, O.; Gunnarsson, J. S., Remediation of Contaminated Marine Sediment Using Thin-Layer Capping with Activated Carbon-A Field Experiment in Trondheim Harbor, Norway. *Environmental Science & Technology* **2011,** *45*, (14), 6110-6116.

34. Kume, A.; Monguchi, Y.; Hattori, K.; Nagase, H.; Sajiki, H., Pd/C-catalyzed practical degradation of PCBs at room temperature. *Applied Catalysis B: Environmental* **2008,** *81*, (3-4), 274-282.

35. Troxler, W. L.; Hunt, J. W.; Taylor, J.; McNiven, C., Thermal desorption treatment of dioxin-contaminated soil at the former allied feeds site, Sydney, Australia. *Environmental Engineering Science* **2010,** *27*, (7), 613-622.

36. Sato, T.; Todoroki, T.; Shimoda, K.; Terada, A.; Hosomi, M., Behavior of PCDDs/PCDFs in remediation of PCBs-contaminated sediments by thermal desorption. *Chemosphere* **2010,** *80*, (2), 184-189.

37. Zhao, L.; Hou, H.; Shimoda, K.; Terada, A.; Hosomi, M., Formation pathways of polychlorinated dibenzofurans (PCDFs) in sediments contaminated with PCBs during the thermal desorption process. *Chemosphere* **2012,** *88*, (11), 1368-1374.

38. Jonker, M. T. O.; Hoenderboom, A. M.; Koelmans, A. A., Effects of sedimentary sootlike materials on bioaccumulation and sorption of polychlorinated biphenyls. *Environmental Toxicology and Chemistry* **2004,** *23*, (11), 2563-2570.

39. Jonker, M. T. O., Absorption of polycyclic aromatic hydrocarbons to cellulose. *Chemosphere* **2008,** *70*, (5), 778-782.

40. Inglezakis, V. J.; Poulopoulos, S. G., 2 - Adsorption, Ion Exchange, and Catalysis. In *Adsorption, Ion Exchange and Catalysis*, Elsevier: Amsterdam, 2006; pp 31-56.

41. Menendez-Diaz, J. A.; Martin-Gullon, I.; Teresa, J. B., Chapter 1 Types of carbon adsorbents and their production. In *Interface Science and Technology*, Elsevier: 2006; Vol. Volume 7, pp 1-47.

42. Bansal, R. C.; Goyal, M., *Activated Carbon Adsorption*. Talyor & Francis Group: Boca Raton, 2005.

43. Sotelo, J. L.; Ovejero, G.; Delgado, J. A.; Martinez, I., Comparison of adsorption equilibrium and kinetics of four chlorinated organics from water onto GAC. *Water Research* **2002,** *36*, (3), 599-608.

44. Van Noort, P. C. M.; Jonker, M. T. O.; Koelmans, A. A., Modeling maximum adsorption capacities of soot and soot-like materials for PAHs and PCBs. *Environmental Science and Technology* **2004,** *38*, (12), 3305-3309.

45. McDougall, G. J., *The Physical Nature and Manufacture of Activated Carbon*. South Africa Inst Min Metal: Marshalltown Transvaal, 1991; Vol. 91.

46. Azargohar, R.; Dalai, A. K., The Direct Oxidation of Hydrogen Sulphide over Activated Carbons Prepared from Lignite Coal and Biochar. *Canadian Journal of Chemical Engineering* **2011,** *89*, 844-853.

47. Amstaetter, K.; Eek, E.; Cornelissen, G., Sorption of PAHs and PCBs to activated carbon: Coal versus biomass-based quality. *Chemosphere* **2012,** *87*, (5), 573-578.

48. Seiler, W.; Crutzen, P., Estimates of gross and net fluxes of carbon between the biosphere and the atmosphere from biomass burning. *Climatic Change* **1980,** *2*, (3), 207-247.

49. Schmidt, M. W. I.; Noack, A. G., Black carbon in soils and sediments: Analysis, distribution, implications, and current challenges. *Global Biogeochem. Cycles* **2000,** *14*, (3), 777-793.

50. Cochrane, M. A., Fire science for rainforests. *Nature* **2003,** *421*, (6926), 913-919.

51. Dickens, A. F.; Gelinas, Y.; Masiello, C. A.; Wakeham, S.; Hedges, J. I., Reburial of fossil organic carbon in marine sediments. *Nature* **2004,** *427*, (6972), 336-339.

52. Koelmans, A. A.; Jonker, M. T. O.; Cornelissen, G.; Bucheli, T. D.; Van Noort, P. C. M.; Gustafsson, O., Black carbon: The reverse of its dark side. *Chemosphere* **2006,** *63*, (3), 365-377.

53. Goldberg, E. D., *Black carbon in the environment: properties and distribution*. J. Wiley: New York, 1985; p xvi, 198 p.

54. Bucheli, T. D.; Gustafsson, O., Quantification of the Soot-Water Distribution Coefficient of PAHs Provides Mechanistic Basis for Enhanced Sorption Observations. *Environmental Science & Technology* **2000,** *34*, (24), 5144-5151.

55. Karapanagioti, H. K.; Kleineidam, S.; Sabatini, D. A.; Grathwohl, P.; Ligouis, B., Impacts of Heterogeneous Organic Matter on Phenanthrene Sorption: Equilibrium and Kinetic Studies with Aquifer Material. *Environmental Science & Technology* **2000,** *34*, (3), 406-414.

56. Rockne, K. J.; Taghon, G. L.; Kosson, D. S., Pore structure of soot deposits from several combustion sources. *Chemosphere* **2000,** *41*, (8), 1125-1135.

57. Sander, M.; Pignatello, J. J., Characterization of Charcoal Adsorption Sites for Aromatic Compounds: Insights Drawn from Single-Solute and Bi-Solute Competitive Experiments. *Environmental Science & Technology* **2005,** *39*, (6), 1606-1615.

58. Braida, W. J.; Pignatello, J. J.; Lu, Y.; Ravikovitch, P. I.; Neimark, A. V.; Xing, B., Sorption Hysteresis of Benzene in Charcoal Particles. *Environmental Science & Technology* **2002,** *37*, (2), 409-417.

59. Griffin, J. J.; Goldberg, E. D., Notes. Impact of fossil fuel combustion on sediments of Lake Michigan: a reprise. *Environmental Science & Technology* **1983,** *17*, (4), 244-245.

60. Ammann, M.; Kalberer, M.; Jost, D. T.; Tobler, L.; Rossler, E.; Piguet, D.; Gaggeler, H. W.; Baltensperger, U., Heterogeneous production of nitrous acid on soot in polluted air masses. *Nature* **1998,** *395*, (6698), 157-160.

61. Morawska, L.; Zhang, J., Combustion sources of particles. 1. Health relevance and source signatures. *Chemosphere* **2002,** *49*, (9), 1045-1058.

62. Armstrong, B.; Hutchinson, E.; Unwin, J.; Fletcher, T., Lung Cancer Risk after Exposure to Polycyclic Aromatic Hydrocarbons: A Review and Meta-Analysis. *Environmental Health Perspectives* **2004,** *112*, (9), 970-978.

63. Jonker, M. T. O.; Smedes, F., Preferential Sorption of Planar Contaminants in Sediments from Lake Ketelmeer, The Netherlands. *Environmental Science & Technology* **2000,** *34*, (9), 1620-1626.

64. Jonker, M. T. O.; Koelmans, A. A., Polyoxymethylene solid phase extraction as a partitioning method for hydrophobic organic chemicals in sediment and soot. *Environmental Science and Technology* **2001,** *35*, (18), 3742-3748.

65. Jonker, M. T. O.; Koelmans, A. A., Extraction of polycyclic aromatic hydrocarbons from soot and sediment: Solvent evaluation and implications for sorption mechanism. *Environmental Science and Technology* **2002b,** *36*, (19), 4107-4113.

66. Cornelissen, G.; Kukulska, Z.; Kalaitzidis, S.; Christanis, K.; Gustafsson, O., Relations between Environmental Black Carbon Sorption and Geochemical Sorbent Characteristics. *Environmental Science & Technology* **2004a,** *38*, (13), 3632-3640.

67. Cornelissen, G.; Elmquist, M.; Groth, I.; Gustafsson, O., Effect of Sorbate Planarity on Environmental Black Carbon Sorption. *Environmental Science & Technology* **2004b,** *38*, (13), 3574-3580.

68. Cornelissen, G.; Gustafsson, O., Sorption of Phenanthrene to Environmental Black Carbon in Sediment with and without Organic Matter and Native Sorbates. *Environmental Science & Technology* **2004c,** *38*, (1), 148-155.

69. Cornelissen, G.; Gustafsson, O.; Bucheli, T. D.; Jonker, M. T. O.; Koelmans, A. A.; Van Noort, P. C. M., Extensive sorption of organic compounds to black carbon, coal, and kerogen in sediments and soils: Mechanisms and consequences for distribution, bioaccumulation, and biodegradation. *Environmental Science and Technology* **2005,** *39*, (18), 6881-6895.

70. Lohmann, R.; MacFarlane, J. K.; Gschwend, P. M., Importance of Black Carbon to Sorption of Native PAHs, PCBs, and PCDDs in Boston and New York Harbor Sediments. *Environmental Science & Technology* **2005,** *39*, (1), 141-148.

71. Schwarzenbach, R. P. G., P.M.; Imboden, D.M. , *Environmental Organic Chemistry*. 2nd ed.; John Wiley & Son, Inc.: Hoboken, New Jersey, 2003; p 165 - 170.

72. Kroto, H. W.; Heath, J. R.; O'Brien, S. C.; Curl, R. F.; Smalley, R. E., C60: Buckminsterfullerene. *Nature* **1985,** *318*, (6042), 162 - 163.

73. Iijima, S., Helical microtubules of graphitic carbon. *Nature* **1991,** *354*, (6348), 56-58.

74. Rao, C. N. R.; Satishkumar, B. C.; Govindaraj, A.; Nath, M., Nanotubes. *ChemPhysChem* **2001,** *2*, (2), 78-105.

75. Choudhary, V.; Gupta, A., Polymer/Carbon Nanotube Nanocomposite. In *Carbon Nanotubes- Polymer Nanocomposites*, Yellampalli, S., Ed. 2011.

76. Chavan, R.; Desai, U.; Mhatre, P.; Chinchole, R., A Review: Carbon Nanotubes. *International Journal Oof Pharmaceutical Sciences Review and Research* **2012,** *13*, (1), 125 - 134.

77. Yang, K.; Xing, B., Adsorption of Organic Compounds by Carbon Nanomaterials in Aqueous Phase: Polanyi Theory and Its Application. *Chemical Reviews* **2010,** *110*, (10), 5989-6008.

78. Peigney, A.; Laurent, C.; Flahaut, E.; Bacsa, R. R.; Rousset, A., Specific surface area of carbon nanotubes and bundles of carbon nanotubes. *Carbon* **2001,** *39*, (4), 507-514.

79. Long, R. Q.; Yang, R. T., Carbon Nanotubes as Superior Sorbent for Dioxin Removal. *Journal of the American Chemical Society* **2001,** *123*, (9), 2058-2059.

80. Chen, W.; Duan, L.; Zhu, D., Adsorption of Polar and Nonpolar Organic Chemicals to Carbon Nanotubes. *Environmental Science & Technology* **2007,** *41*, (24), 8295-8300.

81. Kah, M.; Zhang, X.; Jonker, M. T. O.; Hofmann, T., Measuring and modeling adsorption of PAHs to carbon nanotubes over a six order of magnitude wide concentration range. *Environmental Science and Technology* **2011,** *45*, (14), 6011-6017.

82. Gotovac, S.; Hattori, Y.; Noguchi, D.; Miyamoto, J.-i.; Kanamaru, M.; Utsumi, S.; Kanoh, H.; Kaneko, K., Phenanthrene Adsorption from Solution on Single Wall Carbon Nanotubes. *The Journal of Physical Chemistry B* **2006,** *110*, (33), 16219-16224.

83. Gotovac, S.; Yang, C.-M.; Hattori, Y.; Takahashi, K.; Kanoh, H.; Kaneko, K., Adsorption of polyaromatic hydrocarbons on single wall carbon nanotubes of different functionalities and diameters. *Journal of Colloid and Interface Science* **2007,** *314*, (1), 18-24.

84. Gotovac, S.; Honda, H.; Hattori, Y.; Takahashi, K.; Kanoh, H.; Kaneko, K., Effect of Nanoscale Curvature of Single-Walled Carbon Nanotubes on Adsorption of Polycyclic Aromatic Hydrocarbons. *Nano Letters* **2007,** *7*, (3), 583-587.

85. Shao, D.; Sheng, G.; Chen, C.; Wang, X.; Nagatsu, M., Removal of polychlorinated biphenyls from aqueous solutions using B-cyclodextrin grafted multiwalled carbon nanotubes. *Chemosphere* **2010,** *79*, (7), 679-685.

86. Shao, D.; Hu, J.; Jiang, Z.; Wang, X., Removal of 4,4'-dichlorinated biphenyl from aqueous solution using methyl methacrylate grafted multiwalled carbon nanotubes. *Chemosphere* **2011,** *82*, (5), 751-758.

87. Wang, S.; Chia, P.-J.; Chua, L.-L.; Zhao, L.-H.; Png, R.-Q.; Sivaramakrishnan, S.; Zhou, M.; Goh, R. G. S.; Friend, R. H.; Wee, A. T. S.; Ho, P. K. H., Band-like Transport in Surface-Functionalized Highly Solution-Processable Graphene Nanosheets. *Advanced Materials* **2008,** *20*, (18), 3440-3446.

88. Novoselov, K. S.; Geim, A. K.; Morozov, S. V.; Jiang, D.; Zhang, Y.; Dubonos, S. V.; Grigorieva, I. V.; Firsov, A. A., Electric Field Effect in Atomically Thin Carbon Films. *Science* **2004,** *306*, (5696), 666 - 669.

89. Allen, M. J.; Tung, V. C.; Kaner, R. B., Honeycomb Carbon: A Review of Graphene. *Chemical Reviews* **2009,** *110*, (1), 132-145.

90. Cooper, D. R.; Whiteway, E.; Yu, V.; D'Anjou, B.; Ghattamaneni, N.; Harack, B.; Hilke, M.; Horth, A.; Majlis, N.; Massicotte, M.; Vandsburger, L., Experimental Review of Graphene. *ISRN Condensed Matter Physics* **2012,** *2012*, (6).

91. Zhu, Y.; Murali, S.; Cai, W.; Li, X.; Suk, J. W.; Potts, J. R.; Ruoff, R. S., Graphene and Graphene Oxide: Synthesis, Properties, and Applications. *Advanced Materials* **2010,** *22*, (35), 3906-3924.

92. Catherine M. Santos; Maria Celeste R. Tria; Regina Aileen May V. Vergara; Karina Milagros Cui; Roderick Pernites; Rigoberto C. Advincula, Films of Highly Disperse Electrodeposited Poly(N-vinylcarbazole)–Graphene Oxide Nanocomposites. *Macromolecular Chemistry and Physics* **2011,** *212*, (21), 2371–2377.

93. Safe, S. H., Polychlorinated Biphenyls (PCBs): Environmental Impact, Biochemical and Toxic Responses, and Implications for Risk Assessment. *Critical Reviews in Toxicology* **1994,** *24*, (2), 87-149.

94. De Bruijn, J.; Hermens, J., Relationships Between Octanol Water Partition-Coefficients and Total Molecular-Surface Area and Total Molecular Volume of Hydrophobic Organic-Chemicals. *Quantitative Structure-Activity Relationships* **1990,** *9*, 11-21.

95. Hawker, D. W.; Connell, D. W., Octanol-water partition coefficients of polychlorinated biphenyl congeners. *Environmental Science & Technology* **1988,** *22*, (4), 382-387.

96. Mackay, D.; Shiu, W. Y.; Ma, K. C., *Illustrated Handbook of Physical-Chemical Properties and Environmental Fate for Organic Chemicals*. Lewis Publishers, Inc: Chelsea, 1992.

97. Brodsky, J.; Ballschmiter, K., Reversed phase liquid chromatography of PCBs as a basis for the calculation of water solubility and LogKow for polychlorobiphenyls. *Fres. Z. Anal. Chem* **1988**, (331), 295-301.

98. Gramatica, P.; Navas, N.; Todeschini, R., 3D-modelling and prediction by WHIM descriptors. Part 9. Chromatographic relative retention time and physico-chemical

properties of polychlorinated biphenyls (PCBs). *Chemometrics and Intelligent Laboratory Systems* **1998,** *40*, (1), 53-63.

99. Foo, K. Y.; Hameed, B. H., Insights into the modeling of adsorption isotherm systems. *Chemical Engineering Journal* **2010,** *156*, (1), 2-10.

100. Langmuir, I., The constitution and fundamental properties of solids and liquids. *Journal of the Franklin Institute* **1917,** *183*, (1), 102-105.

101. Langmuir, I., The Adsorption of Gases on Plane Surfaces of Glass, Mica and Platinum. *Journal of the American Chemical Society* **1918,** *40*, (9), 1361-1403.

102. Vijayaraghavan, K.; Padmesh, T. V. N.; Palanivelu, K.; Velan, M., Biosorption of nickel(II) ions onto Sargassum wightii: Application of two-parameter and three-parameter isotherm models. *Journal of Hazardous Materials* **2006,** *133*, (1-3), 304-308.

103. Werner, D.; Karapanagioti, H. K.; Van Noort, P. C. M.; Jonker, M. T. O.; Koelmans, A. A., Comment on "Modeling maximum adsorption capacities of soot and soot-like materials for PAHs and PCBs" [2] (multiple letters). *Environmental Science and Technology* **2005,** *39*, (1), 381-384.

104. van Noort, P. C. M.; Jonker, M. T. O.; Koelmans, A. A., Response to Comment on "Modeling Maximum Adsorption Capacities of Soot and Soot-like Materials for PAHs and PCBs". *Environmental Science & Technology* **2004,** *38*, (22), 6176-6176.

105. Pikaar, I.; Koelmans, A. A.; van Noort, P. C. M., Sorption of organic compounds to activated carbons. Evaluation of isotherm models. *Chemosphere* **2006,** *65*, (11), 2343-2351.

106. Freundlich, H. M. F., Uber die Adsorption in Losungen. *Z. Phys. Chem.* **1906,** *57*, 385-470.

107. Allen-King, R. M.; Grathwohl, P.; Ball, W. P., New modeling paradigms for the sorption of hydrophobic organic chemicals to heterogeneous carbonaceous matter in soils, sediments, and rocks. *Advances in Water Resources* **2002,** *25*, (8â€“12), 985-1016.

108. Crittenden, J. C.; Trussell, R. R.; Hand, D. W.; Howe, K. J.; Tchobanoglous, G., *Water Treatment: Principles and Design*. 2nd ed.; John Wiley & Sons, Inc: Hoboken, 2005; p 1948.

109. Koelmans, A. A.; Meulman, B.; Meijer, T.; Jonker, M. T. O., Attenuation of polychlorinated biphenyl sorption to charcoal by humic acids. *Environmental Science and Technology* **2009,** *43*, (3), 736-742.

110. Jonker, M. T. O.; Barendregt, A., Oil is a sedimentary supersorbent for polychlorinated biphenyls. *Environmental Science and Technology* **2006,** *40*, (12), 3829-3835.

111. USEPA *Method 8082, Revision A, Polychlorinated Biphenyls (PCBs) by Gas Chromatography*; 2007; p 5.

112. Lu, X.; Skwarski, A.; Drake, B.; Reible, D. D., Predicting bioavailability of PAHs and PCBs with porewater concentrations measured by solid-phase microextraction fibers. *Environmental Toxicology & Chemistry* **2011,** *30*, (5), 1109-1116.

113. Mayer, P.; Vaes, W. H. J.; Wijnker, F.; Legierse, K. C. H. M.; Kraaij, R.; Tolls, J.; Hermens, J. L. M., Sensing Dissolved Sediment Porewater Concentrations of Persistent and Bioaccumulative Pollutants Using Disposable Solid-Phase Microextraction Fibers. *Environmental Science & Technology* **2000,** *34*, (24), 5177-5183.

114. McDonough, K. M.; Fairey, J. L.; Lowry, G. V., Adsorption of polychlorinated biphenyls to activated carbon: Equilibrium isotherms and a preliminary assessment of the effect of dissolved organic matter and biofilm loadings. *Water Research* **2008,** *42*, (3), 575-584.

115. Roque-Malherbe, R., Complementary approach to the volume filling theory of adsorption in zeolites. *Microporous and Mesoporous Materials* **2000,** *41*, (1-3), 227-240.

116. Condon, J. B., Equivalency of the Dubinin-Polanyi equations and the QM based sorption isotherm equation. A. Mathematical derivation. *Microporous and Mesoporous Materials* **2000,** *38*, (2-3), 359-376.

Appendix A

Table A.1: Detailed list of the isotherm parameters found in the literature for sorption of PCBs to carbonaceous materials.

Lead Author	Year		PCB Congener	LAN Q_{max} *10^6 (ug/kg)	LAN b (L/ug)	FRE K_F *10^6 $(x/kg)(x/L)^{-n}$	FRE n_F (-)	PDM Q_{max} *10^6 (ug/kg)	PDM Z (kJ/mol)	d (-)
Cornelissen	2004	BC	PCB-3	-	-	0.26	0.62	-	-	-
Cornelissen	2004	BC	PCB-4	-	-	0.035	0.92	-	-	-
McDonough	2008	Fresh AC	PCB-4	-	-	560	0.57	-	-	-
McDonough	2008	Fresh AC	PCB-12	-	-	230	0.73	-	-	-
McDonough	2008	Fresh AC	PCB-18	-	-	170	0.7	-	-	-
McDonough	2008	Fresh AC	PCB-52	-	-	76	0.86	-	-	-
McDonough	2008	Fresh AC	PCB-53	-	-	34	1.08	-	-	-
McDonough	2008	Fresh AC	PCB-54	-	-	66	1.03	-	-	-
McDonough	2008	Fresh AC	PCB-72	-	-	250	0.83	-	-	-
McDonough	2008	Fresh AC	PCB-77	-	-	790	0.82	-	-	-
McDonough	2008	Fresh AC	PCB-126	-	-	890	0.94	-	-	-
McDonough	2008	DOM AC	PCB-4	-	-	11	0.97	-	-	-
McDonough	2008	DOM AC	PCB-12	-	-	25	0.92	-	-	-
McDonough	2008	DOM AC	PCB-18	-	-	33	0.79	-	-	-
McDonough	2008	DOM AC	PCB-52	-	-	13	0.93	-	-	-
McDonough	2008	DOM AC	PCB-53	-	-	8.3	1.03	-	-	-
McDonough	2008	DOM AC	PCB-54	-	-	11	1.02	-	-	-
McDonough	2008	DOM AC	PCB-72	-	-	46	0.78	-	-	-
McDonough	2008	DOM AC	PCB-77	-	-	66	0.85	-	-	-
McDonough	2008	DOM AC	PCB-126	-	-	110	0.87	-	-	-
McDonough	2008	Bio AC	PCB-4	-	-	26	0.8	-	-	-
McDonough	2008	Bio AC	PCB-12	-	-	76	0.72	-	-	-
McDonough	2008	Bio AC	PCB-18	-	-	19	0.81	-	-	-
McDonough	2008	Bio AC	PCB-52	-	-	4.6	0.95	-	-	-
McDonough	2008	Bio AC	PCB-53	-	-	6.6	0.96	-	-	-
McDonough	2008	Bio AC	PCB-54	-	-	10	0.96	-	-	-
McDonough	2008	Bio AC	PCB-72	-	-	38	0.8	-	-	-
McDonough	2008	Bio AC	PCB-77	-	-	130	0.68	-	-	-
McDonough	2008	Bio AC	PCB-126	-	-	230	0.74	-	-	-
Koelmans	2009	BC with HA	PCB-18	0.66 ± 0.37	3.96 ± 2.8	-	-	0.52 ± 0.11	18.7 ± 1.0	4.0 ± 0.47
Koelmans	2009	BC with HA	PCB-28	0.84 ± 0.55	22.9 ± 19	-	-	0.63 ± 0.18	24.3 ± 1.3	5.3 ± 0.82
Koelmans	2009	BC with HA	PCB-52	0.58 ± 0.26	9.64 ± 5.6	-	-	0.54 ± 0.1	16.1 ± 0.87	3.3 ± 0.29
Koelmans	2009	BC with HA	PCB-72	0.52 ± 0.09	63.6 ± 15	-	-	1.02 ± 0.18	14.8 ± 0.91	2.4 ± 0.17
Koelmans	2009	BC with HA	PCB-77	0.89 ± 0.31	198 ± 87	-	-	0.98 ± 0.23	14.0 ± 1.1	2.8 ± 0.30
Koelmans	2009	BC with HA	PCB-101	0.45 ± 0.13	24.2 ± 9	-	-	0.54 ± 0.09	12.5 ± 0.74	2.4 ± 0.17
Koelmans	2009	BC with HA	PCB-118	0.61 ± 0.11	110 ± 26	-	-	1.54 ± 0.45	13.8 ± 1.4	2.2 ± 0.22
Koelmans	2009	BC with HA	PCB-126	0.77 ± 0.24	201 ± 81	-	-	3.96 ± 3.2	8.6 ± 2.8	1.6 ± 0.32
Koelmans	2009	BC with HA	PCB-138	0.7 ± 0.1	46 ± 8.2	-	-	1.25 ± 0.36	8.7 ± 1.1	1.8 ± 0.17
Koelmans	2009	BC with HA	PCB-156	0.84 ± 0.21	93.6 ± 29	-	-	2.57 ± 1.53	8.2 ± 2.1	1.6 ± 0.28
Koelmans	2009	BC with HA	PCB-169	0.92 ± 0.36	132 ± 62	-	-	3.89 ± 4.50	5.6 ± 3.0	1.3 ± 0.38
Jantunen	2010	traffic soot	PCB-18	0.05 ± 0.01	12 ± 3.5	0.16	0.76	1.3 ± 2.3	~ 6 ± 5	1.3 ± 0.5
Jantunen	2010	traffic soot	PCB-28	0.17 ± 0.02	16 ± 1.9	1.1	0.86	1.3 ± 0.77	12 ± 2	2.0 ± 0.3
Jantunen	2010	traffic soot	PCB-52	0.11 ± 0.02	9.6 ± 2.4	0.54	0.9	0.44 ± 0.29	9 ± 2	1.8 ± 0.3
Jantunen	2010	traffic soot	PCB-72	0.09 ± 0.01	55 ± 10	1.8	0.88	1.2 ± 4.1	9 ± 1	1.6 ± 0.1
Jantunen	2010	traffic soot	PCB-77	0.12 ± 0.03	270 ± 68	9.7	0.88	4.7 ± 2.9	3.7 ± 0.9	1.1 ± 0.1
Jantunen	2010	traffic soot	PCB-101	0.13 ± 0.02	26 ± 4.6	1.7	0.91	1.6 ± 0.98	5 ± 1	1.3 ± 0.1
Jantunen	2010	traffic soot	PCB-118	0.15 ± 0.03	83 ± 15	5	0.89	4.6 ± 2.3	6 ± 1	1.4 ± 0.1
Jantunen	2010	traffic soot	PCB-126	0.22 ± 0.08	180 ± 61	14	0.91	65 ± 65	~ 2.1 ± 0.8	~ 0.9 ± 0.1
Jantunen	2010	traffic soot	PCB-138	0.11± 0.04	83 ± 28	3.6	0.9	18 ± 18	~ 1.7 ± 0.7	0.9 ± 0.1
Jantunen	2010	traffic soot	PCB-156	0.17 ± 0.05	140 ± 42	9.8	0.92	6.5 ± 4.7	4 ± 1	1.1 ± 0.1
Jantunen	2010	traffic soot	PCB-169	0.29 ± 0.22	140 ± 110	17	0.92	360 ± 1100	~ 0.5 ± 0.5	~ 0.66 ± 0.12
Jantunen	2010	coal	PCB-18	0.07 ± 0.02	35 ± 12	0.28	0.66	0.15 ± 0.13	17 ± 4	3 ± 1
Jantunen	2010	coal	PCB-28	0.12 ± 0.02	160 ± 39	0.7	0.5	0.13 ± 0.1	26 ± 3	7 ± 7
Jantunen	2010	coal	PCB-52	0.07 ± 0.01	79 ± 17	0.48	0.64	0.12 ± 0.06	18 ± 3	3.1 ± 1.0
Jantunen	2010	coal	PCB-72	0.08 ± 0.01	270 ± 34	2.4	0.76	0.23 ± 0.09	17 ± 1	2.6 ± 0.3
Jantunen	2010	coal	PCB-77	0.08 ± 0.01	1300 ± 210	9	0.77	0.26 ± 0.09	13 ± 1	2.1 ± 0.2
Jantunen	2010	coal	PCB-101	0.09 ± 0.01	200 ± 37	1.8	0.73	0.2 ± 0.1	14 ± 2	2.5 ± 0.4
Jantunen	2010	coal	PCB-118	0.10 ± 0.02	490 ± 92	6.1	0.78	0.33 ± 0.13	17 ± 2	2.6 ± 0.3
Jantunen	2010	coal	PCB-126	0.11 ± 0.03	830 ± 250	9	0.78	2 ± 2	8 ± 3	1.5 ± 0.3
Jantunen	2010	coal	PCB-138	0.09 ± 0.01	350 ± 67	5.6	0.82	0.54 ± 0.32	9 ± 2	1.6 ± 0.2
Jantunen	2010	coal	PCB-156	0.11 ± 0.01	530 ± 83	12	0.85	0.83 ± 0.36	9 ± 1	1.7 ± 0.1
Jantunen	2010	coal	PCB-169	0.16 ± 0.03	390 ± 83	19	0.88	0.79 ± 0.54	8 ± 2	1.6 ± 0.2
Shao	2010	CNT-g-CD	PCB-15	261	-	-	-	-	-	-
Shao	2010	CNT-g-CD	PCB-20	235	-	-	-	-	-	-
Shao	2011	CNT-g-pMMA	PCB-15	240	6	-	-	-	-	-
Shao	2011	CNT	PCB-15	177	3.5	-	-	-	-	-
Amstaetter	2012	Coal AC	PCB-101	-	-	5000	1.22	-	-	-
Amstaetter	2012	Biomass AC	PCB-101	-	-	8100	1.11	-	-	-

Table A.2: Experimental internal standard results and adjustments made for quantification.

Sample #	CCVs	AC	BC	CNT	CNT-OH	GE
1	73245	96034	86625	103850	141970	130879
2	59066	83596	89164	119509	102158	132004
3	90552	79974	81315	119711	112459	134599
4	85966	84373	94211	114028	147845	130792
5	71010	100507	99382	129488	140232	150648
6	87576	106096	94622	131680	152990	147399
7	83737	111688	99229	137340	161083	163476
8	76881	110624	99911	142270	137068	147073
9	72419	104726	100389	138501	157065	142066
10	71129	92055	101874	144549	157276	141137
11	71610	104419	97788	125841	130747	164673
12	74618	104187	90280	121152	145514	147003
13	87380	97831	93042	123551	137882	155281
14	65420	99044	95942	115376	147023	147438
15	81273	101250	93245	118070	145221	156537
16	83515	113195	94354	111340	141503	149735
17	83230	99220	91892	99825	149133	137315
18	101731	94221	100954	99474	132805	123811
19	106903	105731	90697	97140	119430	134319
20	-	91731	100539	114870	120445	128027
21	-	93933	95613	115340	121483	134791
22	-	96278	98576	98469	123211	143881
23	-	100332	-	113666	137635	159801
24	-	99805	-	109901	123712	142283
25	-	102407	-	127385	132318	141274
26	-	98671	-	113719	152868	165368
average	80382	98920	94984	118694	137349	144293
std	11816	8207	5235	13368	14893	11664
CV	0.146992	0.08297	0.055113	0.112622	0.108432	0.080836
min	59066	79974	81315	97140	102158	123811
max	106903	113195	101874	144549	161083	165368

Table A.3: R^2 values of the three isotherm models for the 55 sorbent-congener combinations and two error functions.

SSE

Congener	AC			Best fit
	LAN	FRE	PDM	
PCB-001	0.779	0.628	0.777	LAN, PDM
PCB-002	0.933	0.795	0.929	LAN, PDM
PCB-004	0.865	0.746	0.863	LAN, PDM
PCB-008	0.938	0.898	0.937	LAN, PDM
PCB-015	0.939	0.968	0.968	FRE, PDM
PCB-052	0.962	0.945	0.959	LAN, PDM
PCB-072	0.952	0.932	0.947	LAN, PDM
PCB-077	0.839	0.842	0.842	ALL
PCB-138	0.975	0.975	0.976	ALL
PCB-156	0.813	0.809	0.811	ALL
PCB-169	0.809	0.795	0.817	FRE, PDM

HYBRID

Congener	AC			Best fit
	LAN	FRE	PDM	
PCB-001	0.777	0.597	0.768	LAN
PCB-002	0.931	0.727	0.916	LAN
PCB-004	0.865	0.708	0.858	LAN, PDM
PCB-008	0.929	0.871	0.934	LAN, PDM
PCB-015	0.913	0.966	0.966	FRE, PDM
PCB-052	0.962	0.938	0.957	LAN, PDM
PCB-072	0.952	0.924	0.943	LAN, PDM
PCB-077	0.829	0.842	0.842	FRE, PDM
PCB-138	0.973	0.974	0.976	ALL
PCB-156	0.808	0.809	0.809	ALL
PCB-169	0.805	0.781	0.787	LAN

Congener	BC			Best fit
	LAN	FRE	PDM	
PCB-001	0.965	0.876	0.961	LAN, PDM
PCB-002	0.989	0.962	0.988	LAN, PDM
PCB-004	0.882	0.833	0.881	LAN, PDM
PCB-008	0.981	0.958	0.978	LAN, PDM
PCB-015	0.983	0.961	0.982	LAN, PDM
PCB-052	0.982	0.974	0.981	ALL
PCB-072	0.982	0.977	0.981	ALL
PCB-077	0.986	0.985	0.986	ALL
PCB-138	0.982	0.982	0.982	ALL
PCB-156	0.988	0.987	0.989	ALL
PCB-169	0.974	0.961	0.993	PDM

Congener	BC			Best fit
	LAN	FRE	PDM	
PCB-001	0.965	0.817	0.956	LAN, PDM
PCB-002	0.988	0.924	0.987	LAN, PDM
PCB-004	0.881	0.814	0.880	LAN, PDM
PCB-008	0.979	0.937	0.974	LAN, PDM
PCB-015	0.982	0.933	0.980	LAN, PDM
PCB-052	0.982	0.969	0.978	LAN, PDM
PCB-072	0.982	0.973	0.979	ALL
PCB-077	0.986	0.985	0.985	ALL
PCB-138	0.981	0.982	0.981	ALL
PCB-156	0.987	0.987	0.986	ALL
PCB-169	0.957	0.945	0.975	PDM

Congener	CNT			Best fit
	LAN	FRE	PDM	
PCB-001	0.963	0.971	0.975	FRE, PDM
PCB-002	0.982	0.980	0.986	ALL
PCB-004	0.884	0.837	0.884	LAN, PDM
PCB-008	0.980	0.982	0.984	ALL
PCB-015	0.993	0.988	0.996	ALL
PCB-052	0.996	0.994	0.996	ALL
PCB-072	0.995	0.995	0.997	ALL
PCB-077	0.966	0.935	0.973	LAN, PDM
PCB-138	0.995	0.993	0.994	ALL
PCB-156	0.987	0.979	0.985	ALL
PCB-169	0.814	0.779	0.955	PDM

Congener	CNT			Best fit
	LAN	FRE	PDM	
PCB-001	0.954	0.960	0.975	PDM
PCB-002	0.976	0.964	0.984	LAN, PDM
PCB-004	0.884	0.803	0.882	LAN, PDM
PCB-008	0.966	0.980	0.984	FRE, PDM
PCB-015	0.986	0.977	0.996	LAN, PDM
PCB-052	0.993	0.993	0.995	ALL
PCB-072	0.989	0.992	0.997	ALL
PCB-077	0.953	0.908	0.967	PDM
PCB-138	0.994	0.992	0.994	ALL
PCB-156	0.987	0.975	0.982	LAN, PDM
PCB-169	0.760	0.728	0.846	PDM

Table A.3 (continued).

Congener	CNT-OH			Best fit
	LAN	FRE	PDM	
PCB-001	0.851	0.747	0.847	LAN, PDM
PCB-002	0.952	0.921	0.948	LAN, PDM
PCB-004	0.835	0.840	0.839	ALL
PCB-008	0.947	0.933	0.943	LAN, PDM
PCB-015	0.910	0.858	0.902	LAN, PDM
PCB-052	0.938	0.922	0.942	LAN, PDM
PCB-072	0.933	0.911	0.931	LAN, PDM
PCB-077	0.901	0.820	0.927	PDM
PCB-138	0.917	0.896	0.927	PDM
PCB-156	0.913	0.890	0.933	PDM
PCB-169	0.755	0.625	0.830	PDM

Congener	CNT-OH			Best fit
	LAN	FRE	PDM	
PCB-001	0.848	0.708	0.843	LAN, PDM
PCB-002	0.948	0.873	0.947	LAN, PDM
PCB-004	0.836	0.839	0.838	ALL
PCB-008	0.947	0.925	0.936	LAN
PCB-015	0.909	0.811	0.889	LAN
PCB-052	0.935	0.914	0.922	LAN
PCB-072	0.931	0.897	0.912	LAN
PCB-077	0.883	0.775	0.892	PDM
PCB-138	0.908	0.878	0.898	LAN
PCB-156	0.903	0.874	0.888	LAN
PCB-169	0.604	0.499	0.812	PDM

Congener	GE			Best fit
	LAN	FRE	PDM	
PCB-001	0.879	0.778	0.875	LAN, PDM
PCB-002	0.978	0.964	0.978	LAN, PDM
PCB-004	0.830	0.739	0.829	LAN, PDM
PCB-008	0.977	0.972	0.976	ALL
PCB-015	0.977	0.931	0.974	LAN, PDM
PCB-052	0.977	0.971	0.975	ALL
PCB-072	0.976	0.964	0.973	LAN, PDM
PCB-077	0.981	0.841	0.983	LAN, PDM
PCB-138	0.944	0.917	0.953	LAN, PDM
PCB-156	0.966	0.870	0.969	LAN, PDM
PCB-169	0.958	0.843	0.956	LAN, PDM

Congener	GE			Best fit
	LAN	FRE	PDM	
PCB-001	0.872	0.729	0.872	LAN, PDM
PCB-002	0.977	0.933	0.977	LAN, PDM
PCB-004	0.828	0.699	0.825	LAN, PDM
PCB-008	0.965	0.967	0.976	FRE, PDM
PCB-015	0.976	0.892	0.971	LAN, PDM
PCB-052	0.976	0.969	0.972	ALL
PCB-072	0.974	0.955	0.970	LAN, PDM
PCB-077	0.972	0.740	0.982	LAN, PDM
PCB-138	0.942	0.900	0.927	LAN
PCB-156	0.965	0.795	0.950	LAN
PCB-169	0.950	0.744	0.954	LAN, PDM